

# Meson Spectroscopy with low $Q^2$ electron scattering in CLAS12

M. Battaglieri<sup>\*†</sup>, R. De Vita<sup>†</sup>, M.Osipenko, M. Ripani, M. Taiuti

*Istituto Nazionale di Fisica Nucleare, Sezione di Genova e Dipartimento di Fisica dell'Università, 16146  
Genova, Italy*

A. Afanasev, V. D. Burkert, V. Kubarovsky,

P. Nadel-Turonski, E. Pasyuk, S. Stepanyan<sup>†</sup>, D. Weygand<sup>†</sup>

*Jefferson Lab, Newport News, VA 23606, USA*

D. Glazier<sup>†</sup>, D. Watts

*Edinburgh University, Edinburgh EH9 3JZ, United Kingdom*

C. Salgado<sup>†</sup>, M. Khandaker

*Norfolk State University, Norfolk VA 23504, USA*

A. Szczepaniak

*Physics Department and Nuclear Theory Center, Indiana University, Bloomington, Indiana 47405*

J. Ball, M. Garçon, B. Moreno, H. Moutarde, S. Procureur, F. Sabatié

*CEA-Saclay, Service de Physique Nucléaire, F91191 Gif-sur-Yvette, France*

K. Hicks

*Ohio University, Department of Physics, Athens, OH 45701, USA*

M. Ungaro

*University of Connecticut, Storrs, Connecticut 06269*

D. Ireland, R. Kaiser, K. Livingston, D. MacGregor, B. McKinnon, D. Protopopescu, G. Rosner,  
B. Seitz

*University of Glasgow, Glasgow G12 8QQ, United Kingdom*

W. J. Briscoe, H. Haberzettl, M. Paris, I. I. Strakovsky

*The George Washington University, Washington, D.C., 20052*

A. Kubarovsky, P. Stoler

*Rensselaer Polytechnic Institute, Department of Physics, Troy, NY 12181, USA*

L. Guo

*Florida International University, Miami, Florida 33199*

B.Nefkens, A. Starostin

*University of California at Los Angeles, Department of Physics and Astronomy, Los Angeles, CA  
90095-1547, USA*

---

<sup>\*</sup>Contact Person, email: Marco.Battaglieri@ge.infn.it

<sup>†</sup>Spokesperson

A. D'Angelo, C. Shaerf, V. Vegna

*Istituto Nazionale di Fisica Nucleare, Sezione di Roma 2 e Dipartimento di Fisica dell'Università di Roma  
Tor Vergata, Roma, Italy*

M. Aghasyan, S. Anefalos Pereira, E. De Sanctis, D. Hasch, V. Lucherini, M. Mirazita, P. Rossi  
*Istituto Nazionale di Fisica Nucleare, Laboratori Nazionali di Frascati, P.O. 13, 00044 Frascati, Italy*

M. Capogni, D.M. Castelluccio, E. Cisbani, S. Frullani, F. Garibaldi, F. Meddi, G. M. Urciuoli  
*Istituto Nazionale di Fisica Nucleare, Sezione di Roma e Gruppo Collegato Sanità, e Università La  
Sapienza, Italy*

R. De Leo

*Istituto Nazionale di Fisica Nucleare, Sezione di Bari e Dipartimento di Fisica dell'Università, Bari, Italy*

R. Perrino

*Istituto Nazionale di Fisica Nucleare, Sezione di Lecce 73100 Lecce, Italy*

V. Bellini, A. Giusa, F. Mammoliti, G. Russo, M. L. Sperduto, C. M. Sutera

*Istituto Nazionale di Fisica Nucleare, Sezione di Catania e Dipartimento di Fisica dell'Università, Catania,  
Italy*

L. Barion G. Ciullo, M. Contalbrigo, P. Lenisa, L. Pappalardo

*Istituto Nazionale di Fisica Nucleare, Sezione di Ferrara e Dipartimento di Fisica dell'Università, Ferrara,  
Italy*

A. Fradi, B. Guegan, M. Guidal, S. Niccolai, S.Pisano

*Institut de Physique Nucléaire d'Orsay, IN2P3, BP 1, 91406 Orsay, France*

J. Dumas, C. Maier, Y. Perrin, E.Voutier

*Laboratoire de Physique et de Cosmologie, CNRS/IN2P3, 38026 Grenoble, France*

## Abstract

Understanding quark and gluon confinement in Quantum Chromo Dynamics is one of the main issues in hadronic physics. Meson spectroscopy is a powerful tool to investigate how the QCD partons manifest themselves in strong interaction at the energy scale of the nucleon mass (GeV). A comprehensive study of the meson spectrum with precise determination of resonance masses and properties and search for unconventional states beyond  $q\bar{q}$  configurations in high statistics and high resolutions experiment is needed to assess the role of gluons and identify the relevant degree of freedom. We are proposing to extend the Hall-B CLAS12 capability to run experiments with quasi-real photons to study conventional and unconventional (hybrids and exotics) hadrons. The proposed technique, electroscattering at very low  $Q^2$  ( $10^{-2} - 10^{-1}$  GeV $^2$ ), providing a high photon flux and a high degree of linear polarization, represents a competitive and complementary way to study the hadron spectrum and the production mechanisms with respect to standard real photo-production experiments with Bremsstrahlung beams. A Forward Tagger made by a calorimeter, a veto counter and a tracking device will be added to the standard equipment to detect the scattered electrons in the angular range  $\theta_{e'} = 2.5^\circ - 4.5^\circ$  and energy range  $E_{e'} = 0.5 - 4.5$  GeV, with an effective quasi-real photon flux of  $10^7 - 10^8$   $\gamma/s$ . The operations of the new device will be compatible with standard electron scattering experiments planned for Hall-B, allowing the proposed measurements to be run in parallel to the already approved program. The unique combination of CLAS12 and the new forward tagger facility will give access to an extensive physics program, which belongs to the main physics focus of the Jefferson Lab upgrade.

# Contents

<b>1</b>	<b>Introduction</b>	<b>5</b>
<b>2</b>	<b>Physics motivation</b>	<b>6</b>
2.1	Meson spectroscopy . . . . .	7
2.2	Partial Wave Analysis . . . . .	8
<b>3</b>	<b>Experimental setup</b>	<b>11</b>
3.1	Hadron detection: CLAS12 configuration . . . . .	11
3.2	Electroproduction at very small $Q^2$ . . . . .	13
3.3	Kinematics, rates and backgrounds . . . . .	14
3.4	Electron detection: the Forward Tagger . . . . .	15
3.4.1	The electromagnetic calorimeter . . . . .	17
3.4.2	The tracker . . . . .	18
3.4.3	The veto counter . . . . .	18
3.5	GEMC Simulations . . . . .	20
3.5.1	FT acceptance and resolution . . . . .	20
3.5.2	Electromagnetic background rates . . . . .	23
3.5.3	Radiation dose . . . . .	23
3.5.4	CLAS12 Drift Chamber occupancies . . . . .	26
3.6	Trigger . . . . .	27
3.6.1	CLAS12 trigger system . . . . .	27
3.6.2	Electroproduction trigger rate . . . . .	28
3.6.3	Quasi-real photoproduction rate . . . . .	31
<b>4</b>	<b>Expected results</b>	<b>32</b>
4.1	Benchmark channels . . . . .	32
4.1.1	The reaction $\gamma p \rightarrow n\pi^+\pi^+\pi^+$ . . . . .	34
4.1.2	The reaction $\gamma p \rightarrow n\eta\pi^-$ . . . . .	37
4.1.3	The reaction $\gamma p \rightarrow p\eta\phi$ . . . . .	38
4.1.4	The reactions $\gamma p \rightarrow pK^+K^-\pi^0$ and $\gamma p \rightarrow nK^+K^-\pi^+$ . . . . .	40
4.1.5	Conclusions . . . . .	42
4.2	PWA simulations . . . . .	42
4.2.1	Partial Wave Analysis of the $3\pi$ Channel . . . . .	45
4.2.2	Partial Wave Analysis of the $\eta\pi$ Channel . . . . .	52
4.3	Beam time request and expected results . . . . .	53
4.3.1	Strangeonia . . . . .	59
<b>5</b>	<b>Summary</b>	<b>59</b>
<b>A</b>	<b>Appendix A: the model to describe <math>\gamma p \rightarrow \pi^+\pi^+\pi^-n</math></b>	<b>61</b>

# 1 Introduction

Meson spectroscopy is one of the key tools for studying Quantum Chromodynamics (QCD) in the strong interactions *i.e.*, confinement regime. Light quarks spectroscopy has been an essential component of the physics program with CLAS [1, 2, 3, 4, 5, 6]. To date a large amount of experimental data on electromagnetic production of mesons and baryons has been collected by CLAS while largely focusing on baryon structure. With advances in lattice gauge computations of hadron spectrum more data will be necessary to guide improvements in hadronic phenomenology and to verify lattice QCD predictions. A complete picture of QCD in the strong-coupling regime requires an extension of hadron spectroscopy studies to higher masses and/or higher transferred momenta. Reconstruction of hadron resonances requires complete understanding of reaction mechanisms, *i.e.* both production and decay characteristics. Meson production at higher electron energies that will be available after completion of the CEBAF 12 GeV upgrade is expected to be less affected by baryon resonances while maintaining significant yields

While electron scattering at finite  $Q^2$  is very powerful for detailed studies of hadronic structure, real or (*quasi*-)real ( $Q^2 \sim 0$ ) photon experiments are more advantageous for exploratory studies because of the higher cross section. Furthermore, experiments with tagged real photons would be a natural extension of the proposed physics program as already proved by 12 years of real photon runs with CLAS at 6 GeV (CLAS6). Based on these considerations, we propose to add to the standard electron scattering operations of CLAS12 the capability of running (*quasi*-)real photon scattering experiments in parallel.

A comprehensive experimental program concerning the photoproduction of high-mass mesonic states (consisting of ordinary mesons, hybrids, and mesons with exotic  $J^{PC}$ ) using  $H_2$  will be possible with the CLAS12 detector and the new (*quasi*-)real photon tagging facility.

The proposed technique for obtaining tagged, linearly polarized, real photons is different from the coherent bremsstrahlung presently used in Hall-B and planned for the GlueX [7] experiment in Hall-D. We are planning to use virtual photons produced when electrons are scattered at very forward angles (*i.e.*, scattering angles between  $2.5^\circ - 4.5^\circ$ ). In this kinematics the four-momentum transfer,  $Q^2$ , associated to the virtual photon is less than  $10^{-1} \text{ GeV}^2$  and consequently the virtual photon can be considered as quasi-real. The equivalent photon flux ( $10^7 - 10^8 \gamma/\text{s}$ ), for a nominal luminosity of  $10^{35} \text{ cm}^{-2} \text{ s}^{-1}$ , and the degree of linear polarization ( $\sim 40\%$ ) obtained with this technique is comparable to what is obtained by using the coherent Bremsstrahlung.

The low energy scattered electron (0.5 GeV - 4.0 GeV) will be detected in a Forward Tagger system (FT), made of a calorimeter, a tracking device and a veto counter, in coincidence with the detection of multi-particle final states in CLAS12.

*Electroproduction at these small values of  $Q^2$  using unpolarized electrons is equivalent to photoproduction using partially linearly polarized photons [8].*

The proposed design for the FT system is compatible with the use of the CLAS12 standard equipment with no impact on the acceptance and resolution of the CLAS12 spectrometer. The FT operations will be possible in parallel to the detection of the electron at larger angles as required in CLAS12 electroproduction experiments. In that respect, the new proposed facility can be viewed as an extension of the CLAS12 detector allowing not only the measurement of electrons scattered at small angles but also providing an excellent coverage for charged and neutral particles emitted in the forward direction (e.g. as required in the leading DVCS experiment at 11 GeV).

The physics program using the very small angle electron scattering facility will take advantage of polarized photons with relatively high photon fluxes. Since electrons are tagged after their interaction in the target, no limitations associated to the operation of a standard real photon tagger will be present.

Knowledge of the photon linear polarization, high fluxes, together with the use of the nearly  $4\pi$  coverage for hadronic final states in CLAS12 will allow the study of meson spectroscopy in a competitive and complementary experimental environment to the planned coherent bremsstrahlung photoproduction experiment in Hall-D. Furthermore, the two experimental halls, hosting very different spectrometers (a toroidal-based versus a solenoidal-based detector) with different particle identification capability, angular coverage and resolution, will provide the way to perform independent checks of any possible findings. In the field of hadron spectroscopy, this unique capability will give additional strength to the whole Laboratory.

## 2 Physics motivation

It has been more than thirty years since QCD was postulated as the theory of strong interactions. While much progress has been made in understanding the high energy phenomena, strong-interactions in the non-perturbative regime of hadrons have remained obscured. While mesons and baryons may be viewed differently, their phenomenology reflects common aspects of the strong interaction dynamics. For example, the bulk of hadron mass *i.e.* the visible mass in the universe, is due to gluons. Searching for mesons with gluons as constituent particles that have their own identity and along with quarks form hadronic bound states will thus shed light on the mechanisms of mass generation. Significant portion of the lattice effort has been focused towards to understanding this issue [10].

For many years, speculations on the existence of hybrid mesons ( $q\bar{q}g$ ) and other resonances beyond those predicted by the quark model have been made. Up to now predictions for masses and decay widths were based on various models, *e.g.* the bag model, the flux tube model or the constituent glue model [19, 20, 21, 22]. Recently, first principle computations using lattice gauge techniques have shown signals for such states. Discrimination among the various dynamical assumptions of these models has become possible with the emerging lattice results, that give us confidence that hybrid mesons exist and should be experimentally accessible. Calculations indicate that the decay characteristics of these states are not different from those of regular meson resonance and that the masses of the lowest states are of about 2 GeV. In Fig. 1, the recent lattice results for the isovector meson resonances are shown together and compared with the computed spectrum of exotic states. The good agreement between lattice computations and experimental data for well established states proves the advanced stage of these calculations. In Fig. 2 we show a compilation of several lattice results on the mass of the lightest  $J^{PC} = 1^{-+}$  exotics as a function of the pion mass. It is evident that there is a good agreement between various lattice groups and convergence towards a physical pion mass limit is expected in the future.

To validate these lattice efforts, the predicted hadron properties must be compared with information extracted from high precision measurements. Many experiments have already addressed some of those issues, however the experimental information is still incomplete and a comprehensive experimental program is needed. We propose a dedicated CLAS12 spectroscopy program to complement and enhance the worldwide effort in hadron spectroscopy experiments, which at present, include the GlueX, BES-III and PANDA collaborations. In general, experiments in hadron spectroscopy will require: *i)* analysis of many different decay modes and production channels, *ii)* comprehensive study of partial wave amplitudes and their dependencies on all kinematic variables, *iii)* a dedicated theoretical effort to understand the analytical structure of partial waves aimed at extracting resonance properties (mass, width, decay branches, *etc.*).

In the following we discuss the current status and outlook for development of analysis tools for

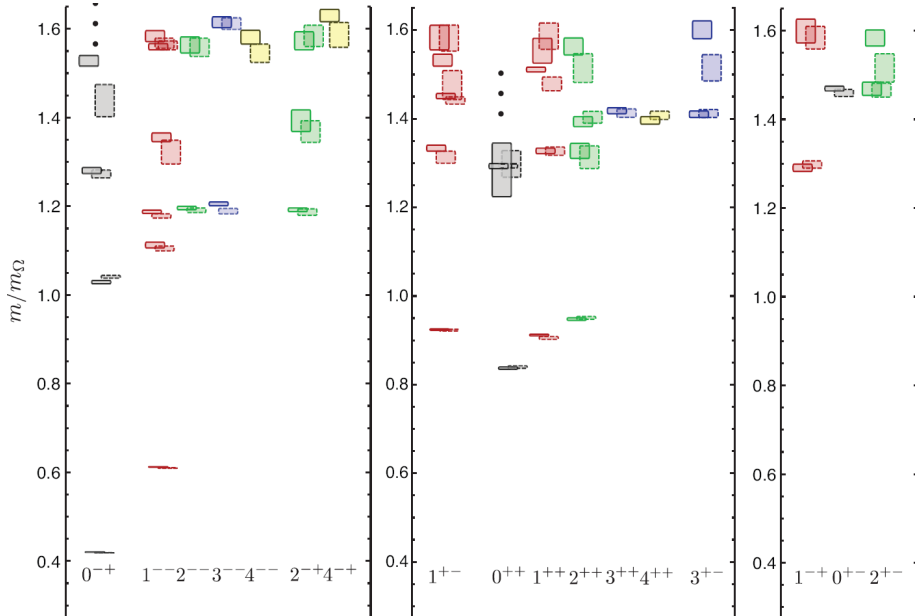


Figure 1: Lattice results from JLab lattice collaboration, Ref. [18] for the low-lying isovector mesons. Masses are given in units of the  $\Omega^-$  baryon.

the present proposal.

## 2.1 Meson spectroscopy

A complete mapping of meson resonances in the mass region of 1 to 3 GeV will be particularly important for a better understanding of QCD where existence of several new types of states beyond the naive quark model (glueballs, hybrids, multi-quark states) is predicted [25, 26]. Gluons play a central role in strong interactions and the cleanest experimental signature for the presence of gluons in the dynamical mass generation process, are exotic hybrid mesons. In a particular model, self interacting gluons form a string-like flux tube between valence quarks [21]. Normal mesons have quantum numbers compatible with a flux tube in the ground state, while in hybrid mesons gluon degrees of freedom of the excited flux tube add to the quark quantum numbers resulting in exotic combination for the total angular momentum, parity, and C-parity. The identification of states with particular  $J^{PC}$  combinations, as  $0^{--}, 0^{+-}, 1^{+-}, 2^{+-} \dots$ , is an unambiguous experimental signature for the presence of gluonic degrees of freedom in the spectrum of mesons. Determining the properties of such states will shed light on the underlying dynamics of quark confinement.

The flux tube excitation will be induced by using a photon beam. Photoproduction of exotics has many advantages compared to traditional hadro-production (pion or kaon beams): lattice and phenomenological models converge on predicting the dominance of the spin-1 component of the valence quark wave function in the ground state  $J^{PC} = 1^{-+}$  exotic meson [?]. This leads to a prediction of large cross-section, of the order of 10-100 nb, *i.e.* comparable to that of regular meson, for the exotic mesons peripheral photoproduction [?].

The identification of these states has been difficult, as high mass resonances are generally broad and overlapping, and often have similar quantum numbers (mixing). Ideally, for a complete mapping of the mesons in this mass region, we will need to study each resonance through as many decay channels and production mechanisms as possible in order to disentangle mixing effects.

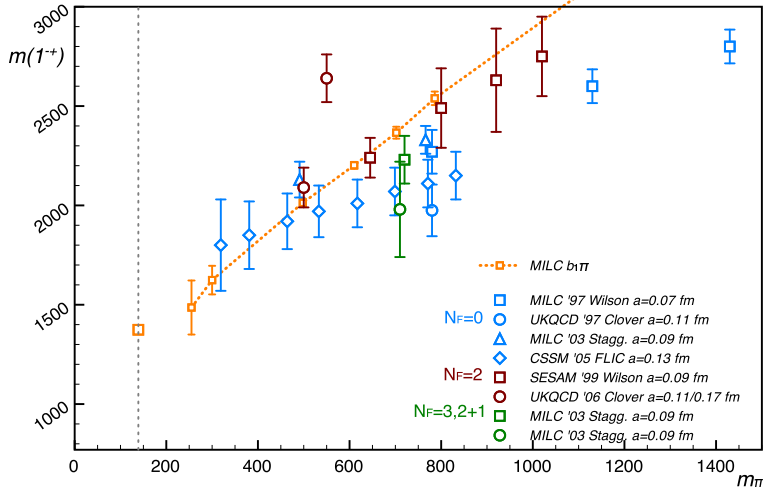


Figure 2: Summary of lattice results for the mass of the  $J^{PC} = 1^{-+}$  exotic meson

To determine meson quantum numbers, we will use partial wave analysis (PWA), that are, in a broad sense, fits to the angular distributions of final states. A complete PWA requires high event statistics, as well as high resolution and geometrical acceptance of the detector. Meson spectroscopy at CLAS12, using the forward tagger, will fulfill many of these stipulations.

Beside exotic mesons, the study of *strangeonia* constitutes a high priority in meson spectroscopy. *Strangeonia* are mesons in the containing  $s\bar{s}$  pairs: these can be conventional states in the Constituent Quark Model CQM or hybrids with or without exotic quantum numbers. The masses are expected to be in the 1-3 GeV range, i.e. a transition region between light (relativistic) and heavy (non-relativistic)  $q\bar{q}$  states. Photoproduction is expected to be an efficient technique to produce  $s\bar{s}$  mesons due to the spin-vector nature of the photon beam. This provides a natural way to favor the presence an  $s\bar{s}$  component in the produced meson system. The excellent CLAS12 particle identification ( $k/\pi$  separation up to  $p=3$  GeV) and acceptance in this mass range makes the upgraded Hall-B the ideal place to study strangeonia production.

The conventional *strangeonia* mesons are associated with the radial and orbital excited states of the  $\phi(1020)$  meson, the ground state of the  $s\bar{s}$  system. Even these 'normal' strangeonia are poorly understood: among the 22 low mass ( $M < 2.5$  GeV) strangeonium states expected, only 5 are well identified. The clarification of the predicted strangeonium spectra in this mass range is, therefore, an important and necessary step for the advancement of meson models and the understanding of meson spectroscopy beyond the CQM. As already mentioned, the study of  $s\bar{s}$  excitations provide a tool to explore the transition between light to heavy quark systems. This property has been pointed out by Barnes, Page and Black [81]: "the similarity between the  $s\bar{s}$  spectrum, the light meson  $n\bar{n}$  and the heavy  $Q\bar{Q}$  systems needs to be understood to bridge the gap between Heavy Quark Effective Theory (HQET) and the light quark world in which we live".

## 2.2 Partial Wave Analysis

The main goal of a hadron spectroscopy program is to identify and extract resonance properties from the measured intensity distribution of their decay products. Resonances correspond to poles in partial waves, *i.e.* amplitudes for production of two or more resonance decay products pro-

jected onto total angular momentum and isospin. In data analysis, theoretical cross sections are parametrized in terms of partial waves which are then fitted to the measured intensity in bins of kinematic variables. A maximum likelihood fit is applied to the intensity distribution by a set of given partial waves. The goodness of the fit is related to the statistics (number of events per binned data) and the rank of the fit as defined by the number of (complex) amplitudes. The fit can be improved by using higher statistics or (equivalently) by reducing the rank of the fit *i.e.* by implementing some of the known theoretical constraints on the amplitudes.

In lepto- and photo- production the knowledge of photon polarization simplifies the extraction of partial waves by giving information on the production mechanisms and therefore reducing the rank of the fit. Electroproduction at very small values of  $Q^2$  using unpolarized electrons *is equivalent to photoproduction using partially linearly polarized photons*. The matrix element for the electron scattering process in the one-photon exchange is:

$$|\mathcal{M}|^2 = (2e^4/Q^2)T_{\mu\nu}L^{\mu\nu} \quad (1)$$

where  $T_{\mu\nu}$  is the hadronic tensor (expressed in terms of nucleon structure functions) and  $L^{\mu\nu}$  is the virtual photon polarization density matrix. Defining  $\nu$  the energy of the virtual photon and  $\theta$  the electron scattering angle, the photon polarization is

$$\epsilon = [1 + 2\frac{(Q^2 + \nu^2)}{Q^2} \tan^2(\theta/2)]^{-1}. \quad (2)$$

The longitudinal polarization is given by  $\epsilon_L = \frac{Q^2}{\nu^2}\epsilon$ , and the polarization density matrix can be written as [8]:

$$\begin{pmatrix} \frac{1}{2}(1+\epsilon) & 0 & -[\frac{1}{2}\epsilon_L(1+\epsilon)]^{1/2} \\ 0 & \frac{1}{2}(1-\epsilon) & 0 \\ -[\frac{1}{2}\epsilon_L(1+\epsilon)]^{1/2} & 0 & \epsilon_L \end{pmatrix}$$

At very low values of  $Q^2$  the virtual photon beam becomes, for all practical purposes, almost a real photon beam, since

$$\epsilon_L = \frac{Q^2}{\nu^2}\epsilon = 10^{-3}\epsilon \approx 0.$$

Since there is no longitudinal contribution, the matrix represents the spin density matrix of real (transverse) photons. The photon polarization produced by an 11 GeV electron beam ranges between 70% (6.5 GeV photons) to 20% (10 GeV photons) and can be calculated from the electron kinematic for each event.

After extraction of partial waves it is necessary to perform their analysis, *i.e.* describe the measured dependence on kinematic variables in terms of a dynamical model. Amplitude analysis is inherently model dependent. This is because there is no first principle, QCD-based description of hadron production reactions. Amplitudes, however, satisfy certain model-independent constraints that can be used to reduce model ambiguities. These constraints originate from the general analytical properties of scattering amplitudes and specify properties of amplitudes when considered as complex functions of their kinematic variables. Amplitudes are real analytical functions except for cuts associated with physical thresholds, with discontinuities in the physical region constrained by unitarity. Thus, for example, an amplitude describing two-meson photo-production is related to that of meson-meson scattering. Unfortunately such constraints do not completely determine reaction amplitudes and various approximations have to be studied to access systematic uncertainties.

As an example of such model dependence in the PWA interpretation we may refer to the  $\pi^- p \rightarrow \pi^- \pi^- \pi^+ p$  reaction. The recent COMPASS results revealed a resonance in the exotic  $J^{PC} = 1^{-+}$  wave decaying to  $\rho\pi$  [12]. The resonance interpretation was, however, based on a particular model, the isobar model, that, when used in the analysis of the same final state measured in the experiment E852 at Brookhaven, lead to conflicting results [13]. In this case the dominant contribution to meson production comes from the pion exchange, the so called *Deck mechanism* [14], leading to an interpretation in terms of forces as opposed to in terms of an elementary excitation. It is worth noting that a fairly comprehensive analysis of  $L^P = 1^+$ ,  $3\pi$  amplitude, was carried out in the past. The broad enhancement seen in the intensity of the  $1^{++}$ ,  $3\pi$  partial wave centered around  $M_{3\pi} \sim 1.2\text{GeV}$  was originally interpreted as originating from the *Deck process* [15, 16] but a subsequent reanalysis has found the existence of a subtle interference with an additional short-range process representing the direct production of the  $a_1$  resonance [17].

Amplitude analysis is a challenging theoretical task which is currently being approached from several fronts and that will continue to progress as data from current and planned experiments are being collected. There is the EBAC effort at JLab, SAID at GW, the NABIS collaboration centered at Julich (and expanding onto the US) that focuses on Dalitz analysis of D and B meson decays, and ongoing amplitude analysis centers at BES III and GSI. These groups are actively sharing their experiences and resources through regular workshops and ongoing collaborations that include members of this collaboration.

*An estimate of the systematic uncertainty related to the partial wave analysis is thus clearly needed. In this area we are capitalizing on the synergy between theoretical and experimental contributions to this collaboration.*

At Jefferson Lab, the study of the meson spectrum already started by using data collected with the CLAS detector and now progresses in developing the analysis tools necessary to identify exotic mesons by testing them on both well and poorly known meson states, such as the  $\rho$  and the  $f_0(980)$  respectively [29]. Figure 3 shows the results of a partial wave analysis of the  $\gamma p \rightarrow p\pi^+\pi^-$  channel. In the upper panel the prominent peak of the  $\rho$ -meson dominates the  $\pi - \pi$   $P$ -wave differential cross section. In the lower panel, the  $S$ -wave shows a clear variation in the vicinity of the  $f_0(980)$ . It has to be noted that this is the first time that the  $f_0(980)$  meson has been measured in a photo-production experiment. The evidence of the  $f_0(980)$  signal in the  $S$ -wave is a sign that photo-production may indeed be a good tool for accessing meson resonances other than vector meson states.

Another example is shown in Fig. 4. The reaction  $\gamma p \rightarrow n\pi^+\pi^+\pi^-$  was studied with CLAS6 to search for the  $\pi_1(1600)$  [?]. The results show clear signals for the  $a_1(1270)$ ,  $a_2(1320)$  and  $\pi_2(1670)$ , but show no signal for the  $\pi_1(1600)$  decaying to three pions. The limited statistics of this experiment with the unfavorable kinematic accessible with the current beam energy prevents to draw definitive conclusions.

The extensive study of these and other reactions will be possible with the CLAS12 detector and the FT facility here proposed. CLAS12 will be able to measure multi-charged and multi-photon particle final states with good acceptances for up to four or five final state particles. PWA of more than four or five final particles becomes difficult and increasingly unreliable, limiting the possible number of decay channels to be analyzed. We plan to obtain the high statistics that will be needed to access channels with four observed particles in the final state by running high beam currents. As an example, current CLAS6 experiments using Bremsstrahlung photon beams at DAQ rates of 2 KHz were able to achieve in about one or two months (*real time*) of running, statistics in three particles final states that are comparable to the whole data yield accumulated in  $\pi$  beam experiments in years.

Description of some the reactions that will be studied in the present experiment and the related

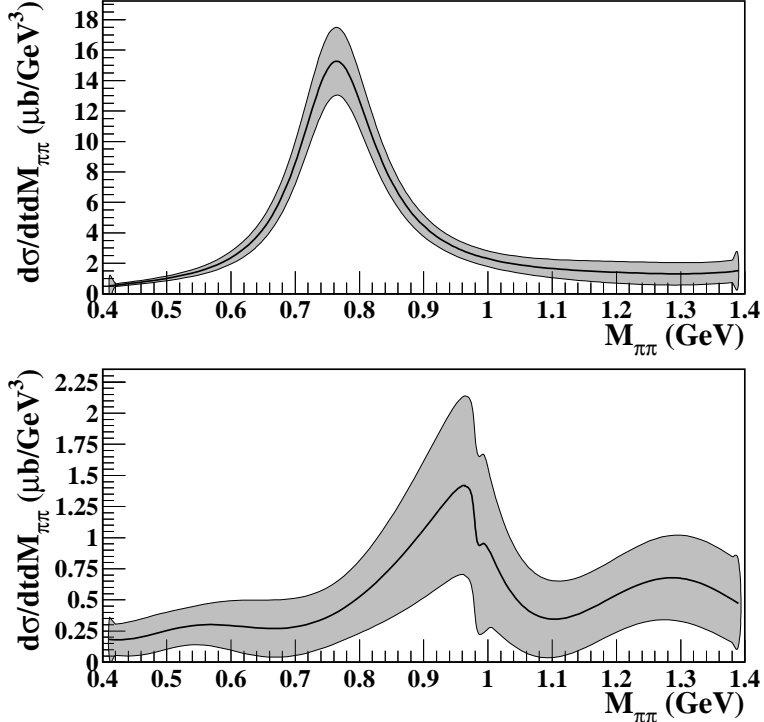


Figure 3: Partial wave cross sections  $d\sigma/dtdM_{\pi\pi}$  for the reaction  $\gamma p \rightarrow p\pi^+\pi^-$  in the photon energy bin  $3.2 < E_\gamma < 3.4$  GeV and momentum transfer  $0.5 < -t < 0.6$   $\text{GeV}^2$ . The top and bottom panels show the  $P$ - and the  $S$ -wave, respectively.

kinematics, CLAS12 acceptance and resolution are presented in the Section 4.1.

### 3 Experimental setup

In this section we briefly outline the CLAS12 configuration and the proposed technique to obtain a (*quasi-*)real ( $Q^2 \sim 0$ ) photon beam in the Hall-B. It is worth to stress that CLAS12 will be used to detect hadrons while the scattered electron will be detected in the Forward Tagger. The experiment will be run with the 11 GeV electron beam on a 5 cm long liquid hydrogen target. This is the standard target foreseen for electroproduction experiments on proton.

#### 3.1 Hadron detection: CLAS12 configuration

The goal of this experiment is to study meson spectroscopy looking for mesons with masses up to 2.5 GeV. The identification of such states requires knowledge about their production mechanisms, identification of their quantum numbers,  $J^{PC}$ , and their decay modes. This imposes stringent requirements on hadron detection. To identify and measure the decay products of produced mesons, the detector has to have:

- good efficiency for multi-particle final states since high mass mesons decay in many particles,

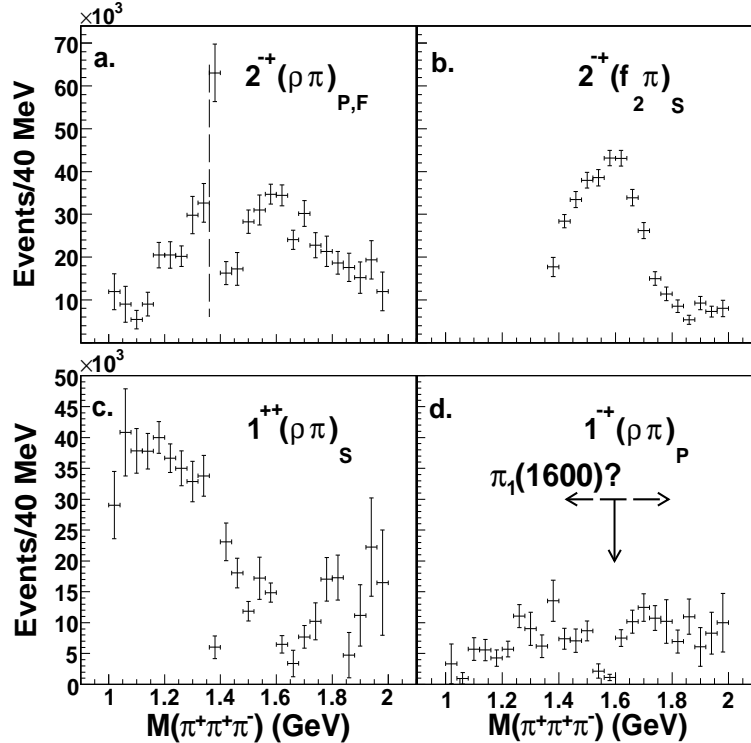


Figure 4: CLAS PWA results on photoproduced three pions.

- good efficiency for both neutral and charged particles,
- good particle identification and in particular good kaon/pion discrimination (up to  $p \sim 3$  GeV/c) to study strangeness-reach mesons,
- large kinematic coverage to study the production mechanisms,
- good particle momentum and angle resolution to use the missing mass technique to reduce the number particles that need to be detected to isolate exclusive final states.

*The standard configuration of CLAS12 detector fulfills all of these requirements.* Charged particle identification will be accomplished using standard tracking in the torus and solenoid magnetic fields and time-of-flight systems in both forward and central detectors. Pions and protons will be identified using time-of-flight (SC/CTOF) and path length plus measured momentum (DC/central tracker). Photons and neutrons will be detected in both the new forward tagger and standard calorimeters (PCAL, EC and CND).

The effect of the torus field setting has been studied for some benchmark reactions (see Sec. 4.1) showing that to increase the acceptance of multi particle final states, a half-strength-field is desirable. With this set-up, the CLAS12 resolution is good enough to apply the missing mass technique to reduce the necessary number of particles detected. Full-field running is also possible with a reduction of the acceptance in the range of the 20-30%.

*We concluded that the CLAS12 torus field setting is not critical for the meson spectroscopy program.*

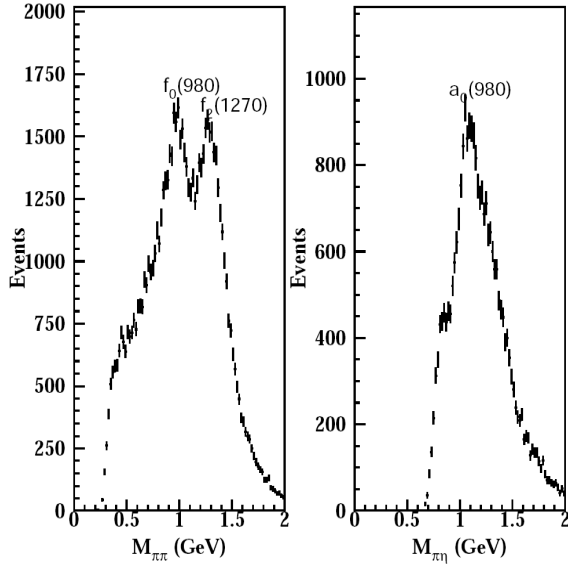


Figure 5: Invariant mass distribution for  $\pi^0\pi^0$  (left) and  $\pi^0\eta$  (right) for the reactions  $ep \rightarrow p\pi^0\pi^0(e)$  and  $ep \rightarrow p\pi^0\eta(e)$ , respectively. In both cases, the protons and 4 photons from the meson decays were detected while the final state electron was unmeasured, being emitted at  $0^\circ$ .

### 3.2 Electroproduction at very small $Q^2$

The current photoproduction setup of CLAS, producing real Bremsstrahlung photons tagged by a magnetic spectrometer, can not be operated at 11 GeV energies because of the limitation of the existing magnet. *Instead, we are planning to use quasi-real photons produced when electrons are scattered at very forward angles (i.e., scattering angles of few degrees).* Electron detection at very small angles, ( $Q^2$  values of about  $10^{-1}$  GeV $^2$  or lower) with the coincidence detection of the hadronic final states in CLAS12, is a very attractive alternative to photoproduction experiments [8]. We plan to use a small angle forward electron tagger extending the CLAS12 acceptance for electrons in the range  $2.5^\circ - 4.5^\circ$ , not covered by the standard equipment.

This technique was used in the past to produce high energy ( $\sim 100$  GeV) photon beams at CERN ( $\Omega$  Collaboration and COMPASS) and DESY (ZEUS and H1 experiments). First tests were performed with CLAS6, by looking for hadronic events where the electron was undetected. Final states where the hadron four-momenta were compatible with an electron scattered at  $\sim 0^\circ$  were selected. The reconstructed mass spectra of  $\pi^0\pi^0$  and  $\pi^0\eta$  show clear evidence of rare mesons expected in these channels ( $f_0(980)$ ,  $f_2(1270)$ ,  $a_0(980)$ ) demonstrating that this technique works quite well (see Fig. 5). Recently, the  $eg6$  run used this technique to study coherent meson production on  ${}^4He$  [32].

To fully exploit the potential of quasi-real photoproduction it is necessary to measure the scattered electron three momentum. The relevant quantities to be determined are:

- the energy  $E_{e'}$ : since the photon energy is given by  $E_\gamma = \nu = E_{Beam} - E_{e'}$  and its linear polarization by  $P_\gamma = \epsilon = [1 + \frac{\nu^2}{2E_{Beam}E_{e'}}]^{-1}$
- the azimuthal angle  $\phi_{e'}$  to determine the polarization plane
- the polar angle  $\theta_{e'}$ : since  $Q^2 = 4E_{Beam}E_{e'} \sin^2 \theta / 2$

$E_{scattered}$	0.5 - 4.5 GeV
$\theta$	$2.5^\circ$ - $4.5^\circ$
$\phi$	$0^\circ$ - $360^\circ$
$\nu$	6.5 - 10.5 GeV
$Q^2$	0.01 - 0.3 GeV $^2$ ( $\langle Q^2 \rangle > 0.1$ GeV $^2$ )
W	3.6 - 4.5 GeV

Table 1: Kinematic range covered by the forward tagger.

The degree of linear polarization (up to 70%) and the quasi-real photon flux (up to  $0.5 \cdot 10^8 \gamma/\text{s}$ ) achievable with the CLAS12 nominal luminosity of  $10^{35} \text{ cm}^{-2} \text{ s}^{-1}$ , are similar to what expected by using the coherent Bremsstrahlung technique planned by the GLUEX experiment in Hall-D.

Virtual ('quasi-real') photoproduction presents several advantages. The photon polarization can be defined on an event-by-event basis measuring the electron scattering plane. Since electrons are tagged after their target interactions, this technique allows the use of high electron currents, permitting to achieve high luminosity on thin (gas) targets not operable with photon Bremsstrahlung beams. Only electrons corresponding to photons that have produced hadronic interactions are registered by the tagger, thus allowing a higher beam flux for a comparable accidental rates.

### 3.3 Kinematics, rates and backgrounds

The kinematic range covered by the forward tagger facility is shown in Tab. 1 for an incoming electron beam of 11 GeV.

The total electron scattering cross section contains contributions from one-photon exchange (Born process), from QED vacuum polarization loops, and from the emission of additional real photons (radiative corrections). The importance of the internal radiative corrections in relation to the Born process depends on the kinematics. Radiative corrections increase with decreasing  $Q^2$  and increasing  $\nu = E_{Beam} - E_{e'} = E_\gamma$ . We have used the program RADGEN 1.0 [55] to calculate the contributions of internal radiative corrections to the total inclusive cross section. Including such effects, the total inclusive electron rate within the geometrical and momentum acceptance of the forward tagger will be of about 130 kHz ( $\Delta E_{e'} = 0.3\text{-}10.8$  GeV and  $\Delta \theta_{e'} = 2.5^\circ\text{-}4.5^\circ$ ). Inelastic processes represent about 45% of the total cross section in our kinematic range. The remaining 55% is due to elastic events where at most one proton will go in the active area of CLAS12. It is, therefore, essential for our measurements to require a tight time coincidence between the forward tagger and the detection of multi-particle final states in the CLAS detector.

The total rate of inelastic events in the forward tagger acceptance with  $E_\gamma = \nu = 6.5\text{-}10.5$  GeV, is expected to be about 6.5 kHz (while the radiated rate in the same energy range is about 40 kHz). The energy and the angular distributions of inelastic events are reported in Fig. 6. Figure 7 shows the  $Q^2$  and the linear polarization for the same events.

Electromagnetic backgrounds in the FT include Bremsstrahlung and Møller processes. Bremsstrahlung photon production peaks at very forward angles (about  $\delta\theta \approx m_e/E$ ), therefore their contribution at angles  $\theta > 0.5^\circ$  is very small. The Møller electrons are the dominant contribution to the expected FT rate. The Møller cross section is almost flat within the FT acceptance with a sizeable value of about  $d\sigma/d\theta \sim 10\text{-}20$  mb/rad. However the Møller kinematic is highly constrained and, for angles above  $2.5^\circ$ , the Møller electron energy is less than 0.5 GeV, i.e. outside the kinematic range of interest. These low energy electrons are bent in the 5T solenoidal field of CLAS12 and focused

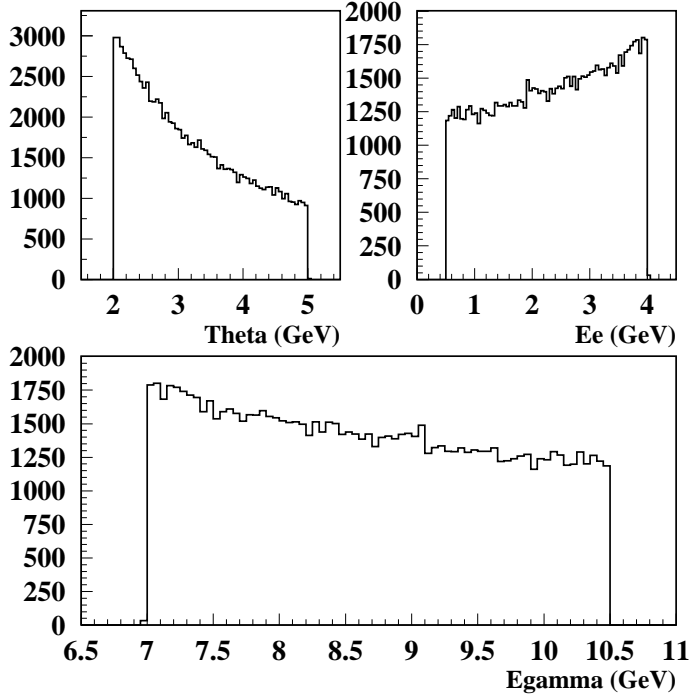


Figure 6: Angular and energy distribution of inelastic events within the geometrical and momentum acceptance of the forward tagger. **TO BE UPDATED**

towards the beam line. Here they enter into a tungsten cone that shields CLAS12 and the FT from this background and from other secondaries produced along the beam line (low energy photons, X-rays, beam halo ...). These backgrounds have been studied using a GEANT4 simulation of CLAS12 (GEMC). All details are reported in Sec. 3.5. The total expected electromagnetic rate is about 50 MHz, dominated by low energy ( $< 100$  MeV) secondaries that will be further suppressed with an optimization of the shield. Suppression at the level of the on-line trigger is discussed in Sec. 3.6. Anyway, this contribution can be almost totally rejected in the off-line analysis when a time coincidence of few nanosecond with the rest of CLAS12 is required, since no hadrons associated to such events will reach the CLAS12 detector.

### 3.4 Electron detection: the Forward Tagger

The angular range of interest ( $2.5^\circ < \theta_{e'} < 4.5^\circ$ ) is outside the acceptance of CLAS12. Therefore a new detector component has to be added. The forward tagger will be made of: **a calorimeter**, to reconstruct the scattered electron energy ( $E_{e'}$ ), **a tracker**, that will measure the scattering angles ( $\theta_{e'}$  and  $\phi_{e'}$ ) with good accuracy and **a veto counter** to have a fast discrimination against neutrals. The calorimeter, the veto counter and one tracker layer will be placed between the high threshold Cerenkov Counter (HTCC) and the torus support, at about 2m downstream of the target (nominal) position. The location very close to the beam line ( $2.5^\circ$  corresponds to  $\sim 8$  cm distance) and the available clearance (at most  $\sim 40$  cm along the beam axes), requires a compact calorimeter with a small radiation length and a very good radiation hardness. Figure 8 shows a cut of the

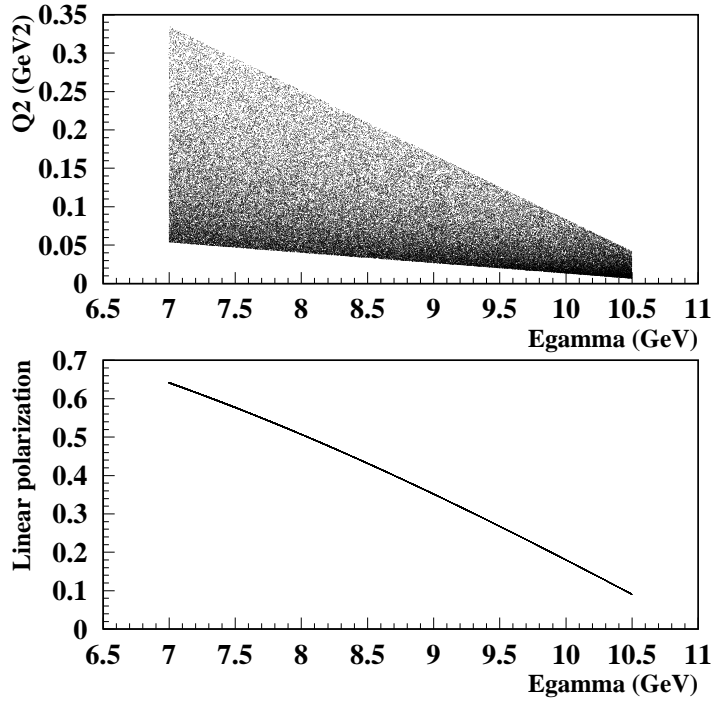


Figure 7:  $Q^2$  and the linear polarization of inelastic events within the geometrical and momentum acceptance of the forward tagger.**TO BE UPDATED**

CLAS12 area (from the target to the torus support) where the forward tagger would be installed. The existing CLAS Inner Calorimeter (CLAS-IC) is shown in the same position that will be taken by the FT. The veto counter, placed in front of the calorimeter, will be made by plastic scintillator tiles read by silicon photomultipliers by mean of light fibers. A second tracking layer will be placed in front of the target extending the CLAS12 forward tracker down to 2.5 degrees. Charged particles with non-zero transverse momentum component are rotated by the 5T solenoidal field. The three-momentum can then be reconstructed measuring the rotation in  $\phi$  between the first tracker layer placed  $\sim 25$  cm downstream, and the second layer placed about 180 cm downstream. With a spacial resolution of  $\pm 200\mu\text{m}$  a  $\sim 1.7\%$  and  $2.8^\circ$  resolution on  $\theta$  and  $\phi$  electron angles respectively, are expected.

The electron energy resolution is not a crucial issue since the relative error on the photon energy determination takes advantage of the large value of  $E_\gamma$  at the denominator reducing by almost an order of magnitude the experimental energy resolution:

$$\frac{\Delta E_\gamma}{E_\gamma} = \frac{\Delta E'_e}{E_{\text{Beam}} - E'_e} \quad (3)$$

An electron energy resolution of few percent (at 1 GeV) would result in an energy resolution of  $\sim 0.1\%$  for the corresponding 10 GeV photon and would be functional to the use the missing mass technique for the most part of the reactions studied (see Sec. 4.1 for details).

The forward tagger has to be fast ( $\sim 10$  ns) providing the scattered electron interaction time with good accuracy ( $< 1$  ns). As previously mentioned, a good timing is necessary to reject the background in the off-line analysis.

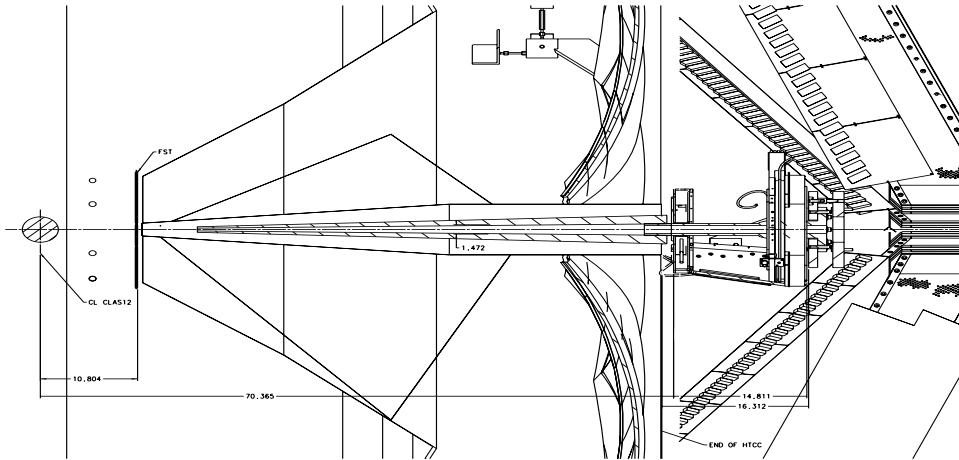


Figure 8: The forward tagger position in CLAS12. The new device will replace the Inner Calorimeter located between the HTCC and the torus support.

A last issue that worth to mention concerns the light read-out: the photodetector are placed in a sizable magnetic field and have to be small in size to fit the available clearance. The standard photomultiplier readout seems to be excluded while photodetectors based on semiconductors, e.g. Avalanche Photo Diode (APD) or Silicon Photo Multipliers (SiPM) should guarantee the requested performance.

### 3.4.1 The electromagnetic calorimeter

The electromagnetic calorimeter has to fulfill demanding requirements in terms of:

- high radiation hardness,
- high light yield,
- small radiation length and Moliere radius,
- good energy and timing resolution.

Due to the expected high rate from electromagnetic background, the calorimeter should be segmented transversely as much as possible in order to maintain each channel at a sustainable readout-rate. The (minimum) size of each pixel should be comparable with the characteristic electromagnetic shower transverse size in order to contain the shower associated to each incident electron. The calorimeter Moliere radius has to be as small as possible to reduce pile-up. To obtain the best performances we focused on a calorimeter based on homogeneous crystals. In fact if the shower is longitudinally and transversely contained, the photoelectron fluctuations is the only sizable contribution to  $\sigma(E)/E$  and  $\sigma(T)/T$ . In the last years materials as PbWO<sub>4</sub> have been extensively studied showing to be very resistant to the radiation damage and are now used in large scale detectors involving hundred thousands of crystals, such as CMS-ECal [56], ALICE-PHOS [57]),PANDA-EMC [58] and CLAS-IC [59]. Against a very fast scintillation decay time (6.5 ns), a very small

radiation length (0.9 cm) and one of the smaller Moliere radius (2.1 cm), the main disadvantage of the PbWO<sub>4</sub> is the poor light yield (only 0.3% of NaI(Tl)). A  $\sim 5\%$  at 1 GeV energy resolution has already been achieved by the existing CLAS-IC with an APD-based readout. According to the PANDA-EMC study, the new crystal manufacturing procedures (PbWO-II from BTCP) and the reduction of the working temperature to -25° should ensure a better performance with a gain of a factor of 8 in light [58]. With this design an energy resolution of  $(2\%/\sqrt{E(\text{GeV})} \oplus 1\%)$  is expected.

*The PbWO<sub>4</sub> option is the leading option for the forward tagger calorimeter.*

Other crystals as LSO/LYSO (or the very recent LaBr) shares almost all the good specifications of the PbWO with a light yield > 100 times bigger. A shortage of extensive studies of radiation hardness and a limited experience in the manufacturing procedures prevent them to be considered as the main option. Nevertheless we are planning to test in parallel some samples of these new crystals and of different light sensors to establish the ultimate performance in terms of time and energy resolution and make the optimal choice.

### 3.4.2 The tracker

The goal of the tracker is to provide the reconstruction of charged particles (essentially electrons) with polar angles between 2.5° and 4.5°. A Forward Vertex Tracker (FVT) is already planned to be part of the standard CLAS12 equipment to improve the vertex resolution of charged particles at larger angles (5°-35°). In the current design, the FVT will be located 30 cm downstream the target, and will consist of 3 double disks of gaseous, Micromegas detectors. Simulations have shown that, even in the presence of a 10 MHz background, an efficient matching with tracks reconstructed in the Drift Chambers can be performed. Using a pitch of 500 microns results in about 6,000 electronic channels.

Studies on a possible extension of the FVT to smaller angles are in progress. As shown in Fig. 9, the background rate rapidly increases below 4°, up to several hundreds of kHz/mm<sup>2</sup>. Assuming a 100 ns gate for the Micromegas, 1 mm<sup>2</sup> pixels would lead to a few percent occupancy. In order to cover the proposed angular range, a doubling of the number of electronic channels is needed (6,000 to 13,000). Additional studies have to be performed on the tracking efficiency with this level of background, but the required 200 microns spatial resolution can be easily achieved with rectangular pixels. In order to reconstruct the electron trajectory, a second layer of Micromegas will be installed in front of the calorimeter. As for the Drift Chambers, the tracks reconstructed in both part of the tracker will be matched, allowing to determine the trajectory parameters in the presence of the solenoid field.

### 3.4.3 The veto counter

The primary aim of the veto system for the forward tagger is to discriminate between uncharged and charged events incident on the calorimeter. Further, the detection of a coincident hit between the veto element and the associated calorimeter element confirms the trajectory of a charged particle reconstructed in the tracking system (previous Section) into the calorimeter. The current veto design will comprise an array of plastic scintillators covering individual or groupings of calorimeter elements. It should be possible to use larger veto tiles covering multiple calorimeter elements at larger radii to reduce the level of instrumentation and readout required.

The high segmentation and restrictive geometry of the forward tagger precludes the use of light readout from the scintillator elements using standard lightguides. Light readout with wavelength shifting (WLS) scintillating fibres embedded into the scintillator tile appears the most viable option and offers flexibility in routing away from the device. For effective operation the timing resolution

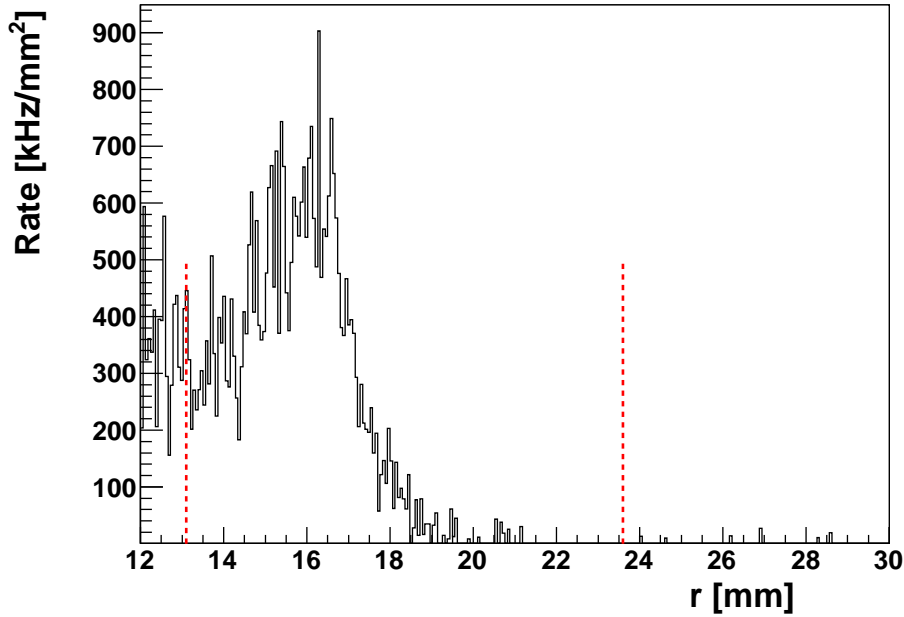


Figure 9: Background rate in the inner part of the extended FVT. The two red lines indicate the proposed angular coverage ( $2.5^\circ$ - $4.5^\circ$ ).

of the veto should be sufficient to select veto-calorimeter coincident hits with a sufficiently low rate of accidentals. The timing resolution of the forward tagger calorimeter elements is expected to be  $\sim 1$  ns so the veto timing should be comparable with this so as not to compromise the achievable coincidence time resolution. Previous systems [78, 79, 80] have employed successful scintillator tile arrays achieving timing resolutions at the level of ns, using combination of WLS fiber coupled to optical fiber.

Measuring the energy deposits in the veto elements with good energy resolution is not critical for our purpose. The vast majority of incident charged particles on the forward tagger will be highly relativistic resulting in a fixed minimum ionizing energy deposit regardless of particle type. The main requirements on the light collection are that sufficient photoelectrons are incident on the photon detection device considering the achievable light coupling in the scintillator and propagation in the fibres. Previous systems using WLS and optical fiber readout have sufficient photoelectrons per minimum ionizing interaction to achieve efficiencies for charged particle detection above 99.7% [79]. Readout sensors compatible with the high magnetic field present in the FT region are silicon photomultipliers (SiPM) that have already been used in this kind of detectors. The scintillator hodoscope developed for the CLAS-IC produced 15 photoelectrons per minimum ionizing event from 1cm thick scintillator tiles with WLS fibers and  $3 \times 3\text{-mm}^2$  SiPM readout [80].

### 3.5 GEMC Simulations

First simulations of the forward tagger facility to understand kinematics, backgrounds and the detector response have been done with GEMC, the GEANT4-based Monte Carlo code for CLAS12 [35]. The forward tagger geometry was implemented in GEMC, assuming the FT calorimeter will be made of PbWO<sub>4</sub> crystals. The calorimeter, consisting of 408 crystals, was placed at a distance of 186 cm from the CLAS12 center. The crystals are parallelepipeds with a section of  $15 \times 15 \text{ mm}^2$  and a length of 200 mm, corresponding to about 23 radiation lengths. The crystals are arranged around the beamline to cover angles from 2. to 5.0 degrees as shown in Fig.10, in order to contain the electromagnetic shower produced by electrons in the angular range from 2.5 to 2.5 degrees. The crystals are placed inside a tungsten case to shield the forward part of CLAS12 from radiation that may exit from the calorimeter because of shower leakages. The veto and second tracking place are located in front of the calorimeter. The FT is shielded from Møller electrons produced by the interaction of the beam in the target by a tungsten cone covering polar angles up to 2.45 degrees. The location and shape of the shield were chosen in order to minimize the radiation on the FT and on CLAS12, compatibly with the most recent design of the CLAS12 beamline. The design of the shield will be finalized with further simulation studies. For these simulation a 5 cm-long liquid-hydrogen target was used.

The purpose of the simulations was to evaluate:

- the acceptance and resolution for the electron detection;
- the background rates on the calorimeter and the related impact of the electron reconstruction;
- the radiation dose on the calorimeter;
- the CLAS12 drift chamber occupancy to verify the compatibility of the FT with the CLAS12 operation at full luminosity.

The results of these studies are described in the next subsections.

#### 3.5.1 FT acceptance and resolution

The GEMC simulations were first used to understand the electron kinematics and the forward tagger acceptance. For this purpose electrons with momentum from 0.05 to 5 GeV and polar angle from 1 to 35 degrees were generated uniformly at the target location.

The trajectory of the electrons is affected by the 5-Tesla solenoidal field, which induces a rotation of the particle around the beamline because of its non-zero transverse momentum component. This results in a significant shift of the azimuthal angle  $\phi$  of the track, while the polar angle  $\theta$  remains almost unchanged, except for very low momenta. This feature does not affect significantly the overall acceptance of the FT in the kinematics of interest, while it provides a mean to reconstruct the particle trajectory using the two tracking planes described in Sec. 3.4.2. The top panels of Fig. 11 show the difference between the azimuthal angle (top-left) and polar angle (top-right) of the electron tracks at the two tracking planes as a function of the momentum. The size of the  $\phi$  rotation directly depends on the momentum and only marginally on the polar angle. By measuring this rotation it is therefore possible to infer the electron momentum and have a full reconstruction of the vertex angles. Assuming a spatial resolution of the tracker of 200  $\mu\text{m}$  and the presence of air between the two tracking planes, the angular resolution estimated from these simulation is of  $\sim 2.8$  degrees in  $\phi$  and about 1.6% in  $\theta$ .

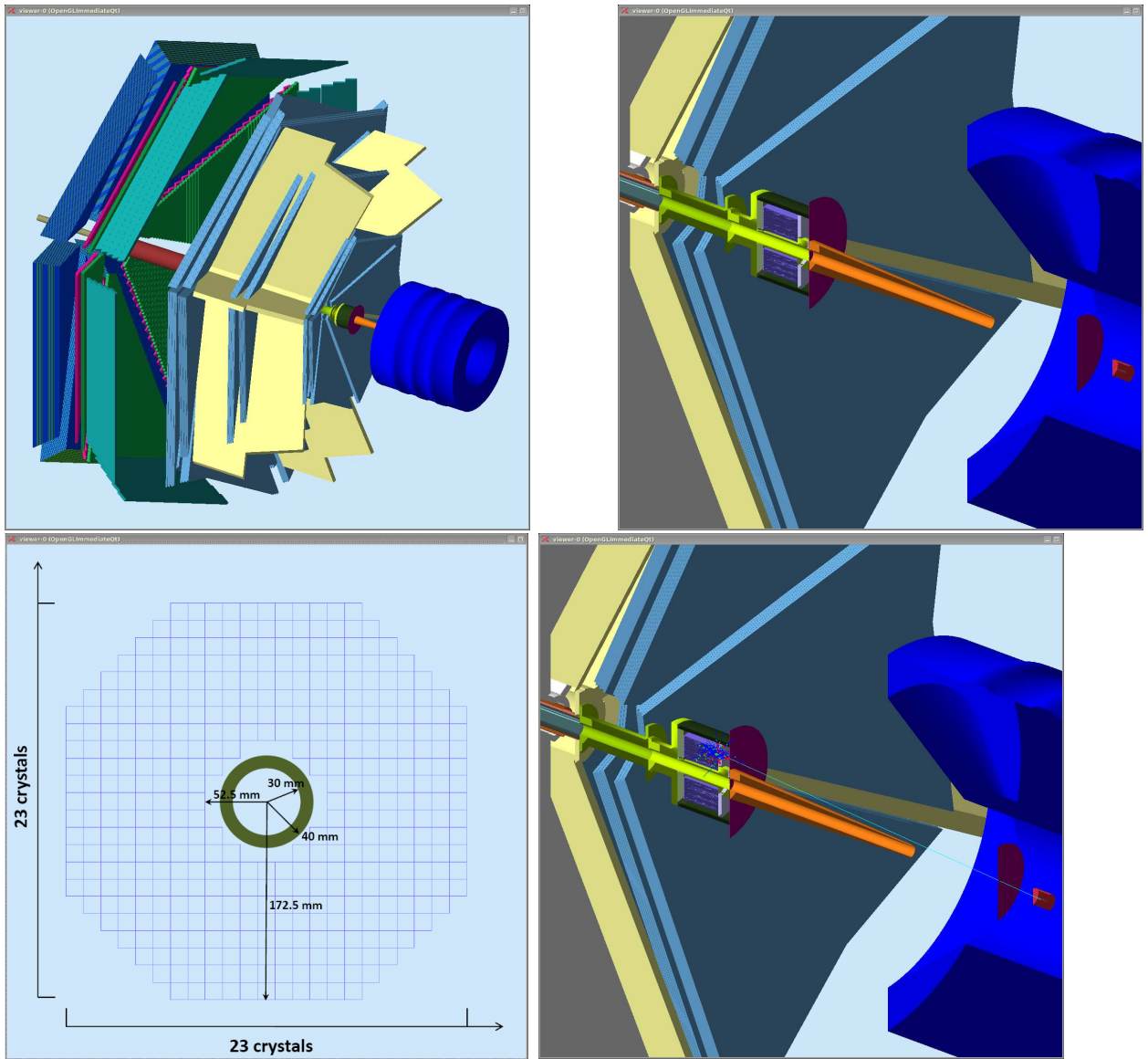


Figure 10: Schematic of the FT facility as implemented in GEMC. The lead tungsten calorimeter, shown in green in the top-left panel, is located at 180 cm from the target (red) and the center of the CLAS12 detector. The magenta disks show the location of the second tracking plane and veto counter. A tungsten cone, shown in orange, shields the detector from Møller electrons generated at the target by the interaction of the beam. The top-right panel shows a section of the FT facility with the  $\text{PbWO}_4$  crystals shown in purple. The crystals are arranged around the beamline as shown in the bottom-left panel to provide coverage for electrons between 2.5 and 4.5 degrees. The bottom-right panel shows how a 2 GeV, 3.5 deg. electron interacts in the calorimeter.

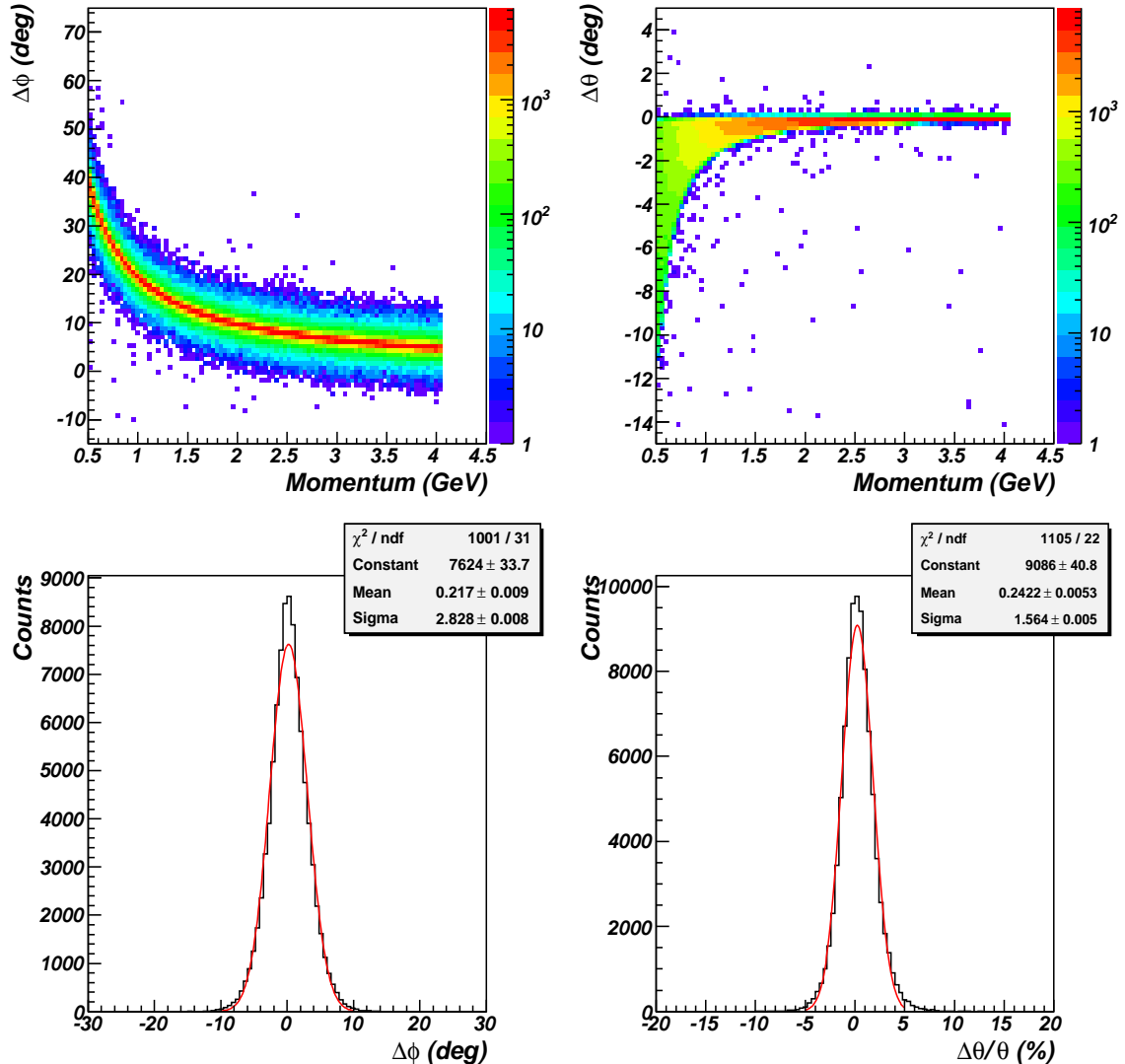


Figure 11: GEMC simulation results. Top: difference between the azimuthal and polar angles measured at two tracking planes as a function of the particle momentum . Bottom: resolution on the reconstruction of the particle vertex angles estimated from the simulation assuming 200  $\mu\text{m}$  spatial resolution of the tarckaer and the presence of air in between the tracking planes.

Electrons entering in the FT calorimeter induce an electromagnetic shower that involves a certain number of crystals that represent a “cluster”. The distribution of number of crystals with deposited energy greater than 10 MeV is shown in the top-left panel of Fig. 12. The energy deposited in the single crystals is distributed between zero and several hundreds MeV, as shown by the top-right panel of the same figure. By summing up the energy “seen” by the crystals involved in a cluster, it is possible to reconstruct the electron energy: the difference between the reconstructed and generated energy as a function of the electron momentum is shown in the bottom-left panel. The overall acceptance is shown in the bottom-right panel of Fig. 12: the ratio of electrons absorbed in the FT calorimeter over the generated ones is shown as a function of the electron momentum and polar angle. The acceptance is very high and uniform throughout the region of interest for this proposal.

### 3.5.2 Electromagnetic background rates

The electromagnetic background produced by the interaction of the electron beam in the target was also simulated. For this purpose, for each primary electron generated in the kinematic of interest, about 115k, 11 GeV electrons were generated 10 cm upstream with respect to the target. The electrons were generated randomly with the 2 ns radiofrequency structure of the CEBAF beam in a 250 ns window, which corresponds to the data acquisition window that will be used for the CLAS12 Drift Chambers. This number of electrons corresponds to a luminosity of  $10^{35} \text{ cm}^{-2}\text{s}^{-1}$ . Fig. 13 shows the energy deposited in the calorimeter in MeV/ns, the energy distribution of particle entering the calorimeter and the corresponding particle rates. The energy deposition per crystals is estimated to be less than 0.04 MeV/ns. Most of this dose is due to very low energy particles as shown by the bottom-right plot. The overall particle rate is of about 50 MHz but only about 4.5 MHz are due to particles with energy above 100 MeV. This is relevant for the trigger rates evaluation described in Sec. 3.6.

The background impact on the reconstruction of “good” electrons has been studied analysing in details the time structure of these events. For the reconstruction of a “good” event, the relevant background is the one that overlaps in time with the ‘good’ signal. The time window that has to be considered is set by the scintillating crystal properties and, in particular, by the  $\text{PbWO}_4$  decay time, which is of about  $\tau = 6.5$  ns. The rates and energy deposition were therefore evaluated in a time window of  $3\tau$ , i.e. 20 ns. The results are shown in Fig. 14. The left plot show the number of hits in the calorimeter in the chosen time window while the right plot shows the energy deposition in MeV. Considering the characteristic of the expected signal for “good” electrons (a number of crystals of the order of 4 and a minimum energy deposition per crystal of 100 MeV), this background is negligible.

### 3.5.3 Radiation dose

The results of the electromagnetic background study were used to estimate the radiation dose deposited in the FT crystals. Radiation dose can be a critical issue for the operation of scintillating crystals in high background environment since radiation induces a deterioration of the light transmission properties of the material due to the creation of color center in the lattice. This defects are not permanent and can be removed with an annealing procedure, that however may be unpractical during data taking.

The energy deposition in each crystal was evaluated from the background simulation and used to calculate the dose per unit of time. The overall radiation dose at  $10^{35} \text{ cm}^{-2}\text{s}^{-1}$  was estimated to be less than 1 rad/h when averaged over the entire calorimeter with a distribution on the calorimeter

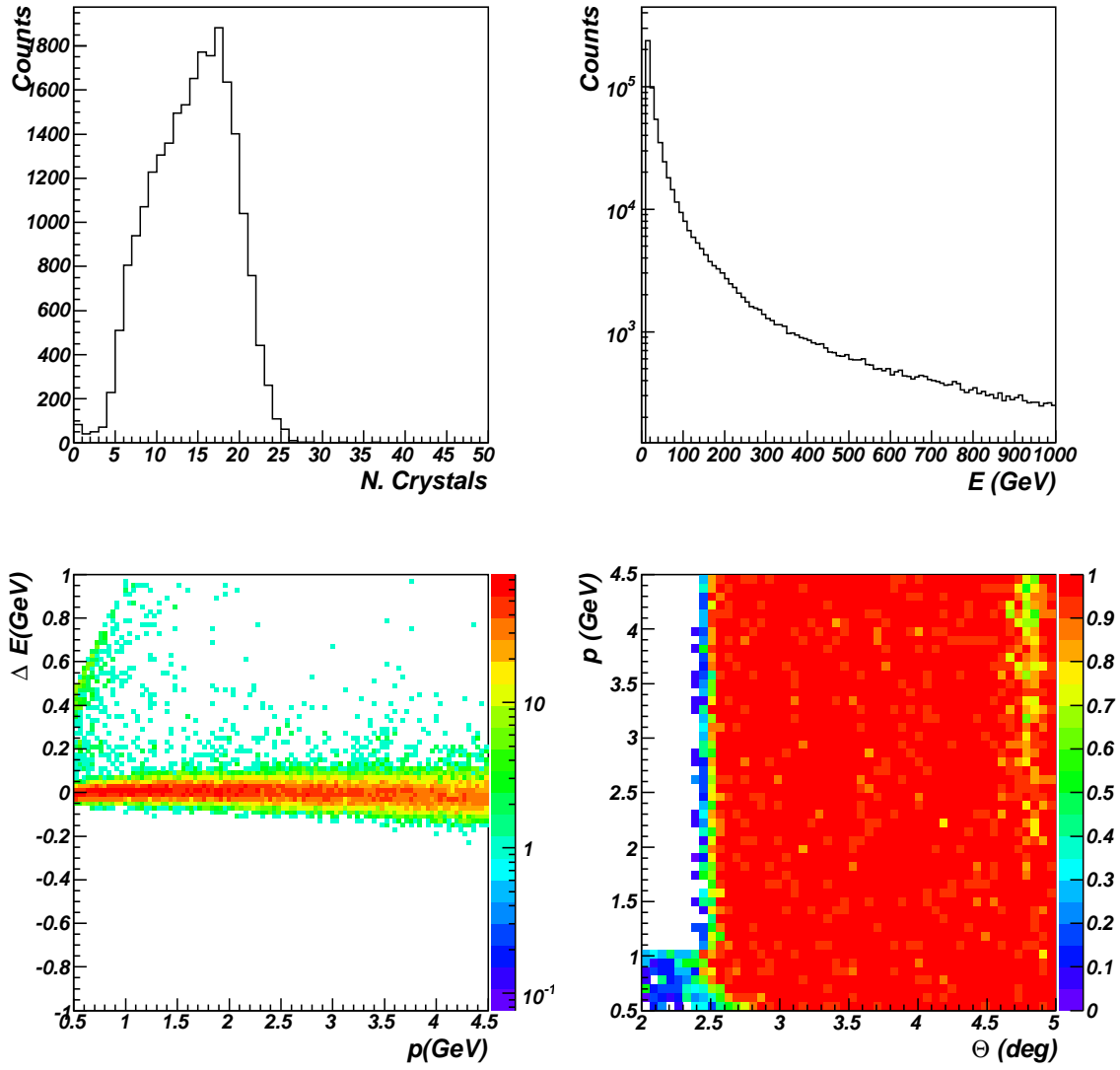


Figure 12: GEMC simulation results. Top-left: Number of crystals with deposited energy greater than 10 MeV involved in the cluster generated by an incoming electron with energy of 0.5-4.5 GeV. Top-right: energy deposited in a single crystal. Bottom-left: difference between the reconstructed and generated electron energy as a function of the electron momentum. Bottom-right: ratio between detected over generated electrons in the kinematic of interest. All plots are based on simulation of electrons generated uniformly in the momentum range 0.05-5 GeV and polar angle range 1-35 degrees.

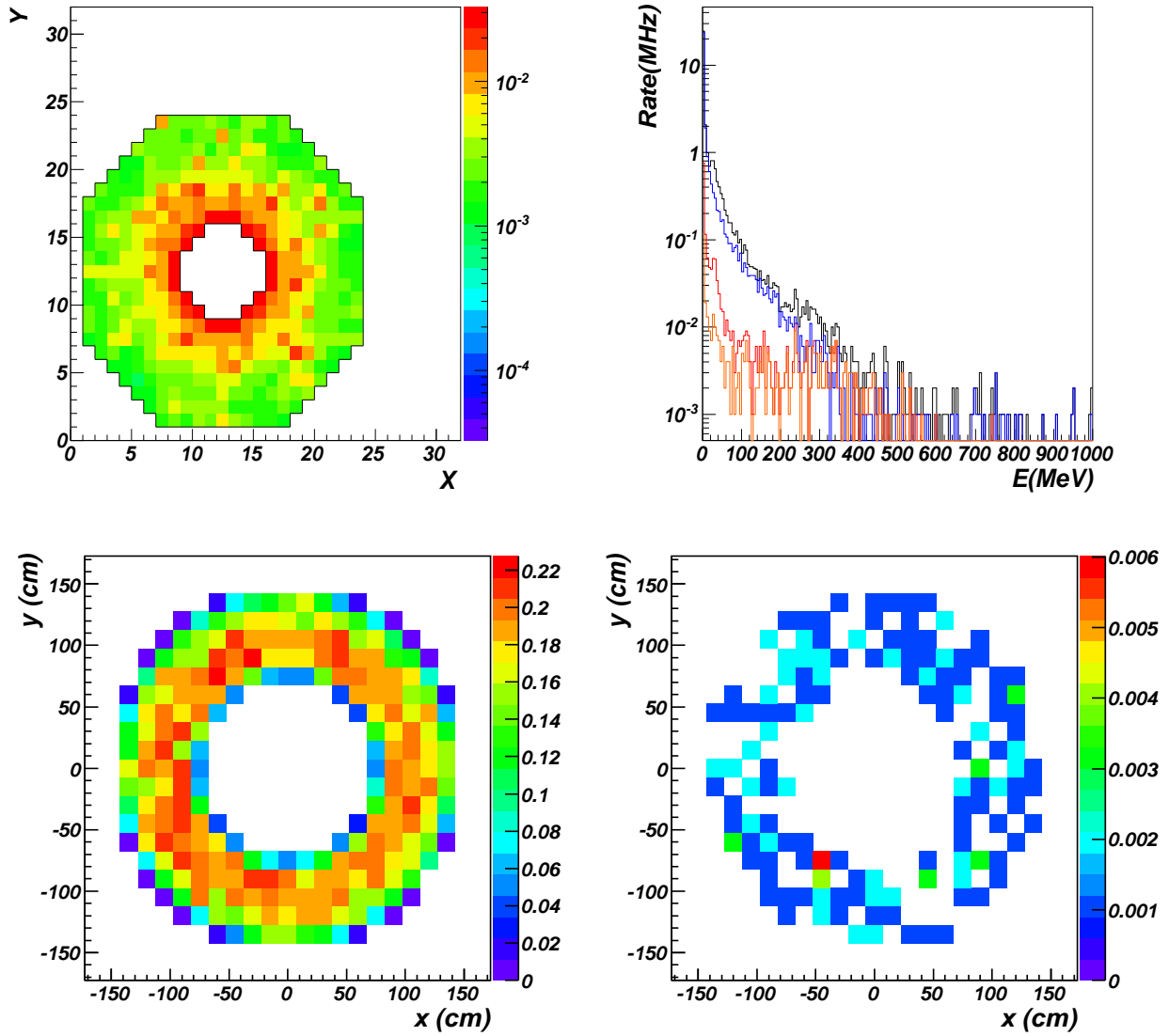


Figure 13: Simulation of the electromagnetic background with GEMC. Top-left: energy deposited in the calorimeter in MeV/ns. Top-right energy distribution of particles hitting the calorimter front face (black-total, red-electrons, blue-photons). Bottom-left: overall particle rate in MHz. Bottom-right: rate of particles with energy grater than 100 MeV in MHz.

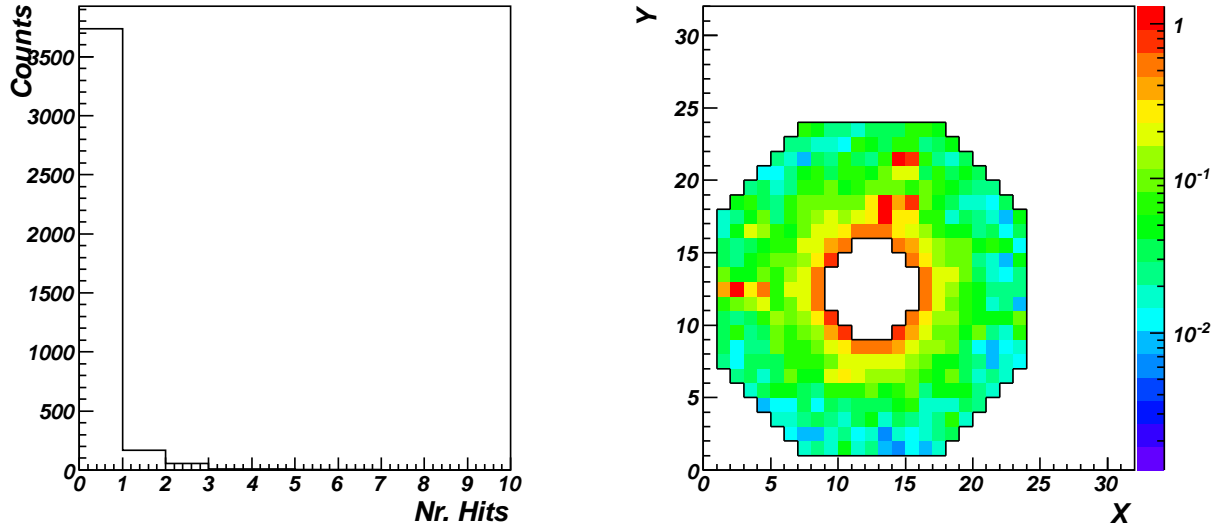


Figure 14: Left: number of crystals in the FT calorimeter with signal above threshold in a 20 ns time window due to the electromagnetic background at a luminosity of  $10^{35} \text{ cm}^{-2}\text{s}^{-1}$ . Right: distribution of the energy deposited in the calorimeter in a 20 ns window; the z-scale is in MeV.

crystals as shown by the left panel of Fig. 15. The maximum dose per crystal is of about 5 rad/h, which would result in an maximum integrated dose per crystal of about 3600 rad in 30 days of beam time. This is similar to what has been estimated for the existing CLAS-IC [59], where no significant worsening of the detector performance were observed.

### 3.5.4 CLAS12 Drift Chamber occupancies

One of the limiting factors for the operation of CLAS12 at high luminosity is the Drift Chambers (DC) occupancy. In the CLAS12 configuration without the Forward Tagger, the DC occupancy is expected to be of the order of 1-2%, as estimated from GEANT3 simulations [?]. This value was obtained by inserting a Møller shield made of aluminum and tungsten and covering angles up to about 4 degrees. This shield is not compatible with the operation of the Foward Tagger. Therefore we performed a dedicated study to evaluate the DC occupancy with the FT, optimizing the FT case and the Møller shield geometries. The interaction of the beam with the target was simulated generating electrons upstream to the interaction region, within a 250 ns window corresponding to the integration time of the DC readout. The secondaries that are produced were tracked throughout the CLAS12 volume and the rates of the different detector components were computed. The resulting DC occupancy for the nominal luminosity of  $10^{35} \text{ cm}^{-2}\text{s}^{-1}$  is shown in Fig. 16. The measured rates are higher in the first two superlayers of Region 1, since the background is dominated by low energy particles coming from the target region and the Møller shield. These secondaries are easily stopped by a small amounts of material, and therefore rates drop in Region 2 and 3. DC occupancy is always below 2% and therefore within acceptable values. It is worth to mention that, implementing the geometry of the standard CLAS12 shield in GEMC, we are able to reproduce the same results obtained with GEANT3 simulations.

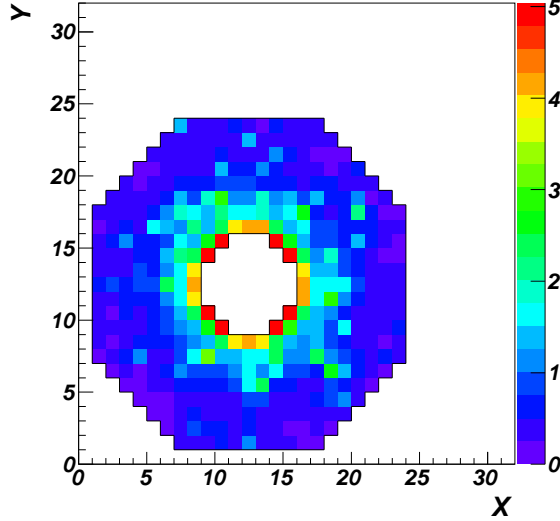


Figure 15: Radiation dose on the FT calorimeter crystals in rad/hour at  $10^{35} \text{ cm}^{-2}\text{s}^{-1}$  luminosity. The maximum values of about 5 rad/h are observed for the innermost crystals, i.e. at the smaller angles.

### 3.6 Trigger

The preferable way to run the meson spectroscopy program, using the Forward Tagger setup, is in parallel to regular CLAS12 electroproduction experiments. In standard runs, both the scattered electron and the hadronic final state are detected in the CLAS12 detector. For meson spectroscopy scattered electron will be detected in the Forward Tagger, while hadronic final state in CLAS12. To be able to collect data for both experiments at the same time, the CLAS12 DAQ system should be able to trigger and record both types of events. For regular electron scattering experiments, single electron trigger will be employed while for meson spectroscopy, DAQ will be triggered by the coincidence of a multi-particle final state in CLAS12 and a signal in Forward Tagger within the relevant energy region. The main requirement for the trigger is to be  $\sim 100\%$  efficient for the final states of interest and do not exceed DAQ readout limit by keeping the background rate as low as possible.

#### 3.6.1 CLAS12 trigger system

CLAS12 will have a free running DAQ system. ADCs and TDCs will collect data in pipeline mode. Readout of data will be done after the trigger decision is made with an expected event rate of  $\geq 10 \text{ kHz}$  [97]. The new CLAS12-DAQ front-end electronics, in particular the use of flash ADCs (fADCs) for calorimeters, time-of-flight and Cherenkov counters, and the availability of fast field-programmable gate arrays (FPGA) will allow to employ a multi layer trigger system [97]. The trigger will have a fast cluster finding algorithm (already implemented in the CLAS-IC read-out) with energy and position reconstruction in EC, hit position and signal strength reconstruction in Cherenkov and time-of-flight counters at Level-1 trigger using features of fADCs and crate trigger processing (CTP) boards. At Level-2, track segment finding, track linking, and track position information in drift chambers will be used. Summing all contributions, the time for Level-1 and Level-2 trigger decision making is  $< 10 \mu\text{s}$ . At the next step, before recording the event, the Level-3

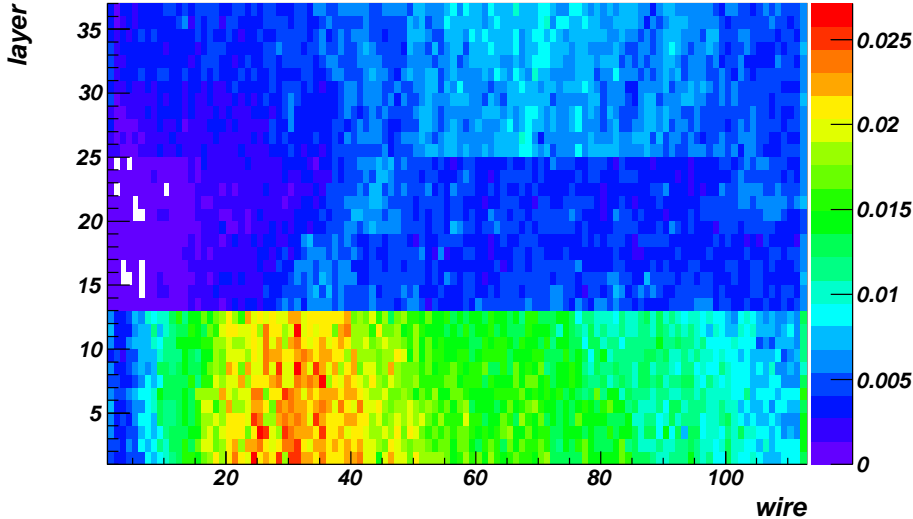


Figure 16: Drift Chamber occupancies at  $10^{35} \text{ cm}^{-2} \text{s}^{-1}$  luminosity as a function of wire and layer number. The maximum occupancy value of about 2% is found in Region 1 while occupancies in Region 2 and 3 are less than 1%. These values are comparable to what estimated in the standard CLAS12 configuration without the FT and are within acceptable values.

software trigger will be employed: combining information from detectors and tracking will make the final decision on the event.

At luminosities and energies foreseen for CLAS12 standard electroproduction experiments, such complex trigger is important even for a single electron trigger data taking. Present experience with CLAS showed that a trigger system that uses sector-based coincidence of signals from calorimeters (with a cut on the total energy sum) and signals from Cherenkov counters (over a certain threshold), while being very efficient, has a very poor electrons-selectivity. For example, at  $E_{beam} \sim 6 \text{ GeV}$  and  $L \sim 2 \times 10^{34} \text{ cm}^{-2} \text{ sec}^{-1}$ , only 7% of triggered events have an electron. Moreover, a simple sector-based Level-2 trigger, involving the tracking, is also inefficient for rejecting background (non-electron) since there is almost always a track found at the sector level. From the analysis of the remaining 97% of non-electron events turned out that most of events were produced via forward photoproduction [32] where a fake trigger was caused by accidental coincidences between the Cherenkov counter and the electromagnetic calorimeter. With higher beam energies (12 GeV) and higher luminosities ( $10^{35} \text{ cm}^{-2} \text{s}^{-1}$ ) operation, the expected results based on a simple trigger system will become worse, of course.

To have a realistic estimate of requirements for trigger selectivity and to calculate the expected trigger rates we studied the CLAS data collected in electron and real photon experiments with production of multi-particle final states.

### 3.6.2 Electroproduction trigger rate

Inclusive electron rates were calculated using parametrization of electron scattering cross section with radiative effects from Ref. [98]. In Figure 17 left-panel, the radiative cross section for  $ep \rightarrow e'X$  as a function of scattered electron energy for several values of scattered electron angles (from  $8^\circ$  to  $28^\circ$ ) is shown. In the calculation the beam energy was assumed to be 11.0 GeV. The corresponding rates at  $L \sim 10^{35} \text{ cm}^{-2} \text{s}^{-1}$  within the CLAS12 geometrical acceptance, are shown in right plot of

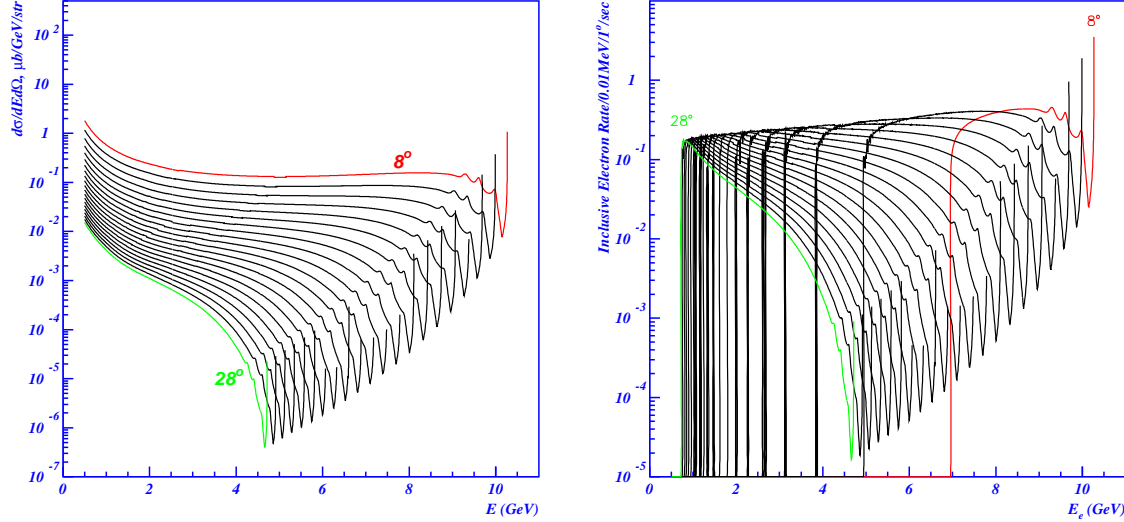


Figure 17: Cross sections (left) and rates at  $10^{35} \text{ cm}^{-2} \text{ sec}^{-1}$  (right) for inclusive electron scattering,  $ep \rightarrow e'X$ , at 11.5 GeV as a function of scattered electron energy, for scattered angles from  $8^\circ$  to  $28^\circ$ . Calculations done using the code of Ref. [98].

Fig. 17. The electron rate integrated over all angles and over the energy range from the minimum threshold energy to the end point as a function of the minimum energy is shown by the red curve in Fig. 18. As one can see from the plot, assuming a minimum momentum cut of  $\sim 0.5 \text{ GeV}/c$ , the total electron rate will be of the order of 1.5 kHz. The main source of background physics triggers is high energy pion production. Pion rates were estimated using pion yields measured in the reaction  $ep \rightarrow \pi^- X$  with CLAS [99], and assuming the  $\pi^+$  yield to be two times higher than the  $\pi^-$  yield. The charged pion rate in CLAS12 was then estimated in a similar way used for electrons, using the simulated performance of the high threshold Cherenkov counter (HTCC) and electromagnetic calorimeters (EC), together with the CLAS12 geometrical acceptances. In Fig. 18 the pions trigger rate is shown with a blue curve. With a low EC threshold ( $\sim 0.5 \text{ GeV}$ ), the pion rate is of the order of 0.3 kHz, resulting in a total trigger rate of *electron-like* particles of less than 2 kHz. We expect the CLAS12 multi-layer trigger system will be 100% efficient for *electron-like* triggers and will be able to reject the other unphysical triggers (accidentals) at level of 50%. With this assumption, we expect to have  $\sim 4 \text{ kHz}$  of trigger rate for electroproduction events.

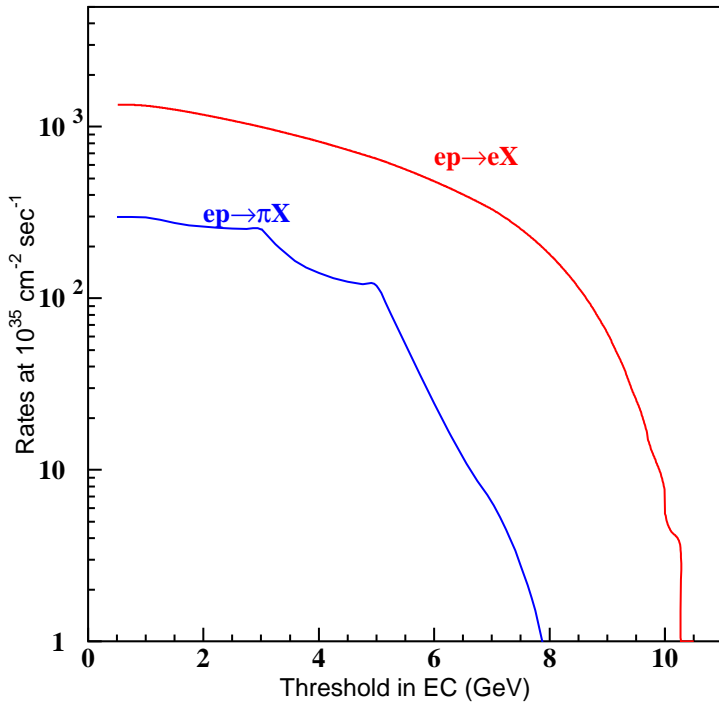


Figure 18: Trigger rates integrated over production angles as a function of the minimum energy (trigger threshold) for inclusive electron and  $\pi^{+/-}$  production at luminosity of  $10^{35} \text{ cm}^{-2} \text{ sec}^{-1}$ .  $\pi^-$  yields from Ref. [99] were used to estimate pion rates, assuming the  $\pi^+$  yield is twice the  $\pi^-$  yield. In the trigger, cuts on the number of photoelectrons in the HTCC and on deposited energy in the EC are used.

### 3.6.3 Quasi-real photoproduction rate

The reactions of interest for meson spectroscopy have three or more particles in final state. Most of the rate comes from reactions with multiple pion photoproduction. As shown in Fig. 19, the cross section of processes with three or more pions levels-out around  $100\mu\text{b}$  for photon energies  $> 3.5 \text{ GeV}$ . With a luminosity of  $10^{35}\text{cm}^{-2}\text{s}^{-1}$ , the inclusive electroscattering rate on the FT, in the energy range of interest ( $E_{e'}=0.5\text{--}4.5 \text{ GeV}$ ) is  $R_{FT-good} = R_{Hadronic}=6.7 \text{ kHz}$ <sup>‡</sup>. This is the hadronic rate useful to study meson spectroscopy. From simulations we estimated the CLAS12 geometrical acceptance for 3 particle final state is  $\epsilon_{3prongs E_{e'}=0.5\text{--}4.5\text{GeV}} \sim 20\%$  and therefore the expected trigger rate from multi-prong events (three or more particles) in CLAS12 will be:  $R_{FT-good} \times \epsilon_{3prongs E_{e'}=0.5\text{--}4.5\text{GeV}} \sim 1.3 \text{ kHz}$ .

On top of this, we should consider accidentals between hadronic events in CLAS12 and the total rate in the FT. The latter is given by two main contributions: the elastic radiative tail and the electromagnetic background. Both of them have no multi-particle events in CLAS12. The elastic radiative rate within the acceptance of the FT was estimated to be of  $R_{FT-rad} \sim 40 \text{ kHz}$ . As discussed in Sec. 3.5.2, the contribution of the electromagnetic background associated to the beam (Møller electrons and secondaries) is much higher than the total hadronic rate mentioned above. The overall electromagnetic background rate is of the order of 50 MHz but, assuming a threshold on the total energy deposited in the FT calorimeter of 500 MeV and limiting the maximum energy to 4.5 GeV we calculated  $R_{FT-em}=180 \text{ kHz}$ . Since the optimization of the tungsten shield geometry is still on progress we are confident that  $R_{FT-em}$  can be further reduced. The suppression of the background outside the energy range of interest, requires the implementation of a trigger system, for both CLAS12 and the FT, capable of reconstructing clusters in the FT with thresholds on the minimum and maximum energy that will be developed for the experiment. To estimate the random coincidences between the FT and the CLAS12 we should consider the total hadron rate due to electroproduction. This is dominated by electroscattering below  $2.5^\circ$ , outside the FT coverage. From Ref. [9] the total electroproduction rate is equivalent to the photoproduction rate given by a Bremsstrahlung beam at a luminosity approximately equal to 1/50 of the electron luminosity (multiplied by a factor that accounts for energy range). In our case this leads to

$$R_{CLAS12} \sim \sigma_{Total}(E_\gamma \sim 10\text{GeV}) \times 3.6 \cdot 10^{33} \text{cm}^{-2}\text{s}^{-1} \times \epsilon_{3prongs 1E_{e'}=0.5\text{--}10.0\text{GeV}} \sim 36 \text{kHz} \quad (5)$$

where  $\epsilon_{3prongs 1E_{e'}=0.5\text{--}10.0\text{GeV}}$  was estimated of the order of 10% averaged over the whole energy range. Assuming a total rate in the forward tagger of  $\sim 250 \text{ kHz}$ , accidentals between CLAS12 and forward tagger in a coincidence window of 100 ns is expected to be in the order of 1.8. kHz, leading to a total rate ( $R_{FT-good}+R_{CLAS12}$ ) of coincidences between FT and CLAS12 of 3.1 kHz. Assuming, as in case of electron trigger, a CLAS12 trigger system selectivity for accidental triggers of 50%, the expected trigger rate for multi-prong events in CLAS12 from photoproduction events will be of the order of 6.2 kHz. This is a conservative estimate that can be refined by reducing rates in FT and CLAS12 and the time coincidence window between the two.

In summary, with a new, multi-level trigger system of CLAS12 and on the FT, electroproduction

---

<sup>‡</sup>Given this value one can calculate the equivalent real-photon flux for a typical target for a photoproduction experiment ( $L_T=30 \text{ cm liquid hydrogen}$ ):

$$\Phi_\gamma = \frac{R_{Hadronic}}{L_T \times \rho_{LH} \times N_{Av} \times \sigma_{Total}(E_\gamma \sim 10\text{GeV})} \quad (4)$$

where  $\rho_{LH}=0.07 \text{ g/cm}^3$ ,  $N_{Av}=6 \cdot 10^{23}$  and  $\sigma_{Total}(E_\gamma \sim 10\text{GeV}) \sim 100\mu\text{b}$ , obtaining  $\Phi_\gamma \sim 5 \cdot 10^7 \text{ g/s}$ . This value is similar to what GlueX is expecting to run with [36].

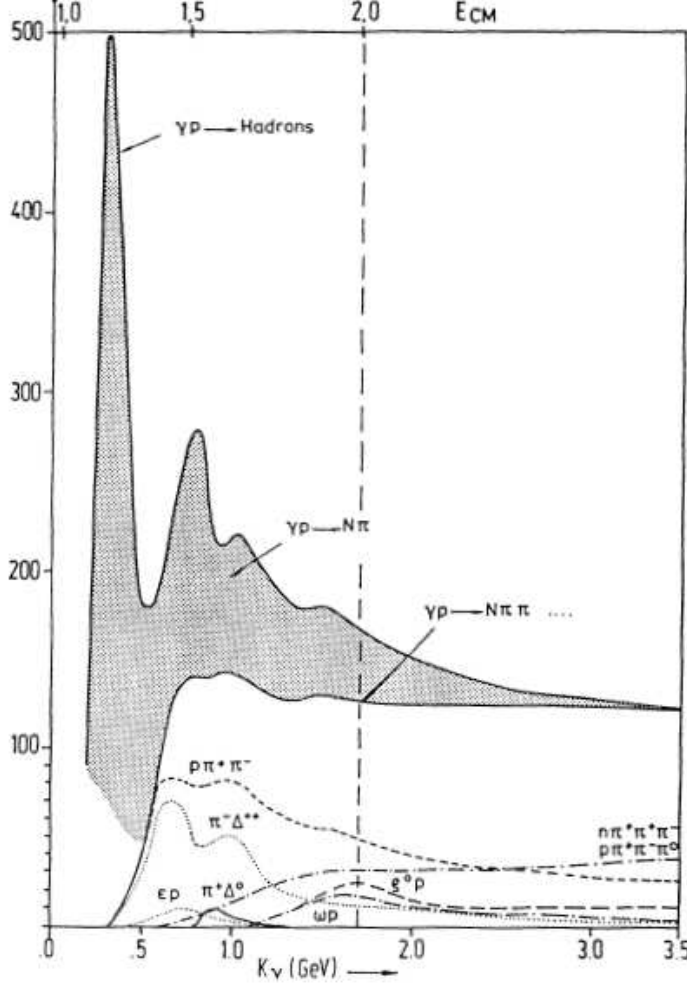


Figure 19: Total photoproduction cross section on proton as a function of photon energy, broken down into major final states which contribute.

and quasi-real photoproduction experiments can be run together. The total trigger rate, with 50% purity of accidentals in both electron and multi-prong triggers, will be  $\sim 10$  kHz, within limit of CLAS12 DAQ event rate.

## 4 Expected results

### 4.1 Benchmark channels

In the following we will discuss in more details some of the reaction channels that we aim at investigating, reporting results obtained from Monte Carlo Simulations for the detection of these channels.

The simulations were based on the CLAS12 Fast Monte Carlo (FASTMC) [64], which uses parametrization of the detector acceptance and resolution for different particle types. The parametrization of angular resolutions were updated to agree with the most recent Monte Carlo tracking results [65, 34] and are shown in Fig. 20.

The acceptance for the tagger was assumed to be 100% in the range  $1 < E_{e'} < 4$  GeV and  $2^\circ < \theta_{e'} < 5^\circ$ . The angular resolution was determined from GEMC simulation studies, detailed in

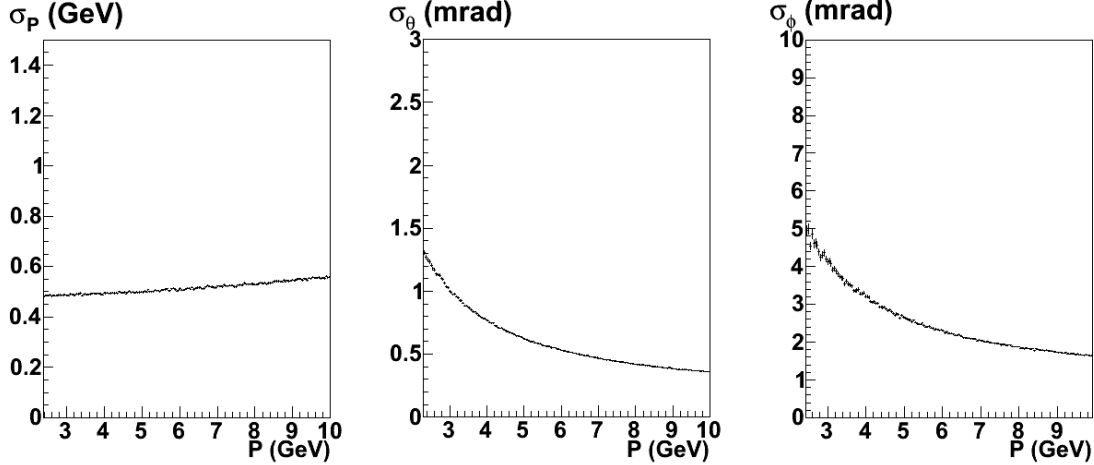


Figure 20: FASTMC resolutions for  $e^-$  at  $\theta = 15^\circ$ . The curves are based on GEANT4 simulation of the CLAS12 tracking system and reconstruction by the SOCRAT package ??.

Sec. 3.5, assuming a spatial resolution for the tracking detector of  $200 \mu\text{m}$  and vertex resolution of  $2.5 \text{ cm}$ . The resulting angular resolutions used were,  $\sigma_\theta = 0.017 \cdot \theta$  and  $\sigma_\phi = 2.8^\circ$ . The energy resolution of the FT was parametrized for three different assumptions on the calorimeter structure:

1. the existing CLAS-IC PbWO<sub>4</sub> calorimeter [59]
  - $\sigma_P = \sqrt{0.02^2 + 0.03^2 P + 0.024^2 P^2} \text{ GeV}$ ,
2. the proposed PANDA-EMC PbWO<sub>4</sub> calorimeter [58]
  - $\sigma_P = \sqrt{0.02^2 P + 0.01 P^2} \text{ GeV}$ ,
3. a poorer resolution sampling calorimeter or equivalent
  - $\sigma_P = 0.2\sqrt{P} \text{ GeV}$ .

Different reactions were studied using reasonable assumptions on production mechanisms. Events were generated via the Monte Carlo technique, projected onto the detector to determine acceptances and the 4-vectors smeared according to the above parametrization.

In the following section we described the results obtained for four specific reactions:

- $\gamma p \rightarrow n\pi^+\pi^+\pi^+$ ,
- $\gamma p \rightarrow n\eta\pi^-$ ,
- $\gamma p \rightarrow p\eta\phi$ ,
- $\gamma p \rightarrow pK^+K^-\pi^0$  and  $\gamma p \rightarrow nK^+K^-\pi^+$ .

#### 4.1.1 The reaction $\gamma p \rightarrow n\pi^+\pi^+\pi^+$

One of the most interesting final state for the search of exotic mesons is the  $3\pi$  channel. For example, exotics with  $J^{PC} = 1^{-+}$  are expected to contribute to this final state, via their decay to  $\rho\pi$ . In fact evidence for the exotic  $\pi_1(1600)$  in this decay mode was reported first by the VES Collaboration [66], followed by the E852 Collaboration at Brookhaven [67]. The latter results are highly controversial, since the initial observation of an exotic  $1^{-+}$  signal at a mass of  $M = (1593 \pm 8)$  MeV with a width of  $\Gamma = (168 \pm 20)$  MeV was not confirmed by a later analysis that used more statistics and a larger set of waves in the PWA [68]. More recently, the same reaction channel was investigated by the CLAS Collaboration [69], that found no evidence for the exotic  $\pi_1(1600)$  state from the analysis of about 83000  $\gamma p \rightarrow \pi^+\pi^+\pi^-n$  events. An upper limit of 13.5 nb on for  $\pi_1(1600)$  production cross section, less than 2% of the  $a_2(1320)$  production, was set. Finally in September 2009, the Compass Collaboration reported the observation of a resonance with  $J^{PC} = 1^{-+}$ , a mass of  $(1660 \pm 10_{-64}^{+0})$  MeV and a width of  $(269 \pm 21_{-64}^{+42})$  MeV, in diffractive dissociation of negative pions into  $\pi^-\pi^-\pi^+$  final state using a 190 GeV/c pion beam hitting a lead target [70].

In spite of the large number of experiments that have investigated the  $3\pi$  system, no definitive conclusion on the existence of an exotic signal in this final state has been obtained. For this reason further studies of these reactions channel are highly desirable.

The  $\gamma p \rightarrow n\pi^+\pi^+\pi^-$  reaction can be easily accessed in the CLAS12 experimental setup by detecting the three charged pions in the forward part of the CLAS12 detector. The exclusivity of the reaction can be ensured by using the FT to determine the energy of the initial state photon and then applying the missing mass technique to select events with a missing neutron. The exotic wave will then be isolated performing a full partial wave analysis of the final state as discussed in Section 2.2. Known mesonic states as the  $a_1(1260)$ ,  $a_2(1320)$  and  $\pi_2(1670)$  will be used as a benchmark of the analysis procedure. To show such techniques will be possible with CLAS12 a detailed Monte Carlo and partial wave analysis was performed for this channel.

Initially, events were generated with a flat  $3\pi$  invariant mass and exponential  $t$  channel distribution,  $\frac{d\sigma}{dt} \propto e^{5t}$ . The response of the CLAS12 and FT system to this channel was then analyzed after tracking with FASTMC. Important acceptances for the reaction are: the invariant mass of the  $3\pi$  system, corresponding to the resonance mass; the momentum transfer or  $t$ -distribution, on which the PWA may show some dependence due to the production mechanism and the angles of the isobar (e.g.  $\rho$ ) in the meson resonance decay. These angles are commonly defined in the meson rest frame with the  $z$ -axis along the negative photon momentum, and the  $y$ -axis  $\underline{n} \times \underline{z}$ , where  $\underline{n}$  is the neutron direction and are known as the Godfried-Jackson angles  $\theta_{GJ}$ ,  $\phi_{GJ}$ . The acceptances for these 4 quantities are shown in Fig. 21 for CLAS12 half field setting and Fig. 22 for the full field setting. Clearly the overall acceptance depends strongly on  $M_{3\pi}$  and the three other variables are shown for fixed  $M_{3\pi} = 1.4$ ,  $1.7$  and  $2.0$  (GeV/c $^2$ ). Although the overall magnitude changes for the 3 masses, the shape of the other acceptances is similar for each. For the full field the acceptance is significantly poorer at low  $M_{3\pi}$ , approximately a factor 5 at  $M_{3\pi} = 1.4$  and 2 at  $M_{3\pi} = 1.7$ . Nevertheless, the angular coverage is reasonable for  $\theta_{GJ}$  and almost flat for  $\phi_{GJ}$ , which is qualitatively good for a PWA, as is tested in more detail later.

Next, the exclusivity of the final state selection was tested by simulating the main possible background channel  $\gamma p \rightarrow n\pi^+\pi^+\pi^-\pi^0$ , which just required an additional  $\pi^0$  in the generator. In this case it is possible for the CLAS12 detector to miss both of the  $\pi^0$  decay photons, so only the 3 charged pions are reconstructed and this final state must be rejected by kinematics. Figure 23, shows the missing mass spectra of the 3 pions for the different models of the FT energy resolution described earlier. The plots only contain events with  $M_{3\pi} < 2.5$  (GeV/c $^2$ ) since the background is lower above this mass. The  $3\pi$  and  $4\pi$  reactions were assumed to have the same cross sections

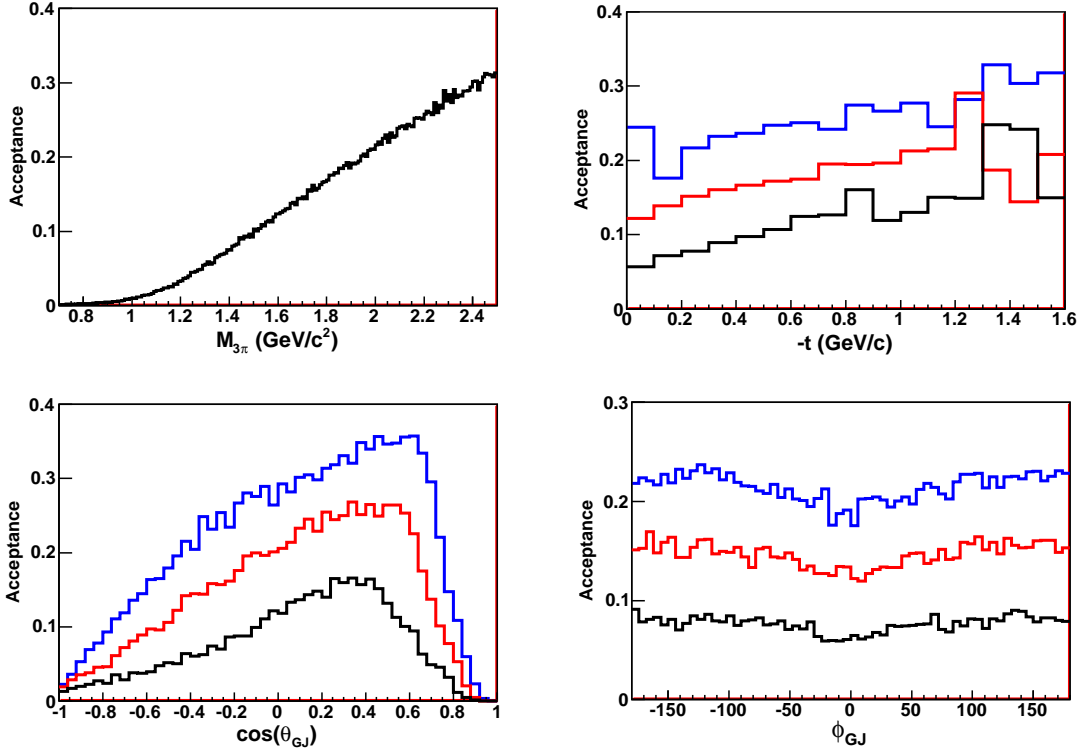


Figure 21: Acceptances for the  $\pi^+\pi^+\pi^-n$  final state and half CLAS12 field setting. Top left the  $3\pi$  invariant mass  $M_{3\pi}$ , right the momentum transfer  $t$ , bottom left,  $\cos \theta_{GJ}$  and right,  $\phi_{GJ}$ . For the latter 3 plots the black, red and blue lines correspond to  $M_{3pi} = 1.4, 1.7$  and  $2.0$  ( $\text{GeV}/c^2$ ) respectively.

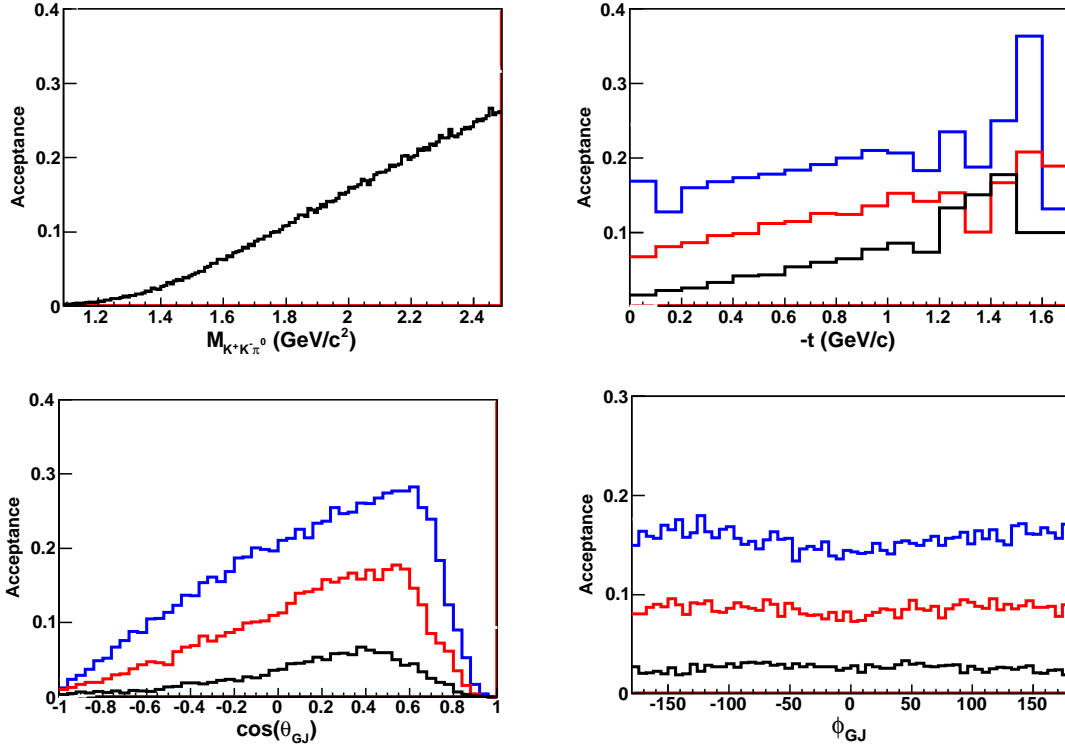


Figure 22: Acceptances for the  $\pi^+\pi^+\pi^-n$  final state and full CLAS12 field setting. Top left the  $3\pi$  invariant mass  $M_{3\pi}$ , right the momentum transfer  $t$ , bottom left,  $\cos \theta_{GJ}$  and right,  $\phi_{GJ}$ . For the latter 3 plots the black, red and blue lines correspond to  $M_{3pi} = 1.4, 1.7$  and  $2.0$  (GeV/c<sup>2</sup>) respectively.

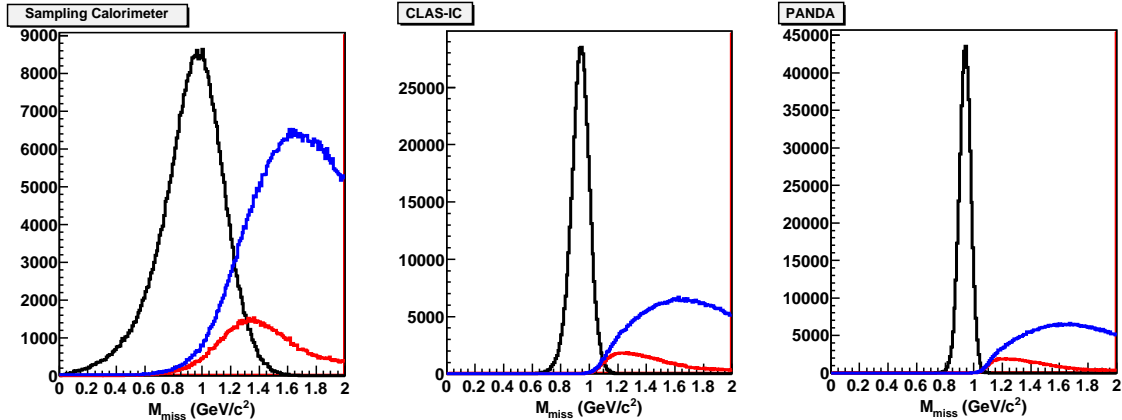


Figure 23: Missing mass of the detected  $3\pi$  system for generated  $3\pi$  events in black, generated  $4\pi$  events with 3 charged  $\pi$  detected, in blue and in red the same but with an additional cut on zero  $\pi^0$  decay photons detected. The left plot is for the sampling calorimeter model, middle, the CLAS-IC and right the expected PANDA calorimeter energy resolution.

for this test. For the  $4\pi$  events two cases are shown, with and without analyzing the  $\pi^0$  decay photons, to show the potential suppression from kinematics alone. It is clear from the plots that the two PbWO<sub>4</sub> calorimeters offer substantial improvement in final state selection compared to a sampling calorimeter. The PANDA calorimeter resolution gives near perfect rejection with the  $4\pi$  background amounting to just 0.03% within  $2\sigma$  of the neutron peak, while the CLAS-IC gives 0.7%. The sampling calorimeter by comparison contains almost 30%  $4\pi$  events in the  $2\sigma$  range. This analysis strongly supports the use of a homogeneous calorimeter with scintillating crystals comparable or superior to PbWO<sub>4</sub> for the FT and that such a detector would allow identification of almost background free  $3\pi$  final states.

#### 4.1.2 The reaction $\gamma p \rightarrow n\eta\pi^-$

Claims of an exotic meson decaying to  $\eta\pi^-$  with a mass around 1400 MeV have a rich history, starting with observations by the GAMS experiment [100] and VES [103]. One of the first evidences for a meson outside the CQM model came from the study of  $\eta\pi^-$  final states in pion production by Brookhaven's E852 experiment [102]. They found a  $J^{PC} = 1^{-+}$  exotic meson candidate now known as the  $\pi_1(1400)$ . At present, there is not a clear understanding of the nature of the  $\pi_1(1400)$  [104, 105]. The observation, or lack, of exotic  $\pi_1(1400)$  in  $\eta\pi$  photoproduction would provide critical information regarding the nature of the  $\pi_1(1400)$ . The good acceptance of CLAS12 for neutral particles and its extension to low angles provided by the FT calorimeter results in a sizeable detection acceptance for the neutral-rich final state of the  $\gamma p \rightarrow n\eta\pi^+$  reaction. We are currently analyzing the CLAS data at 6 GeV (g12 run), exploring the possibility of  $\eta\pi$  meson production off of a recoiling  $\Delta^{++}$ . This channel has the advantage of pre-determine the naturality of the exchanged particle (a pion) and to reduce the background associated to baryon resonances. An order of magnitude more data, as expected from this proposal, would provide enough statistics to explore the resonant nature of the  $\eta\pi^-$  system and to search for the  $\pi_1(1400)$  exotic meson.

Events of the form  $\gamma p \rightarrow pX \rightarrow p\eta\pi \rightarrow p\gamma\gamma\pi^+$  were generated according to  $t$ -channel phase space with a  $d\sigma/dt \propto e^{5t}$ . Acceptances were derived using FASTMC requiring that the  $\pi^+$  and the two photons were measured in CLAS12 (and the FT calorimeter). The neutron was reconstructed by using the missing mass technique. Figure 24 shows acceptances as a function of detected

production	mass(MeV)	width(MeV)	experiment	decay	ref
$e^+e^-$	1650		DM1	$K_L K_S$	[86]
	1650			$K^+ K^-$	[87]
	1650		VEPP-2M	$K^+ K^-$	[88]
	1680		DM2	$K^+ K^-$	[89]
	1677	102		$K_S K^+ \pi^-$	[84]
	1680	185	DM1	$KK, KK\pi$	[90]
	1657	146	DM2	$K^+ K^-$	[91]
photo-	1748	80	CERN Omega	KK	[92]
	1760	80	CERN WA57	KK	[93]
	1726	121	Fermi E401	KK	[94]
	1753	122	Fermi FOCUS	KK	[85]

Table 2: Experimental data on the  $\phi(1680)$

particle angles in the lab frame. The overall acceptance is of about 16%. It worth to note that the acceptance is only slightly dependent on the magnetic field intensity since the most part of the produced particles are neutral.

#### 4.1.3 The reaction $\gamma p \rightarrow p\eta\phi$

A summary of the current data on the  $\phi(1680)$  is shown in Table 2. The interpretation of the current data is not conclusive. Photoproduction and electroproduction experiments observed different properties of the  $\phi(1680)$  decay modes. The resonance mass is consistently higher in photoproduction than in  $e^+e^-$  production. Furthermore, there is no evidence of  $KK^*$  decay in photoproduction, found to be dominant in  $e^+e^-$  production.

The different behavior of the  $\phi(1680)$  observed in photo- and electroproduction may be explained by the presence of two states interfering with  $n\bar{n}$  states. To understand this problem one will need to measure relative branching ratios of the  $\phi(1680)$  into the neutral and charged  $KK$  and  $KK^*$  pairs. However, the  $\phi\eta$  decay mode is the cleanest to study since the interference with  $n\bar{n}$  states is highly suppressed. According to the Zweig rule, the  $\phi\eta$  channel can arise *only* from  $s\bar{s}$  initial states. This decay mode has not been yet observed, and its study is one of the goals of this proposal. Just the mere identification (or not identification) of a resonance in the  $\phi\eta$  system will prove the presence of a  $s\bar{s}$  state. This reasoning is also applicable to the  $\phi(1850)$  and other higher mass excitations.

It is generally accepted that diffraction [95] is the dominant mechanism to photo-produce vector meson resonances. This is certainly true at high energies (Hera or FermiLab), where data are well explained by the Pomeron exchange. However, at intermediate energies of JLab, the situation is not so clear because other mechanisms have to be considered: e.g., the pion exchange could contribute since  $\pi$  strongly couples to the  $\rho$  leading to significant pseudo-vector and tensor meson production.

Preliminary results from the analysis of data taken with CLAS at 6 GeV (g12 run) are promising, indicating that we should be able to extract information about strangeonia resonances. However, due to some limitation of this experiment, limited statistics, limited kaon and neutral identification, the current data will probably provide a limited insight of the strangeonium sector. It worth to note that the GlueX detector, in its current planned setup, will not provide kaon identification and therefore is not suitable to study strangeonia.

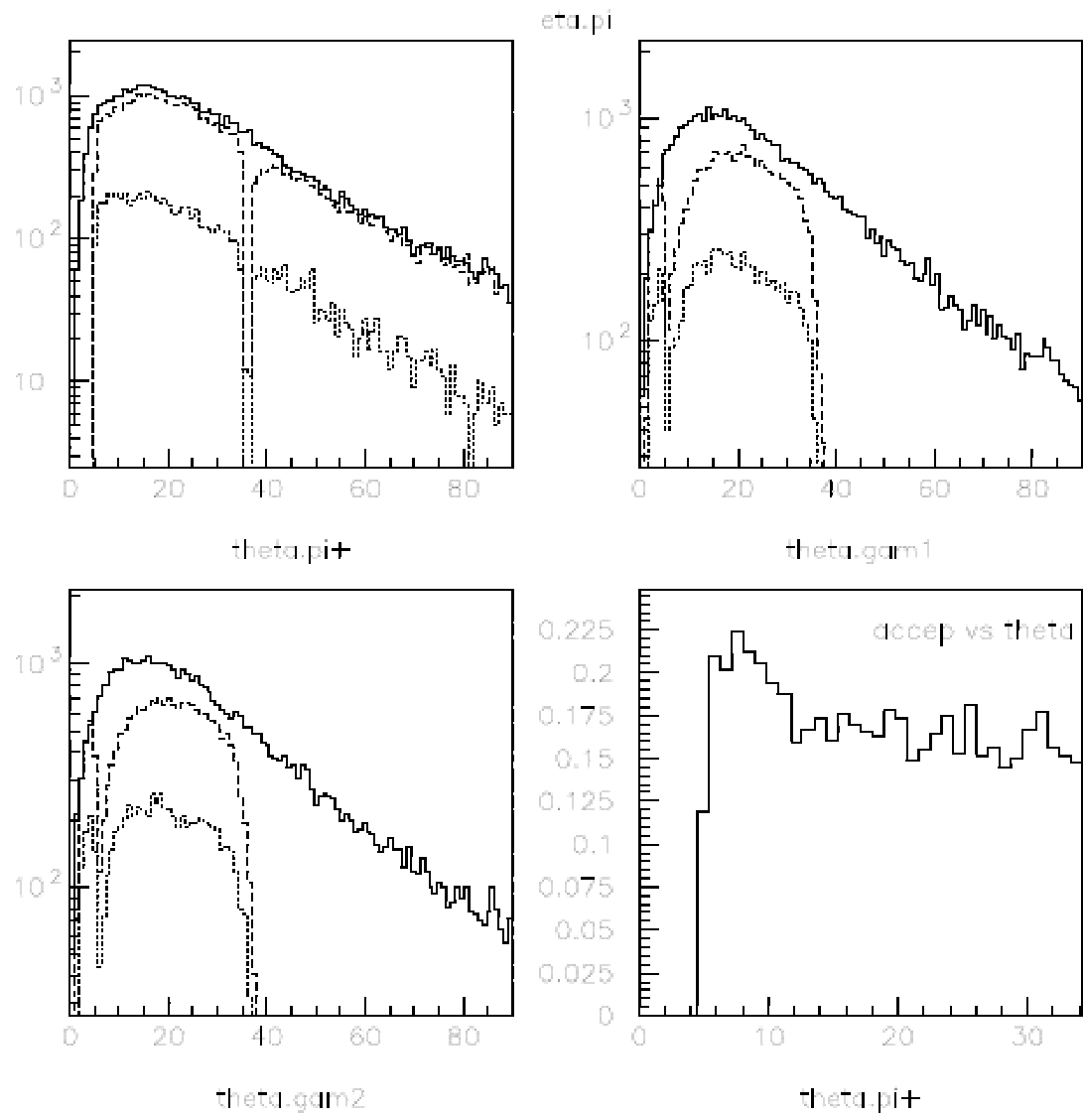


Figure 24: The  $\theta_{Lab}$  distributions for  $\eta\pi$  events. Shown are the generated, particle accepted and event accepted distributions.

The acceptance of CLAS12 to the decay of  $\phi(1850)$  to  $\phi\eta$  has been simulated using the FASTMC. The channel was identified by detecting the proton, the  $\eta$ , via its two photons decay, and a  $k^+$  while the missing  $k^-$  was reconstructed by the missing mass technique. Due to the good acceptance for neutrals in the forward direction, mainly due to the extention to low angles brought by the FT calorimeter, we estimated an overall acceptances of about 18%. Figure 25 shows the angular acceptances for detected particles.

#### 4.1.4 The reactions $\gamma p \rightarrow pK^+K^-\pi^0$ and $\gamma p \rightarrow nK^+K^-\pi^+$

One very attractive method to identify exotic mesons is through the  $\phi\pi$  decay mode. Any  $s\bar{s}$ -meson decay to  $\phi\pi$  is forbidden due to the conservation of isotopic spin. This decay mode is forbidden by the Okubo-Zweig-Iizuka (OZI) rule for any  $n\bar{n}$ -meson (where  $n$  is  $u$  or  $d$  quarks) as well. On the other hand, multiquark or hybrid mesons are expected to have a strong coupling to the  $\phi\pi$  system [?]. The discovery of a  $\phi\pi$  resonance would indicate a new kind of hadron and suggest a  $q\bar{q}g$  or  $q\bar{q}q\bar{q}$  state. This is true for  $f'\pi$  and  $J/\psi\pi$  decay modes as well [71].

There is some experimental evidence for the existence of a resonance with strong  $\phi\pi$  coupling. In experiments at the LEPTON-F spectrometer [72, 73], the charge exchange reaction

$$\pi^- p \rightarrow (\phi\pi^0)n, \quad (6)$$

has been studied at a  $\pi^-$ -momentum of 32 GeV/c. In the mass spectrum of the  $\phi\pi^0$  system a new meson,  $C(1480)$ , with mass  $1480 \pm 40$  MeV and width  $130 \pm 60$  MeV, was observed. The angular distributions of the sequential decay  $C(1480) \rightarrow \phi\pi^0, \phi \rightarrow K^+K^-$  have been studied, and the quantum numbers for  $C(1480)$  meson have been determined:  $I^G = 1^+, J^{PC} = 1^{--}$ . For this meson an anomalously large value of the ratio

$$BR(C(1480) \rightarrow \phi\pi^0)/BR(C(1480) \rightarrow \omega\pi^0) > 0.5 \quad (7)$$

at 95% C.L. has been obtained. This value is more than two orders of magnitude higher than the expected ratio for mesons with the standard isovector quark structure. At the present time the only consistent explanation of these properties can be obtained with the assumption that the  $C(1480)$  meson is a four quark or hybrid state.

At the  $\Omega$ -spectrometer [74] the cross section for the reaction  $\gamma p \rightarrow \phi\pi^0 p$  has been measured. Although the number of events is not large ( $\sim 25$ ), an excess of events in the mass spectrum of the  $\phi\pi^0$  system at  $\sim 1.4$  GeV is observed. The  $\phi\pi^0$  photoproduction cross section was estimated as

$$\sigma(\gamma p \rightarrow \phi\pi^0 p) = 6 \pm 3 \text{ nb} \quad (8)$$

(at 95% C.L.)

The existence of the structure in the same mass range was confirmed with the study of inclusive  $\phi\pi^+$  production with a pion beam [75].

Recently the BaBar Collaboration published new data on the cross section for the annihilation  $e^+e^- \rightarrow \phi\pi^0$ . There is a prominent structure in the cross section near the total energy 1.5 GeV [76].

Quasi-real photoproduction is likely to be one of the more promising mechanisms for the production of exotic mesons with hidden strangeness due to the relatively large  $s\bar{s}$  content of the photon. Photons are also expected to be efficient in the production of spin-1 hybrids.

The first attempts to explore existing data from CLAS runs g6a and g6b showed that the multiparticle reactions

$$\gamma p \rightarrow (\phi\pi^0)p, \quad \phi \rightarrow K^+K^-, \quad \pi^0 \rightarrow \gamma\gamma \quad (9)$$

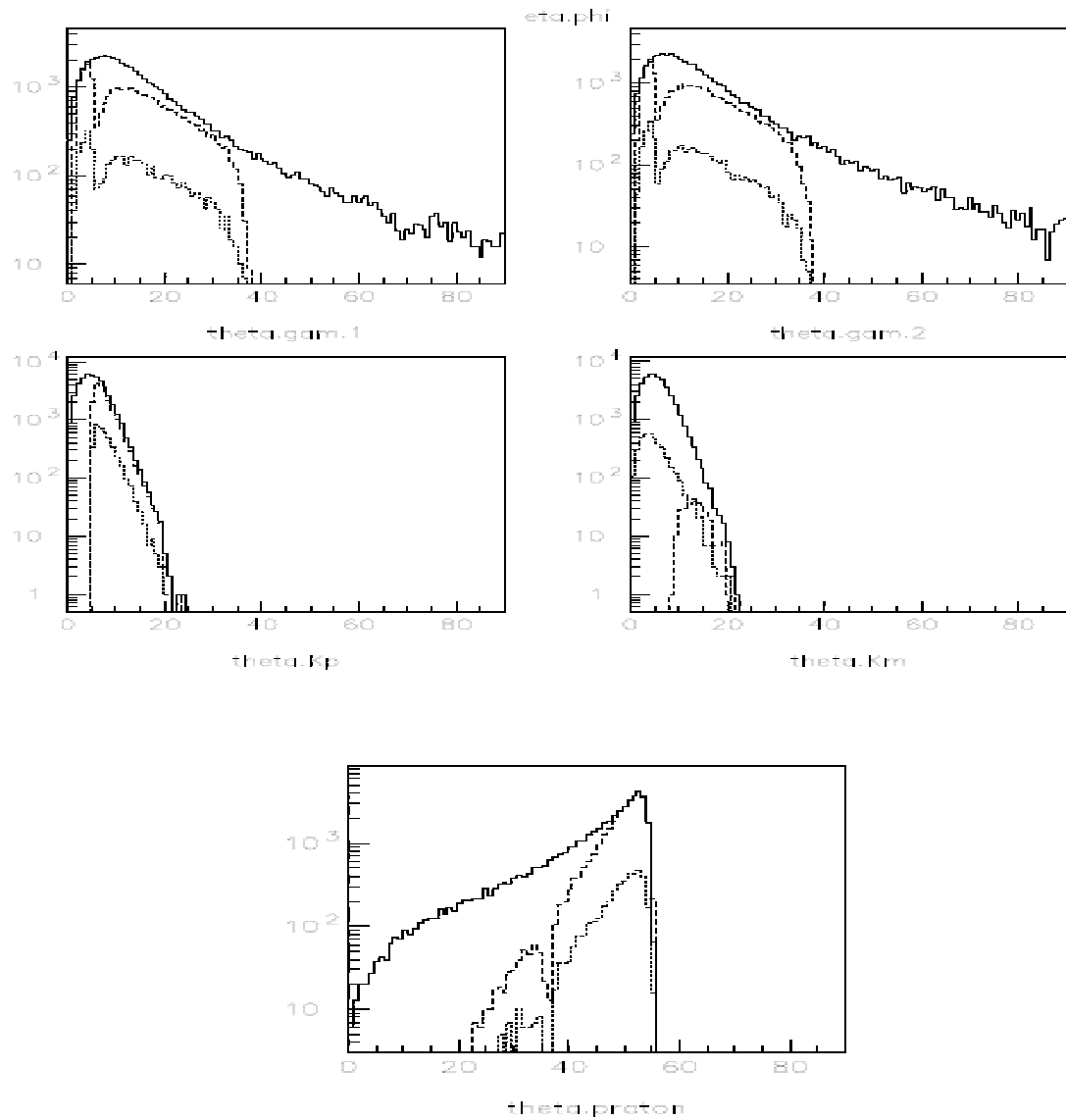


Figure 25: The  $\theta_{Lab}$  distributions for  $\phi\eta$  events. Shown are the generated, particle accepted and event accepted distributions.

$$\gamma p \rightarrow (\phi\pi^+)n, \quad \phi \rightarrow K^+K^- \quad (10)$$

can be investigated [77].

The CLAS12 spectrometer has excellent momentum and angular resolution and particle identification. These features are extremely important for the mass determination and background reduction.

The acceptance and resolution for resonances decaying to  $\phi\pi^0$  was studied assuming the resonance to be produced and decay via the reaction  $\gamma p \rightarrow Xp \rightarrow \phi\pi^0p \rightarrow K^+K^-\gamma\gamma p$ . Again the resonance  $X$  was produced with a  $t$  distribution,  $\frac{d\sigma}{dt} \propto e^{5t}$ . In this case, the  $K^-$  from the decay of the  $\phi$  meson is mainly produced at very forward angle, i.e. typically below 15 degrees in the lab with an overall detection efficiency of about 2% due to the inbending of negative particles in the toroidal field. The detection of this particle leads therefore to a very strong reduction of the overall acceptance. A more efficient identification of this final state is achieved by detecting the proton, the  $K^+$ , the  $\pi^0$  via its decay to two photons and selecting the  $K^-$  in missing mass. In this way the overall acceptance was estimated to be of the order of 9%, to be compared with  $\sim 2\%$  achieved by detecting proton,  $K^+$  and  $K^-$ . The acceptance for the mass of the  $\phi\pi$  system  $M_{K^+K^-\pi^0}$ ,  $t$  distribution and resonant decay angles  $\theta_{GJ}$  and  $\phi_{GJ}$  are shown in Fig. 26 for the half field setting for CLAS12. They are similar to those obtained for the  $3\pi$  analysis and so the conclusions discussed in the next Sections about the feasibility of PWA can be extended to this reaction as well. There is little effect on these acceptances for full magnetic field as the  $K^-$  which would be most effected by this is already reconstructed in the analysis.

Figure 27 shows the reconstructed masses from the  $pK^+\gamma\gamma$  final state. Also shown is a phase space  $\gamma p \rightarrow K^+\pi^0\pi^-p$  background. The missing masses have widths of 0.054 and 0.093 GeV for the CLAS-IC and low-resolution tagger respectively. The resolution is the same for the reconstructed  $\phi$  mass. Again, the capability to determine the photon energy with a good resolution is crucial to be able to study this reaction channel with a sizable efficiency and a good signal to background ratio.

#### 4.1.5 Conclusions

The results of the study on benchmark reactions presented in the previous sections has clearly shown that the possibility of inferring the energy of the quasi-real photon from measuring the scattered low angle electron gives significant advantages for the study of exclusive multiparticle final states. First of all, the complete determination of the initial state provided by the FT makes it possible to use the missing mass technique to ensure the exclusivity of the reaction. Without such information, a full measurement of the final state particles would be necessary, resulting in acceptances of the % level or below for many of the studied reactions. To fully exploit the missing mass technique, a good energy resolution for the tagger is desirable. In cases where full detection of the final state is possible, the determination of the initial state allows to apply further constraints to suppress backgrounds coming from other reactions and extract small cross section signals.

## 4.2 PWA simulations

As described in Sec. 2.2, the first step in partial wave analysis is to extract amplitudes from fits to the measured particle distribution. At this stage it is necessary to establish to what extent the finite detector acceptance and resolution distorts the underlying reaction mechanism. For a specific reaction this is done by generating events using a realistic differential cross-section, processing them through a detector simulation and reconstruction programs, and fitting with a set of partial waves

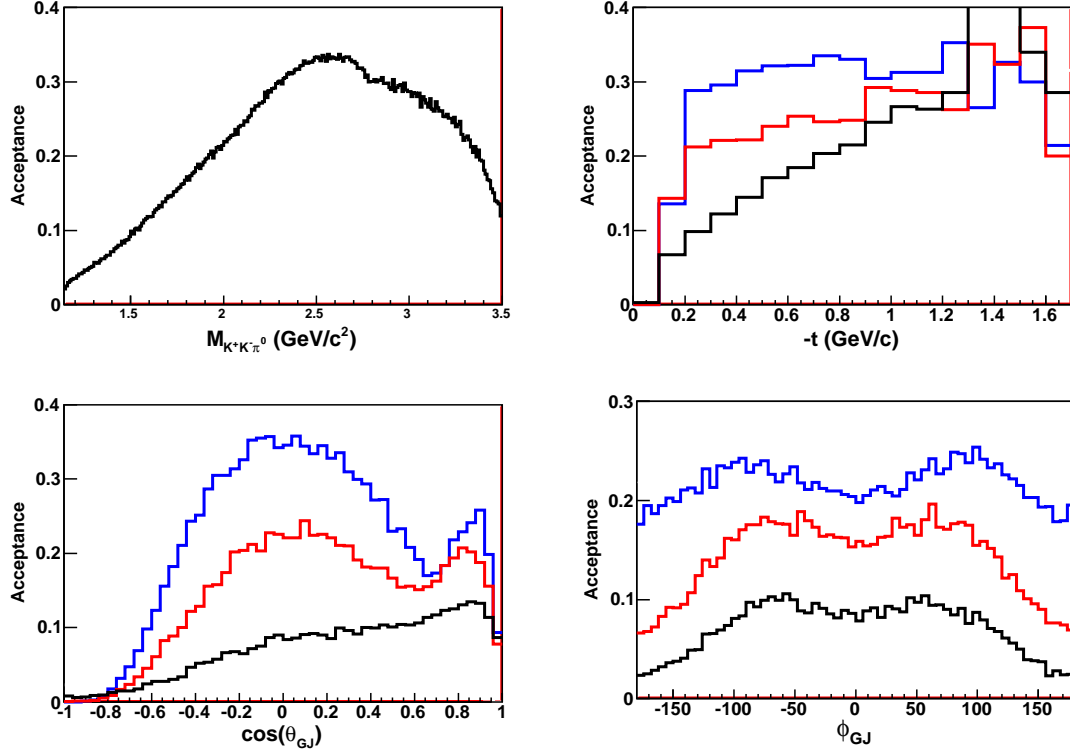


Figure 26: Acceptances for the  $K^+K^-\pi^0p$  final state, with the  $K^-$  reconstructed. Top left the  $K^+K^-\pi^0$  invariant mass  $M_{K^+K^-\pi^0}$ , right the momentum transfer  $t$ , bottom left,  $\cos \theta_{GJ}$  and right,  $\phi_{GJ}$ . For the latter 3 plots the black, red and blue lines correspond to  $M_{K^+K^-\pi^0} = 1.4, 1.7$  and  $2.0$  ( $\text{GeV}/c^2$ ) respectively.

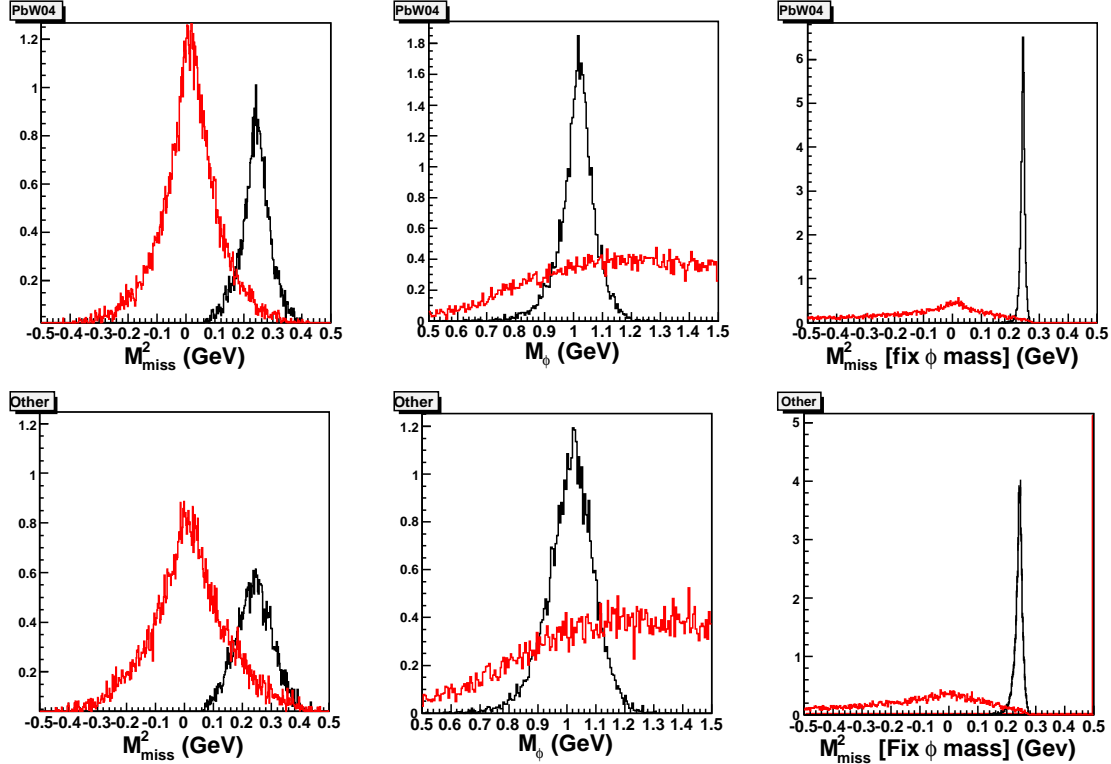


Figure 27: Reconstructed masses from the  $pK^+\gamma\gamma$  final state for the CLAS-IC tagger (top) and the lowest resolution tagger (bottom). In all plots, the black line shows the final state of interest, while the red line is for a phase space  $\gamma p \rightarrow K^+\pi^0\pi^-p$  reaction. The left plot shows the missing mass ( $\sim K^-$ ), the middle the reconstructed  $\phi$  mass and the right plot the missing, mass having fixed the reconstructed  $\phi$  mass to 1.020 GeV.

State	$J^{PC}$	L	Decay Mode
$a_1(1260)$	$1^{++}$	D	$\rho\pi$
$a_2(1320)$	$2^{++}$	D	$\rho\pi$
$\pi_2(1670)$	$2^{-+}$	P	$\rho\pi$
$\pi_2(1670)$	$2^{-+}$	F	$\rho\pi$
$\pi_2(1670)$	$2^{-+}$	S	$f_2\pi$
$\pi_2(1670)$	$2^{-+}$	D	$f_2\pi$
$\pi_1(1600)$	$1^{-+}$	P	$\rho\pi$

Table 3: The meson states produced in the model of  $\pi^+\pi^+\pi^-$  production, detailed in Appendix A.

and bins of kinematical variables. We currently have two partially independent PWA codes and two groups doing PWA. We performed detailed partial wave analysis studies for the two reactions:  $\gamma p \rightarrow \pi^+\pi^+\pi^-n$  and  $\gamma p \rightarrow n\eta\pi^+$ .

Results are reported in the following sections.

#### 4.2.1 Partial Wave Analysis of the $3\pi$ Channel

This is the channel where exotic,  $J^{PC} = 1^{-+}, I = 1$  can be produced. Even though the charged  $3\pi$  state is not an eigenstate of charge conjugation,  $I = 1$  vector resonance decaying to three pions would correspond to a (charged) member of the  $\pi_1^{\pm,0}$  exotic multiplet. From the theoretical point of view, charge exchange photo-production is expected to be well described in terms of the leading Regge pion exchange trajectory which has been thoroughly studied in the past. The alternative, neutral  $3\pi$  production is dominated by the enigmatic Pomeron exchange which leads to large backgrounds from  $I = 0$  vector meson diffractive production. Furthermore, there are well established  $I = 1$   $3\pi$  resonances,  $a_1$ ,  $a_2$  and  $\pi_2$ , that enhance the sensitivity by interfering with the small exotic wave. The model for 3 pion production, detailed in Appendix A, has been used to test the suitability of events reconstructed from CLAS12 and the forward tagger for Partial Wave Analysis. The model defines 8 possible final states, summarized in table 3, decaying to  $\pi^+\pi^+\pi^-$ , with an additional recoiling neutron in the final state. The  $\pi_1$  is a proposed exotic state. In the model, its contribution to the final state is around 2%, corresponding to a 200 nb cross section, for a total  $\pi^+\pi^+\pi^-$  cross section of around 10  $\mu\text{b}$ . To allow a series of PWA tests to be performed in a reasonable time, the number of generated events was limited to 1 million. This would be equivalent to around 1 thousandth of the total number of events, we estimate would be produced in a 3-month beamtime. Therefore, for the experimental data we will have many more times the statistics than for our current tests, allowing fine binning in a number of kinematic variables such as  $E_\gamma$ ,  $t$  and  $M_{3\pi}$ .

The testing algorithm proceeded as follows,

- The model was used to generate 1 million events, “data”, from low  $Q^2$  electron scattering reactions accepted by the forward tagger, with an electron beam energy of 11 GeV. Events were generated in two  $t$  bins at 0.2 and 0.5  $(\text{GeV}/c)^2$ , 0.25 and 1 MeV wide respectively to give comparative numbers of events in the same beamtime.
- 5 million phase space Monte Carlo events, “mc”, were generated in the same kinematics and were used to calculate the acceptance during the PWA fit.

- Both “data” and “mc”, were tracked through the detectors via the FASTMC programme. A number of tracking options were used including full and half CLAS12 torus field and CLAS-IC or PANDA-EMC resolutions for the forward tagger.
- Final states with 3 reconstructed pions were accepted for the PWA.
- The accepted events were split into 40 bins in the mass of the  $3\pi$  system, between 0.7 and 2.2 GeV.
- Maximum likelihood fits were performed, using the model described before to calculate the event-by-event amplitudes, for each  $3\pi$  mass bin. The generated and accepted “mc” events are used to calculate the normalization integrals and subsequent acceptance. The complex production amplitude of each channel was a free parameter in the fit.
- The resulting intensity of each channel was calculated from the fit results and compared to the generated one.

The first comparison presented in Figure 28 is between the generated waves and a fit for each  $t$  bin (0.2 and 0.5) at half CLAS12 field and CLAS-IC Forward Tagger resolution. The fits for both  $t$  bins reproduce the generated waves very well for all channels including the hypothetical  $\pi_1$  exotic. The mass region with  $M_{3\pi}(< 1.2 \text{ GeV}/c^2)$  has been excluded from this analysis because of the very low acceptance. Even with a  $\pi_1$  contribution of just 2% to the total, a clear statistically significant signal is reproduced using a small statistics compared to the expected yield for the proposed experiment. *This leads to the conclusion that the CLAS12-Forward Tagger system is intrinsically capable of meson spectroscopy measurements via partial wave analysis.*

However, in reality we will not have such perfect knowledge of the CLAS12 response and physics of the production and decay. To test the effects of possible distortions and leakages we have performed a number of fits with imperfect knowledge of the detector or model.

1) The “data” were tracked through FASTMC with an incorrect field strength, 2% higher at the half field setting, compared to the accepted “mc” events. This effectively creates a different acceptance between the “data” and “mc” due to charged particles of a given momenta seeing different holes in the detector. The results are shown in Figure 29, and at this level of field discrepancy no sizeable distortion effect is seen on the fitted waves.

2) The angular and momentum resolutions of the FASTMC were decreased by 20% for the “data” only. This tests how accurately we will be required to know the resolutions from the tracking in CLAS12. The results are shown in Figure 30 and very little deviation is seen between the ideal case and the degraded resolution case.

3) The standard model events were fit without the  $\pi_1$  D-wave and the results are shown in Figure 31. The intensity of the generated  $\pi_1$  clearly has to be given to another wave or waves by the fit. In this case it is the  $a_1$  S and D wave which acquires most of the yield, while the  $\pi_2$  P and F waves are underestimated. This shows the importance understanding the components of the model used to perform the fit. As discussed in section 2.2, a collaborative worldwide effort is underway to refine the tools and models required to perform such amplitude analysis. The timescales for this work will coincide well with the prospective data from the CLAS12 experiment.

4) The full model fit was performed on events generated without a  $\pi_1$ . The resulting  $\pi_1$  intensity is consistent with zero within its uncertainty and for the statistics generated is around 10 counts at  $1.6 \text{ GeV}/c^2$ . This is a factor 200 less than for the  $\pi_1$  generated in the model which contributed 2% to the  $3\pi$  yield.

5) We have shown in Sec. 4.1 that the half field setting provides the optimal acceptance for this channel. However, as mentioned before, this experiment is conceived to run in parallel to other

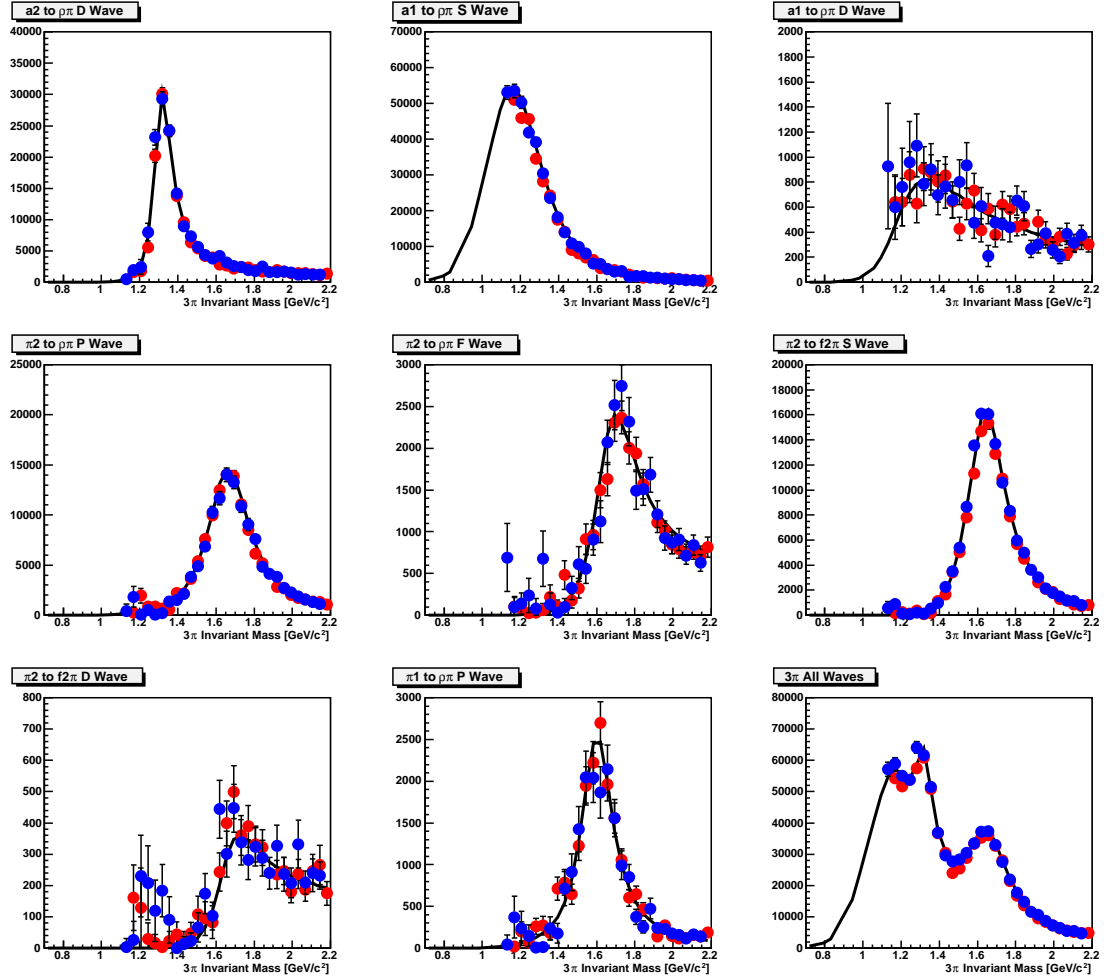


Figure 28: The intensities of the 8 different isobar channels in the  $3\pi$  model, see table 3. The bottom right plot shows the total intensity. The black line shows the generated waves, while the blue and red points are the fit results for  $t = 0.2$  and  $0.5(\text{GeV}/c^2)$ , respectively.

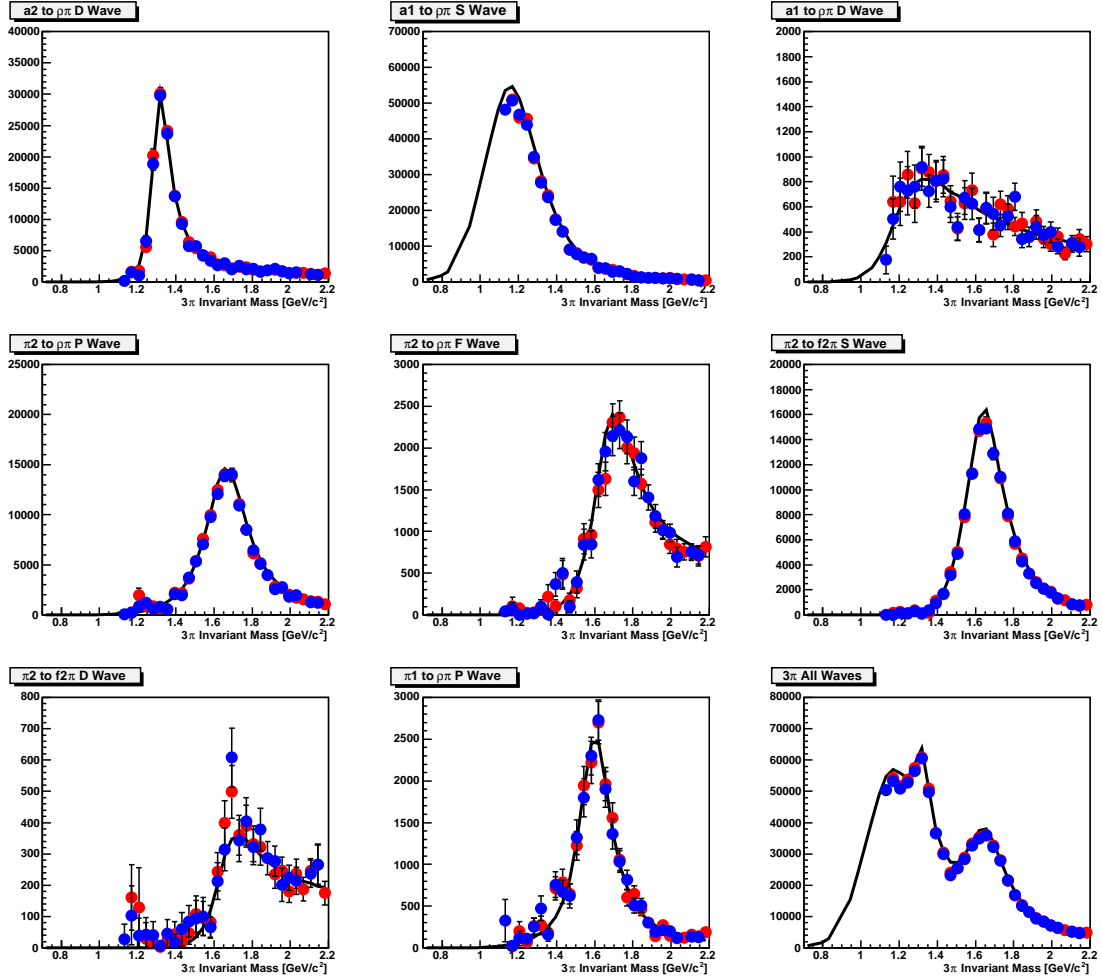


Figure 29: The intensities of the 8 different isobar channels in the  $3\pi$  model, see table 3. The bottom right plot shows the total intensity. The black line shows the generated waves, while the red points are the fit results for  $t = 0.5(\text{GeV}/c)^2$ , half field and the blue points are for “data” tracked with the field incorrectly set 2% higher than for the “mc” events.

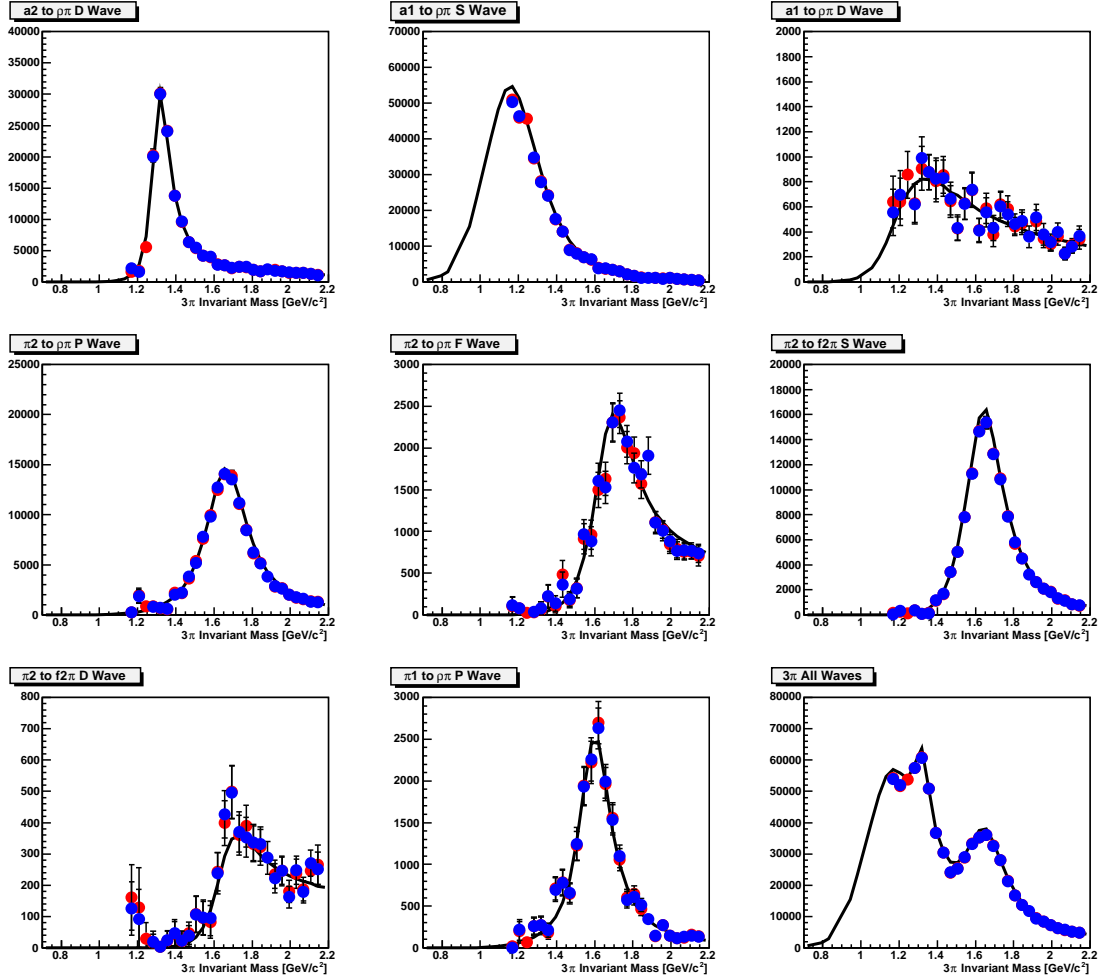


Figure 30: The intensities of the 8 different isobar channels in the  $3\pi$  model, see table 3. The bottom right plot shows the total intensity. The black line shows the generated waves, while the red points are the fit results for  $t = 0.5(\text{GeV}/c)^2$ , half field and the blue points are for “data” tracked resolutions 20% greater than standard, while the corresponding “mc” used standard resolutions.

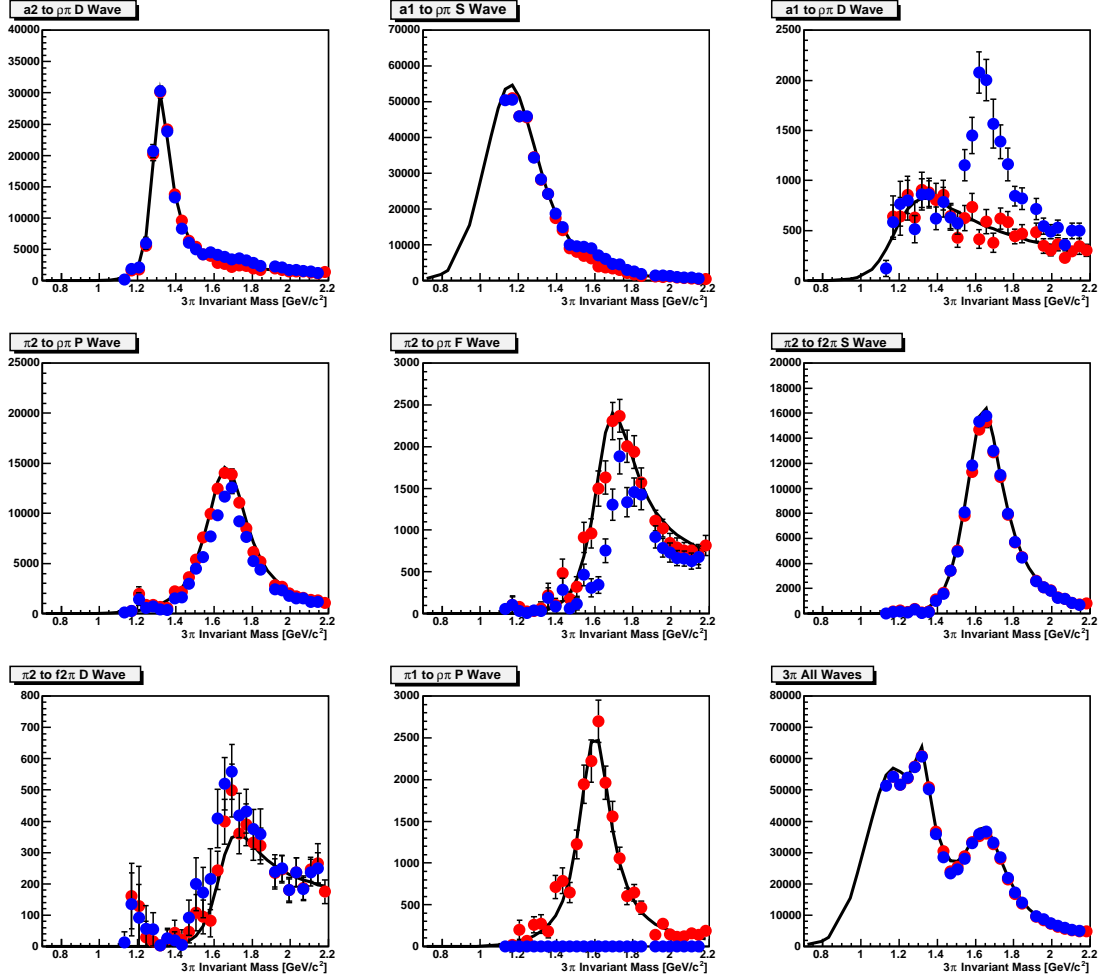


Figure 31: The intensities of the 8 different isobar channels in the  $3\pi$  model, see table 3. The bottom right plot shows the total intensity. The black line shows the generated waves, while the red points are the fit results for  $t = 0.5(\text{GeV}/c)^2$ , half field and the blue points are for a fit without the  $\pi_1$  D wave.

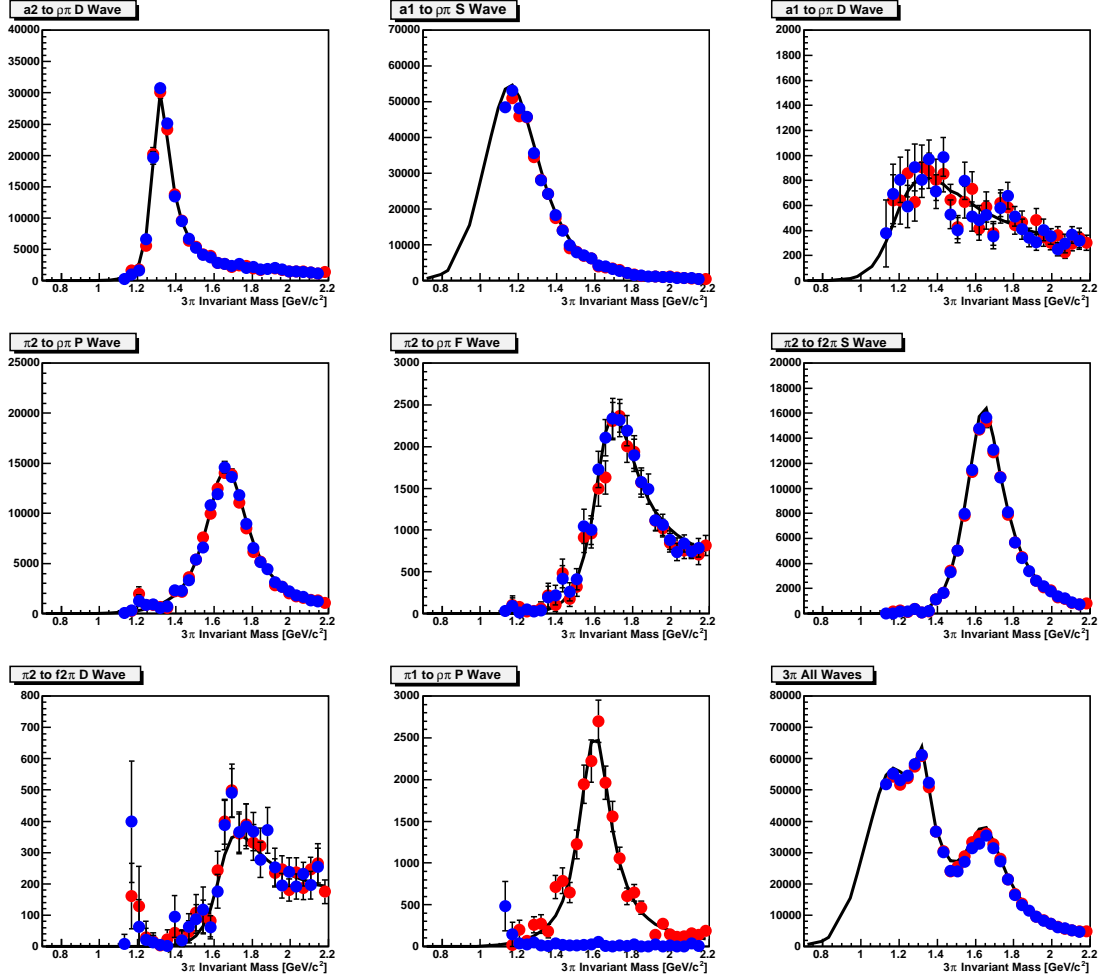


Figure 32: The intensities of the 8 different isobar channels in the  $3\pi$  model, see table 3. The bottom right plot shows the total intensity. The black line shows the generated waves, while the red points are the fit results for  $t = 0.5(\text{GeV}/c)^2$ , half field and the blue points are for a generated without the  $\pi_1$  D wave.

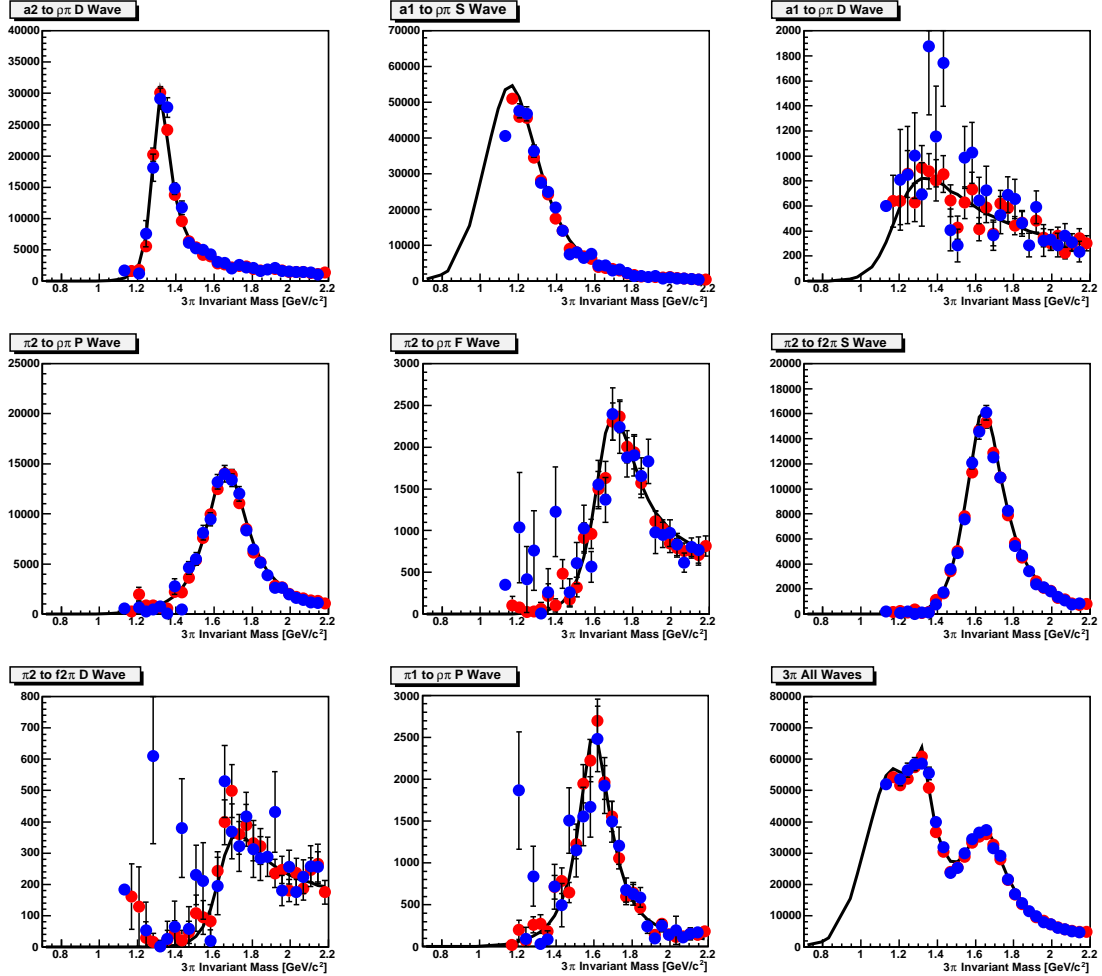


Figure 33: The intensities of the 8 different isobar channels in the  $3\pi$  model, see table 3. The bottom right plot shows the total intensity. The black line shows the generated waves, while the red points are the fit results for  $t = 0.5(\text{GeV}/c)^2$ , half field and the blue points are for full field.

electroscattering experiments that may have higher field setting. The results of the PWA with the full field setting are shown in Fig. 33. Again the fits are successful for the full field setting. In general the error bars are larger particularly at low  $M_{3\pi}$ , and are around 25% larger around the  $\pi_1$  peak. As our test results only use a small amount of the statistics we will achieve with this channel, parasitic running will also provide valuable data for the PWA of mesonic states.

#### 4.2.2 Partial Wave Analysis of the $\eta\pi$ Channel

For the following study we considered an electron beam of 11 GeV, a scattered electron of  $E_{e'} = 2$  GeV (ie. a 9 GeV virtual photon) and  $\theta_{e'}=3^\circ$ . By fixing those parameters, the photon linear polarization is fixed at  $\epsilon = 0.35$ . The azimuthal angle  $\phi_{e'}$  is taken randomly from 0 to 360 degrees, therefore, the angle  $\alpha$ , between the polarization vector and the perpendicular to the production plane, results randomly distributed within the same interval.

The virtual photon information enters solely through its energy and spin density matrix (related

to  $\epsilon$  and  $\alpha$ ). Those three values were smeared with a Gaussian distribution of standard deviation calculated by propagating the energy and angles resolutions measured by the FT.

Events were then weighted according to a photoproduction cross-section for  $E_\gamma=9\text{ GeV}$  photons and with a one-pion-exchange production (OPE) mechanism. In addition, two resonances were included: the  $\pi_1(1400)$  and the  $a_2(1320)$ . Decays were produced only for  $m = +1$  waves leading to two combinations of quantum number:  $J^{PC}M = 1^{-+}1$  and  $2^{++}1$ . These events were then put through FASTMC, a simulation of the CLAS12 detector, that parametrizes its acceptance and resolution.

Our first test was to determine if the asymmetries in  $\phi$  created by the beam polarization, remained through the angular distribution distortion produced by the CLAS12 and FT acceptance and resolution. We knew that the experimental resolution may introduce some distortions but we expected that most of the structure created by the polarization were preserved. A good test is to look at the distributions of  $\phi_{GJ}$  ( $\phi$  angle in the Gottfried-Jackson frame) vs.  $\alpha$  (polarization vector angle) before and after acceptance and resolution smearing. Figures 34 and 35 show these distributions. Also the  $\phi_{GJ}$  distributions for a given range in alpha, before and after acceptances, are shown in figures 36 and 37. We conclude that the  $\phi$  information produced by the beam polarization is still present in the data after the acceptances and resolutions of the CLAS12 and the FT are taken into account.

Furthermore, a mass independent partial wave analysis of the simulated data was performed using  $20\text{ MeV}/c^2$  wide mass bins from  $1.0\text{ GeV}/c^2$  to  $1.6\text{ GeV}/c^2$ . We used a new updated version of the PWA2000 code used for the CLAS-g6c data analysis and currently being used to analyze CLAS-g12 run data. Three partial waves were used in the PWA fit. For each of  $J^{PC}|M|L$  there was one wave corresponding to positive reflectivity (pion exchange). The waves used in the fit were:  $2^{++}1D$ ,  $1^{-+}1P$ , the same used as input for the simulation, and an additional  $2^{++}0D$  wave. The PWA intensities resulting from the many mass independent PWA fits are shown in Fig. 38. The fit populates the  $P1$  and  $D1$  waves, with no contribution to the  $D0$  wave. This result demonstrates the capability of the PWA to extract different resonances in their proper partial waves.

PWA results performed on the two channels, studied independently by the two groups, lead to the conclusion that it is possible to perform a full partial wave analysis using CLAS12 and the Forward Tagger system. Furthermore, information from the beam polarization is maintained in asymmetries observed on the  $\phi$  distributions. This information will be important to determine the naturality of the production mechanisms and to disentangle possible PWA ambiguities.

### 4.3 Beam time request and expected results

As mentioned above, the meson spectroscopy program can run in parallel to the standard electroproduction experiments on hydrogen target planned for CLAS12, collecting in a multi-year campaign a statistic comparable to the foreseen Gluex data yield. Nevertheless some dedicated beam time will be necessary for the Forward Tagger commissioning and to collect data with minimum bias trigger; in addition, periodic dedicated calibration runs have to be foreseen. In particular we would require the following dedicated beam time:

- 2 weeks commissioning time to test and optimize the FT configuration (energy threshold, equalization, time calibration ...);
- 2 weeks of dedicated beam time with low luminosity ( $\sim 10^{34}\text{cm}^{-2}\text{s}^{-1}$ ) and minimum bias triggers (2 prongs) to test the overall trigger configuration;

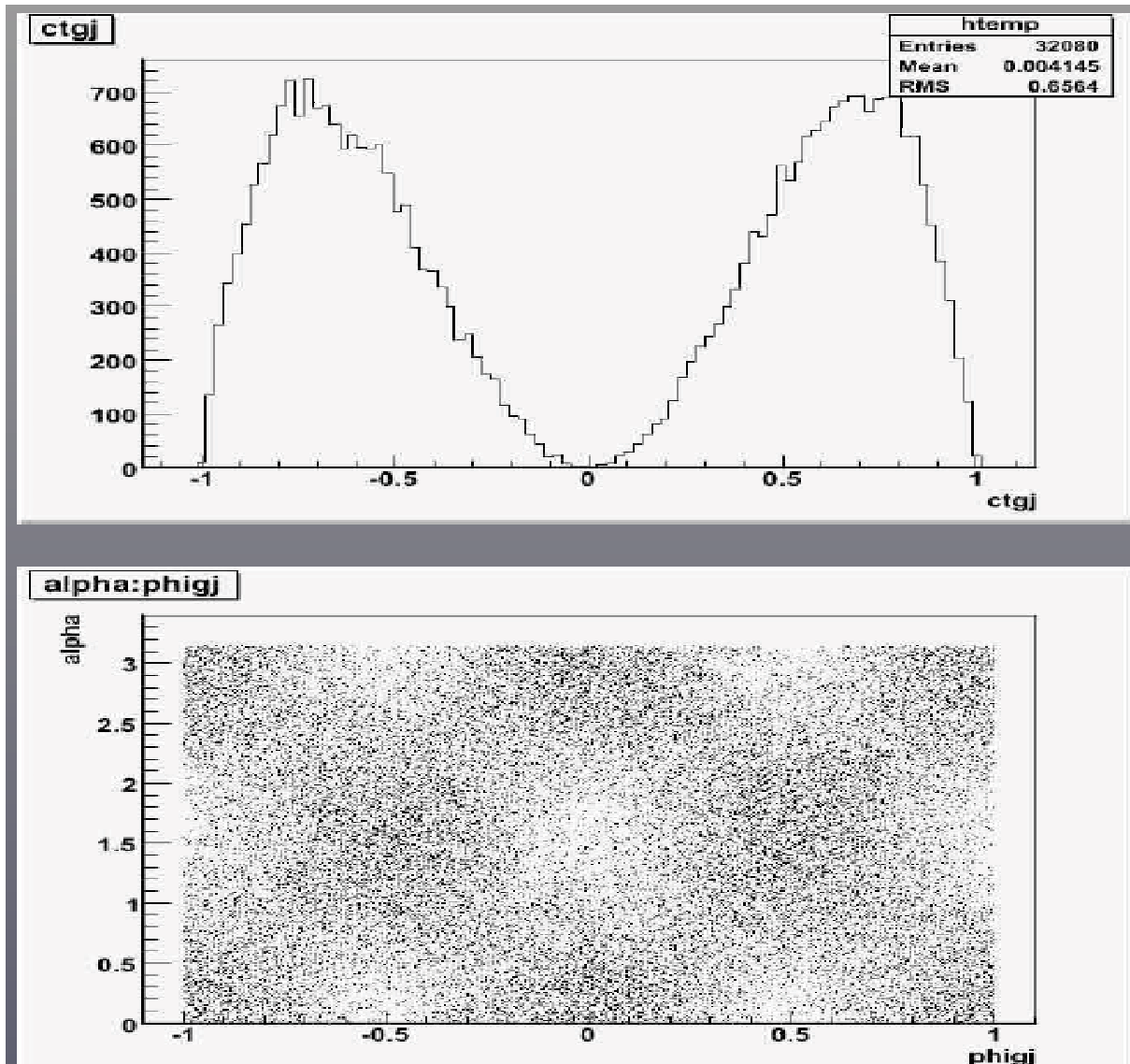


Figure 34: The raw  $\phi_{GJ}$  vs  $\alpha$  and  $\cos(\theta_{GJ})$  distributions

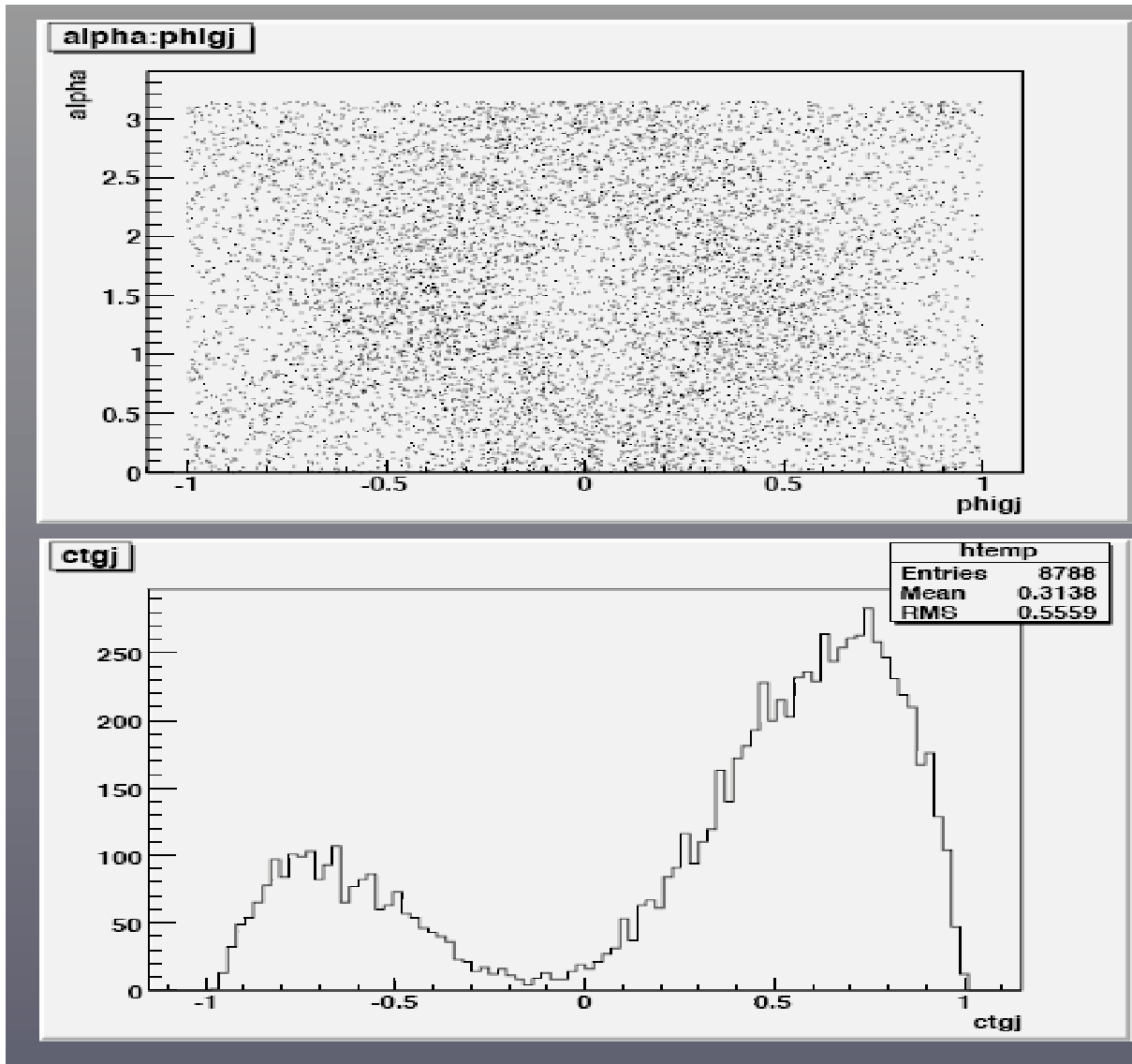


Figure 35: The accepted  $\phi_{GJ}$  vs  $\alpha$  and  $\cos(\theta_{GJ})$  distributions

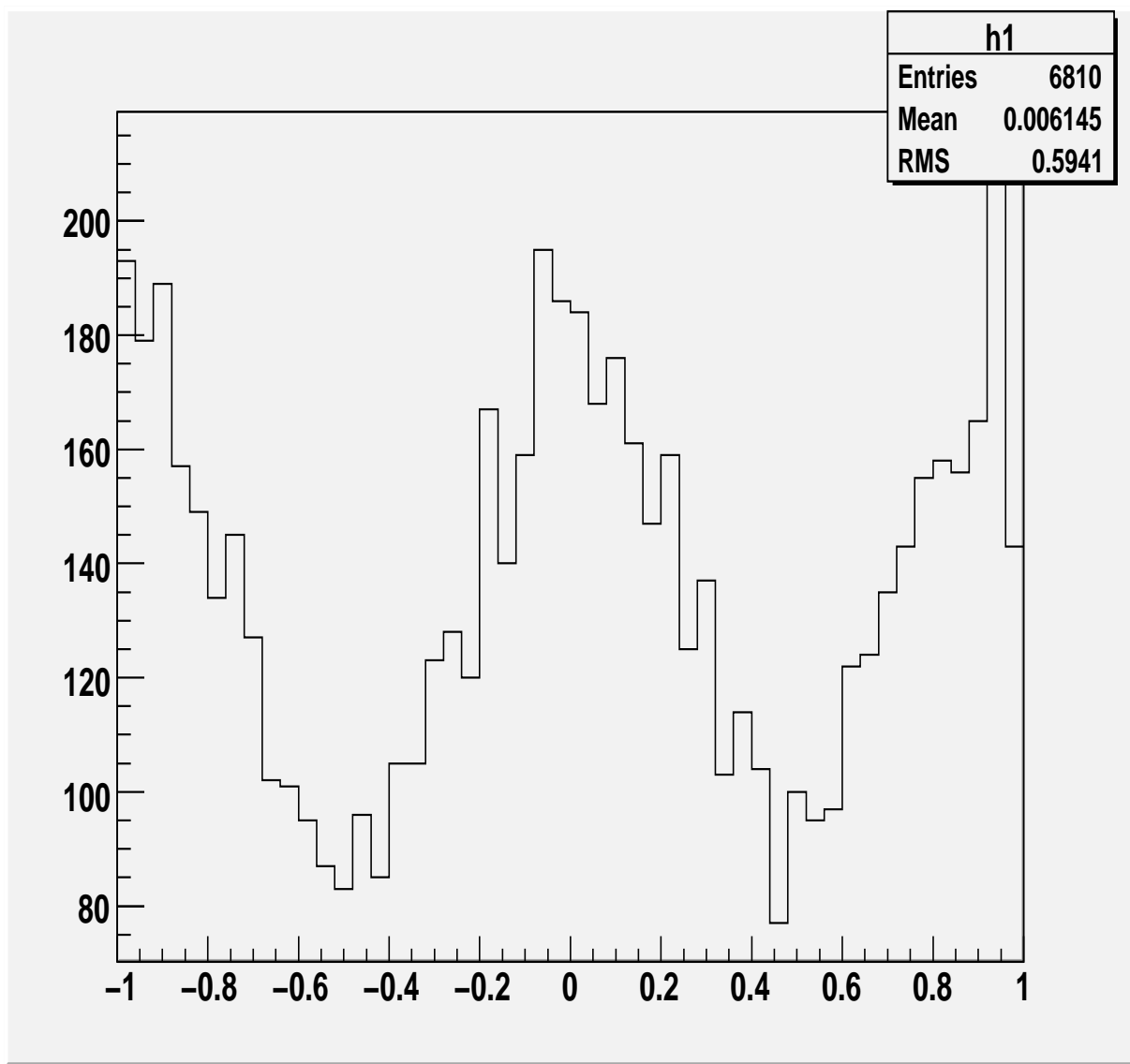


Figure 36: The raw  $\phi_{GJ}$  distribution

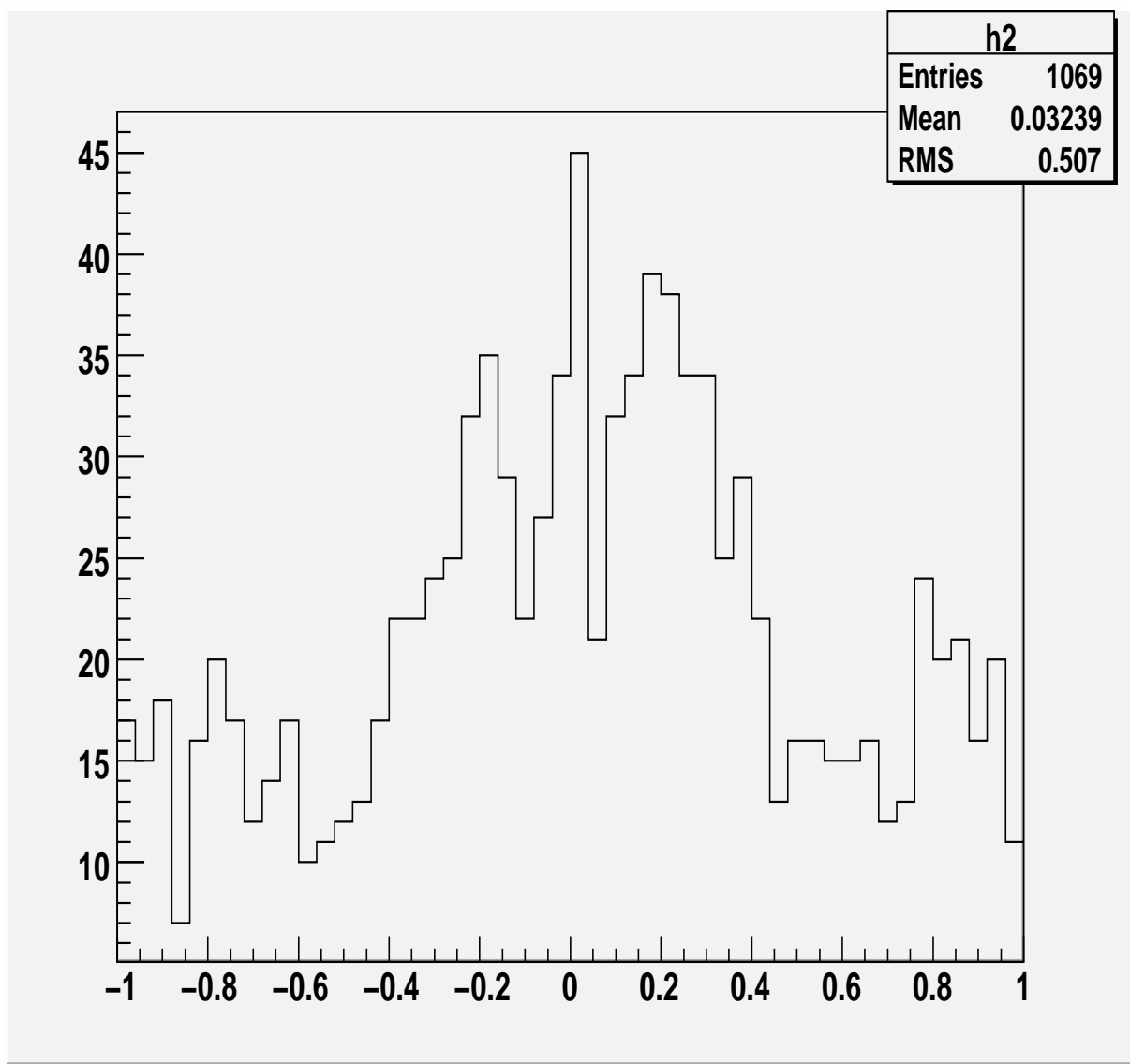


Figure 37: The accepted  $\phi_{GJ}$  distribution

## Acceptance (fit6) D1 + P1

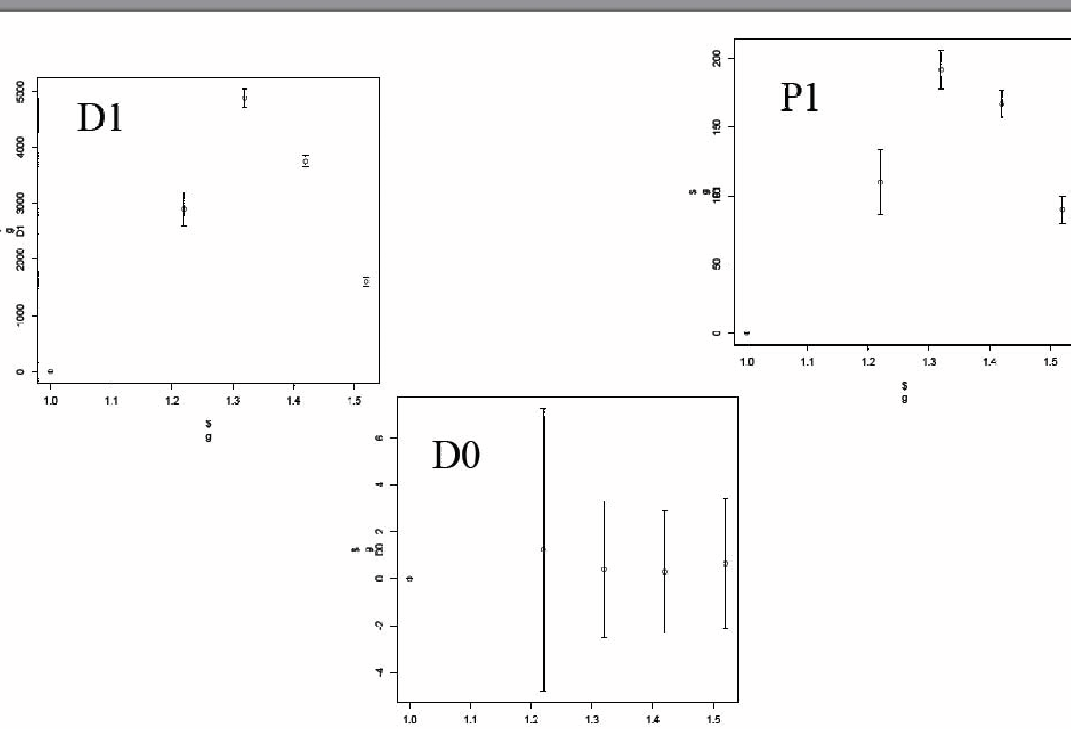


Figure 38: The PWA intensities resulting from the mass independent PWA fits of the simulated data. One expects not to observe resonance structure in these partial waves.

- 2 months of dedicated time at full luminosity ( $\sim 10^{35} \text{ cm}^{-2} \text{s}^{-1}$ ) to accumulate enough statistics in order to perform reliable PWA on the reaction with higher cross sections and optimize all reconstruction and analysis tools;
- during normal electroproduction, special runs for a total time of 8 h/weeks to perform calibration runs and low luminosity runs.

## TO BE COMPLETED

### 4.3.1 Strangeonia

The decay into  $\phi\eta$  of strangeonia has never been observed before. Being one of the channels with the lowest cross section, we might use it to determine runtimes. We can estimate rates using theoretical predictions by Barnes, Black and Page [81]. They predict

$$\frac{Br(\phi\eta)}{Br(K^+K^-)} = 0.5$$

The cross section for  $K^+K^-$  photoproduction was measured at 45 GeV by the  $\Omega$  collaboration [83]. They obtained a cross section of about 8 nb per 50 MeV mass bin. Our lower beam energy should increase the yield somewhat for resonance production so we estimate a cross section of 14 nb per 50 MeV bin for  $K^+K^-$  production which agrees with preliminary g12 values. The data will be sorted into approximately 20 mass bins. This will produce an event rate of 0.0013 events/sec/50 MeV bin. Applying the CLAS12 acceptance (0.18) we will detect a total rate of 15 events/hour distributed over the whole mass range. Therefore in a 30 days run (a full field and in parallel with other CLAS12 experiments) we can obtain about 500 events per 50 MeV bin, enough to determine establish resonances. For PWA of these data, it will neccesary to obtain about two to three times more statistics.

Our goal is to obtain data samples which will enable us to perform an accurate partial-wave analysis in most channels. High statistics are critical to the ability to separate partial waves with good accuracy. Using a reasonable value of 3000 events per mass bin for a typical expected rate like those listed above, we arrive at a total beam-time request of 60-90 days. This will yield a factor of ten increase in the total integrated luminosity over that of g12 (!check that!).

## 5 Summary

We are proposing to add to the CLAS12 equipment a new quasi-real photon tagging facility that will allow to address fundamental questions about hadron spectroscopy and QCD via photo-production experiments. This facility will detect electrons scattered at very small angles, namely from  $2.5^\circ$  to  $4.5^\circ$ , providing the possibility to perform experiments at very small four-momentum transfer  $Q^2$ , below  $10^{-1}$  GeV $^2$ . In this kinematics, the virtual photon can be considered as quasi real and low- $Q^2$  electron production can be treated as photoproduction. The effective photon flux and the degree of linear polarization that can be reached with this technique are of the order of  $10^7 - 10^8 \gamma/\text{s}$  and  $\sim 40\%$ , respectively, that are comparable with what is obtained by using coherent bremsstrahlung as planned in the new Hall-D. The device we are proposing will consist of a calorimeter to measure the energy of the scattered electron, and therefore infer the energy of the virtual photon, a Veto counter to discriminate electrons against photons and a tracking device to determine precisely the scattering plane, and therefore the photon polarization.

This new facility will allow to continue with CLAS12 the extensive photoproduction program that was started with CLAS. The highest photon energy that will be achieved with the 11 GeV electron beam ( $E_\gamma = 7 - 10.5$  GeV) will allow to address several fundamental topics in hadronic physics as the precise determination of the meson spectrum and the search for exotics or hybrids on proton. The spectroscopy program will provide important information for the understanding of the dynamics of strong interaction and address the origin of confinement, the role of gluons in determine the spectrum of hadrons and the origin of their mass.

The design of the forward tagger will be compatible with the CLAS12 standard running, so that the tagger operation will be possible in parallel to standard electron scattering measurements that are part of the already approved physics program. The proposed detector will therefore extend the CLAS12 detection capabilities for electron down to  $2.5^\circ$ , also providing an excellent acceptance for photons emitted in the forward direction. The proposed technique gives access to an extensive physics program that is complementary to the program planned in Hall-D by the GLUEX Collaboration. The meson spectroscopy program proposed in Hall-D has been one of the driving forces for the Jefferson Lab 12 GeV upgrade and the additional contribution to this fundamental physics that CLAS12 with the new forward tagging facility would give will strengthen the role of the Laboratory in answering key questions in non-perturbative QCD.

## A Appendix A: the model to describe $\gamma p \rightarrow \pi^+ \pi^+ \pi^- n$

For reaction  $\gamma p \rightarrow \pi^+ \pi^+ \pi^- n$  the hadronic tensor  $T^{\mu\nu}$  from Eq. 1 is given by the current matrix elements  $T^{\mu\nu} = \langle 3\pi n | J^\mu | p \rangle^* \langle 3\pi n | J^\nu | p \rangle$  where

$$\langle 3\pi n | J^\mu | p \rangle = \sum_{\lambda_\gamma=\pm 1,0} \epsilon^\mu(Q, \lambda_\gamma) T(p_i, p', p, q; \lambda', \lambda, \lambda_\gamma) \quad (11)$$

with  $\lambda_\gamma, \lambda, \lambda'$  being the photon, proton and neutron, helicities in the center of mass, respectively, and  $p_i, i = \pi^+(1), \pi^+(2), \pi^-(3)$ ,  $p', p, q$  denoting the pion, recoil, target and photon momenta, respectively. The amplitude  $T$  is symmetrized with respect to the two  $\pi^+$ . Assuming the pion exchange dominance and rewriting in a factorized form

$$T(p_i, p', p, q; \lambda', \lambda, \lambda_\gamma) = \sum_X \sum_{\lambda_X=-J_X}^{J_X} P_{\lambda', \lambda_X, \lambda, \lambda_\gamma}^X(s, t) D_{\lambda_X}^X(p_i) \quad (12)$$

The amplitude  $P^X$  denotes the one-pion-exchange amplitude for production of a  $3\pi$  isobar,  $X = a_1, a_2, \pi_1, \pi_2$  with the quantum numbers  $J_X^{P_X C_X} = 1^{++}, 2^{++}, 1^{-+}, 2^{-+}$  respectively,

$$P_{\lambda', \lambda_X, \lambda, \lambda_\gamma}^X = \delta_{\lambda', -\lambda} V_{\lambda_\gamma \lambda_X} \left( -\frac{t'}{4m_N^2} \right)^{\frac{|\lambda' - \lambda|}{2} + \frac{|\lambda_\gamma - \lambda_X|}{2}} \frac{1 + e^{-i\pi\alpha_\pi(t)}}{2} \Gamma[-\alpha_\pi(t)] s^{\alpha_\pi(t)} e^{5t \text{GeV}^{-2}}, \quad (13)$$

with  $t' = t_{min}$  where  $t = (p' - p)^2$  is the momentum transfer squared,  $s = (q + p)^2$  is the center of mass energy squared and  $\alpha_\pi(t) = 0.9(t - m_\pi^2) \text{GeV}^{-2}$  is the pion Regge trajectory. The "upper" vertex  $V_{\lambda_\gamma \lambda_X}$  is given by

$$\begin{aligned} V_{\lambda_\gamma \lambda_X} &= [\delta_{\lambda_\gamma, 1} \delta_{\lambda_X, 0} + \eta_X \delta_{\lambda_\gamma, -1} \delta_{\lambda_X, 0}] \beta_1^{\gamma \pi X} + [\delta_{\lambda_\gamma, 1} \delta_{\lambda_X, |\lambda_X|} + \eta_X (-1)^{\lambda_X} \delta_{\lambda_\gamma, -1} \delta_{\lambda_X, -|\lambda_X|}] \beta_{|\lambda_X|-1}^{\gamma \pi X} \\ &+ [\delta_{\lambda_\gamma, 1} \delta_{\lambda_X, -|\lambda_X|} + \eta_X (-1)^{\lambda_X} \delta_{\lambda_\gamma, -1} \delta_{\lambda_X, |\lambda_X|}] \beta_{|\lambda_X|+1}^{\gamma \pi X} + \delta_{\lambda_\gamma, 0} [\delta_{\lambda_X, |\lambda_X|} - \eta_X (-1)^{\lambda_X} \delta_{\lambda_X, -|\lambda_X|}] \beta_{|\lambda_X|}^{\gamma \pi X} \\ &+ \delta_{\lambda_\gamma, 0} \delta_{\lambda_X, 0} \frac{1 - \eta_X}{2} \beta_0^{\gamma \pi X} \end{aligned} \quad (14)$$

where  $\eta_X = P_X(-1)^{J_X}$  and the various linear combination reflect parity conservation. The factors  $\beta_n^{\gamma \pi X}$ ,  $n = 0, 1, \dots, \lambda_X + 1$  give the strength of various helicity couplings and in simulations we have assumed dominances of  $s$ -channel helicity conservation *i.e.* only use  $\beta_0^{\gamma \pi X} \neq 0$ . The resonance decay amplitudes  $D^X$  are given by

$$D_{\lambda_X}^X = D_{\lambda_X}^X(12, 3) + D_{\lambda_X}^X(31, 2) + D_{\lambda_X}^X(23, 1) \quad (15)$$

where  $D_{\lambda_X}^X(ij, k)$  represents a quasi-two body decay of the  $X$ -isobar to a  $(\pi^i \pi^j)$ , di-pion resonance defined by its spin,  $j_{ij}$ , isospin  $t_{ij}$  and parity  $P_{ij}$ , and the spectator,  $\pi^k$ , with the orbital angular momentum  $L_{ij}$  between the di-pion resonance and the spectator,

$$\begin{aligned} D_{\lambda_X}^X(ij, k) &= \sum_{t_{ij} j_{ij} L_{ij}} N_{L_{ij}} N_{j_{ij}} g_{j_{ij} P_{ij} L_{ij}}^{j_X^P I_X} \frac{1 + P_X P_{ij} (-1)^{L_{ij}+1}}{2} \frac{1 + P_{ij} (-1)^{j_{ij}}}{2} \frac{1 + (-1)^{j_{ij} + t_{ij}}}{2} \\ &\times \sum_{m_{ij}, \mu_{ij}} \langle 1m_i; 1m_j | t_{ij} m_{ij} \rangle \langle t_{ij} m_{ij}; 1m_k | 11 \rangle \langle j_{ij} \mu_{ij}; L_{ij} 0 | j_X \mu_{ij} \rangle D_{\mu_{ij}, 0}^{j_{ij}}(\psi_i \theta_i 0) D_{\lambda_X, \mu_{ij}}^{j_X}(\tilde{\phi}_k \tilde{\vartheta}_k 0) \end{aligned} \quad (16)$$

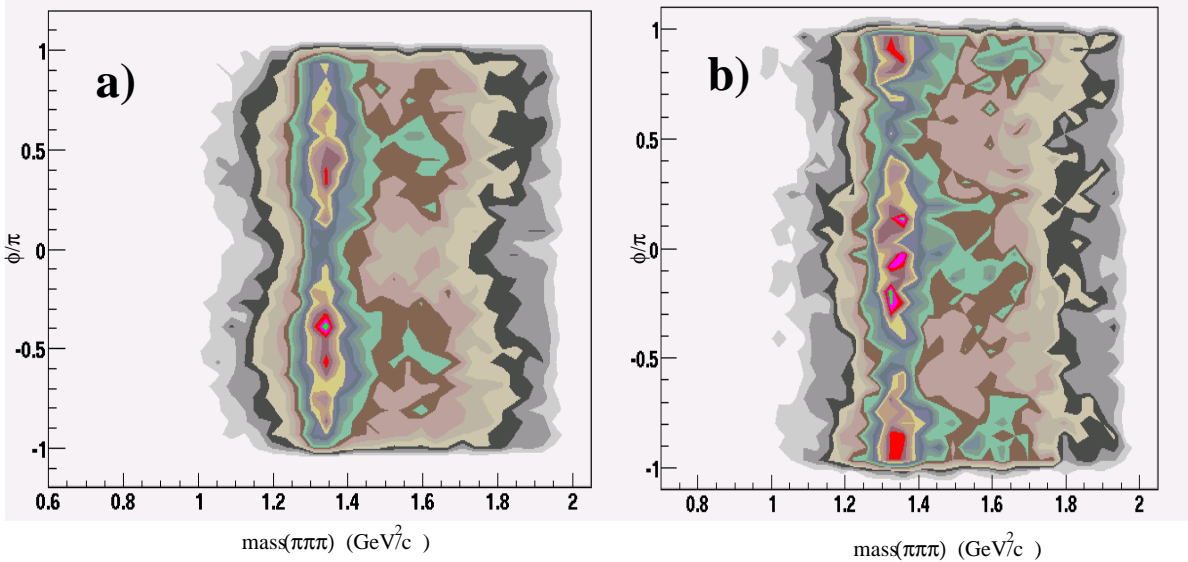


Figure 39: The  $\phi/\pi$  vs. Mass[ $3\pi$ ] for those events with the polarization perpendicular to the production plane (left) and in the production plane (right). The simulated polarization was set to 60%.

The angles  $\tilde{\vartheta}_k, \tilde{\phi}_k$  are the polar and the azminuthal angle of the spectator pion ( $\pi^k$ ) in the helicity frame of the (*i.e.* the rest frame of the  $3\pi$  system with the  $y$  axis perpendicular to the hadron reaction plane and the  $-z$  axis along the recoil neutron) and  $\theta_i, \psi_i$  are the polar and the azminuthal angle of the  $\pi^i$  in the rest frame of the  $\pi^i\pi^j$ . In simulations we used: the  $L = S, D$  decay modes of the  $a_1$  to  $\rho\pi$ , the  $L = D$  decay modes of the  $a_2$  to  $\rho\pi$ , the  $L = P, F$  decay modes of the  $\pi_2$  to  $f_2\pi$  and the  $L = P, F$  decay modes of the  $\pi_2$  to  $\rho\pi$ . The coupling constants  $g$  were fixed by the known decay widths for these modes. In addition we simulated the  $L = P$  decay mode of the exotic,  $\pi_1$  to  $\rho\pi$  with varied coupling strength and mass of the  $\pi_1$  resonance.

The effects related to the polarization can be directly seen in Figure 39. Because pion exchange corresponds to unnatural parity exchange the  $\phi$  dependence of the produced  $3\pi$  system will flip depending on the naturality  $\eta_X = P_X(-1)^{J_X}$  of the state [28]. These two figures differ only in the direction of the photon polarization and correspond to the two eigenstates of reflectivity. In Figure 39 (a) are those events where the photon polarization is normal to the production plane, and (b) are those events where the photon polarization is in the production plane. Due to parity conservation in the production process, states of the same reflectivity but opposite naturality will have opposite  $\phi$  distributions, which may be observed in the figure. It is most clearly seen for the band at the  $a_2(1320)$  mass. This distribution is  $\cos^2(\phi)$  in one figure and  $\sin^2(\phi)$  in the other. Another band at a mass near 1.7 GeV has the opposite  $\phi$  behavior of the  $a_2(1320)$ . It corresponds to the  $\pi_2(1670)$  which has a naturality opposite that of the  $a_2(1320)$ .

Further details of the simulations are presented in Sec. 4

## References

- [1] M. Ripani *et al.*, Phys. Rev. Lett. **91**, 022002 (2003).
- [2] S. Stepanyan *et al.*, Phys. Rev. Lett. **91**, 25001 (2003).
- [3] V. Kubarovsky *et al.*, (CLAS), Phys. Rev. Lett. **92**, 032001 (2004).
- [4] R. Thompson *et al.*, , Phys. Rev. Lett. **86** 1702 (2001).
- [5] J.W.C. McNabb *et al.*, , Phys. Rev. C **69**, 042201R (2004).
- [6] J. W. Price *et al.*, Phys. Rev. C **71**, 058201 (2005).
- [7] The GlueX Collaboration, Hall D CDR.
- [8] N. Dombey, Rev. Mod. Phys. **41**, 236 (1969).
- [9] Y.S. Tsai, Rev. Mod. Phys. **46**, 815 (1974).
- [10] For review see, J. Greensite, Prog. Part. Nucl. Phys. **51**, 1 (2003).
- [11] S. Dürr, *et al.*, Science 21, 322, 1224 (2008).
- [12] M. Alekseev *et al.* [COMPASS Collaboration], Phys. Rev. Lett. **104**, 241803 (2010).
- [13] A. R. Dzierba *et al.*, Phys. Rev. D **73**, 072001 (2006).
- [14] G. Ascoli, L. M. Jones, B. Weinstein and H. W. Wyld, Phys. Rev. D **8**, 3894 (1973).
- [15] R.T. Deck, Phys. Rev. Lett. **13**, 169 (1964).
- [16] E.L. Berger, Phys. Rev. 166, 1525 (1968).
- [17] M. G. Bowler, M. A. V. Game, I. J. R. Aitchison and J. B. Dainton, Nucl. Phys. B **97**, 227 (1975).
- [18] J. J. Dudek, R. G. Edwards, M. J. Peardon, D. G. Richards and C. E. Thomas, Phys. Rev. D **82**, 034508 (2010)
- [19] D. Horn and J. Mandula, Phys. Rev. D **17**, 898 (1978).
- [20] T. Barnes, F. E. Close, F. de Viron and J. Weyers, Nucl. Phys. B **224**, 241 (1983).
- [21] N. Isgur and J. E. Paton, Phys. Rev. D **31**, 2910 (1985).
- [22] P. Guo, A. P. Szczepaniak, G. Galata, A. Vassallo and E. Santopinto, Phys. Rev. D **78** (2008) 056003
- [23] Colin Morningstar, nucl-th/0308026; AIP Conf. Proc. **698**, pp. 530-534 (AIP, New York, 2003).
- [24] N. Mathur, Y. Chen, S.J. Dong, T. Draper, I Horvath, F.X. Lee, K.F. Liu, and J.B. Zhang, hep-ph/0306199; to appear in Phys. Lett. B.
- [25] N. Isgur and J. Paton, Phys. Rev. D **31**, 2910 (1985).
- [26] N. Isgur, R. Kokoski, and J. Paton, Phys. Rev. Lett. **54**, 869 (1985).

- [27] S. U. Chung, BNL-QGS-93-05 (1995).
- [28] S. U. Chung and T. L. Trueman, Phys. Rev. D **11** (1975) 633.
- [29] M. Battaglieri *et al.* (CLAS Collaboration), Phys. Rev. Lett. **102**, 102001 (2009) and M. Battaglieri *et al.* (CLAS Collaboration), Phys. Rev. **D80**, 072005 (2009).
- [30] A. Szczepaniak *et al.*, *A Topical Collaboration in the Analysis of the Light Hadron Spectrum*, <http://www.physics.indiana.edu/~aszczepa/doepprop/doepprop.pdf>.
- [31] H. C. Fenker *et al.*, E-03-012: *The Structure of the Free Neutron Via Spectator Tagging*, <http://www.jlab.org/exp-prog/proposals/03/PR03-012.pdf>. H. C. Fenker *et al.*, Nucl. Instrum. Meth. A **592**, 273 (2008).
- [32] S. Stepanyan *et al.*, E-07-009: *Meson spectroscopy in the Coherent Production on  $^4\text{He}$  with CLAS*, <http://www.jlab.org/exp-prog/proposals/07/PR-07-009.pdf>. K. Hafidi *et al.*, E-08-024: *Deeply Virtual Compton Scattering off  $^4\text{He}$* , <http://www.jlab.org/exp-prog/proposals/08/PR-08-024.pdf>.
- [33] S. Stepanyan *et al.*, JLAB PAC 23 LOI-03-003 (2002).
- [34] CLAS12 Technical Design Report,  
[http://clasweb.jlab.org/wiki/index.php/CLAS12\\_Technical\\_Report](http://clasweb.jlab.org/wiki/index.php/CLAS12_Technical_Report)
- [35] M. Ungaro, CLAS12 GEANT-4 simulation package GEMC,  
[http://clasweb.jlab.org/wiki/index.php/CLAS12\\_Software](http://clasweb.jlab.org/wiki/index.php/CLAS12_Software)
- [36] The Gluex Collaboration, Presentation to PAC30,  
<http://www.jlab.org/exp-prog/proposals/06/PR12-06-102.pdf>
- [37] M.J.M. van Sambeek et al., NIM **A 409**, 443-446 (1998).
- [38] K. Assamagan et al., NIM **A 426**, 405 (1999).
- [39] S.J. Brodsky et al., *Phys. Lett.* **B498**, 23-28 (2001).
- [40] K. Abe et al., *Phys. Rev. D* **30**, 1 (1984)
- [41] M.P. Rekalo and E. Tomasi-Gustafsson, *Phys. Lett.* **B500**, 53-58 (2001).
- [42] B. Gittelman et al., *Phys. Rev. Lett.* **35**, 1616 (1975)
- [43] U. Camerini et. al., *Phys. Rev. Lett.* **35**, 483 (1975)
- [44] F.E. Close and H.J. Lipkin, *Phys. Rev. Lett.* **41**, 1263 (1978).
- [45] *Production of the Strangest Baryon with CLAS12*, JLAB PAC35 Letter-of-Intent, Contact Person: E. Pasyuk
- [46] Review of Particle Physics, *Phys. Lett.* **B 592** (2004).
- [47] D. O. Riska, *Eur. Phys. J.* **A17**, 297 (2003).
- [48] N. Byers and S. Fenster, *Phys. Rev. Lett.* **11**, 52 (1963).
- [49] S. Capstick and N. Isgur, *Phys. Rev. D* **34**, 2809 (1986).

- [50] A. R. Bijker, F. Iachello, A. Leviatan, Annals Phys. **284**, 89 (2000).
- [51] Y. Oh, Phys. Rev. D **75**, 074002 (2007).
- [52] S. Basak *et al.*, [LHP Collaboration], arXiv:hep-lat/0409082; S. Basak *et al.*, [LHP Collaboration], Nucl. Phys. Proc. Suppl. **129**, 209 (2004) [arXiv:hep-lat/0309091]; R. Edwards *et al.*, [LHP Collaboration], Nucl. Phys. Proc. Suppl. **129**, 236 (2004) [arXiv:hep-lat/0309079]; and D. Richards, private communication.
- [53] L. Guo *et al.*, Phys. Rev. C **76**, 025208 (2007).
- [54] R. Gothe, M. Holtrop, E. Smith, S. Stepanyan, E-04-010: *Search for Exotic Cascades with CLAS Using an Untagged Virtual Photon Beam*, <http://www.jlab.org/exp-prog/proposals/04/PR04-010.pdf>.
- [55] I. Akushevich, H. Bottcher and D. Ryckbosch, arXiv:hep-ph/9906408.
- [56] <http://cms.web.cern.ch/cms/Detector/ECAL/index.html>.
- [57] D. C. Zhou *et al.* (ALICE Collaboration), J. Phys. G **34** (2007) 719.
- [58] PANDA Collaboration, “Technical Design Report for PANDA Electromagnetic Calorimeter (EMC),” arXiv:0810.1216
- [59] I. Bedlinskiy *et al.*, “An Inner Calorimeter for CLAS/DVCS experiments”, unpublished.
- [60] B. Andrieu et al., Test beam results of the tungsten/quartz-fibre calorimeter for the luminosity measurement in H1, Proc. of the IX Int. Conf. on Calorimetry in Particle Physics, (CALOR2000) Annecy Oct. 2000, Frascati Physics Series(2001).
- [61] C. Adler et al., The RHIC zero degree calorimeters, nucl-ex/0008005.
- [62] Nucl. Instrum. Meth. A **372**, 359 (1996).
- [63] C. Adloff *et al.* [CALICE Collaboration], J. Phys. Conf. Ser. **160** (2009) 012065 [arXiv:0811.2354].
- [64] M. Mestayer, *private communication*.
- [65] S. Procureur, *private communication*. See also [http://www.jlab.org/~procureu/CLAS12/2008-10-30\\_CollabMeeting.ppt](http://www.jlab.org/~procureu/CLAS12/2008-10-30_CollabMeeting.ppt)
- [66] Y. Khokhlov *et al.* (VES Collaboration), Nucl. Phys. A **663**, 596 (2000).
- [67] G. S. Adams *et al.* (E852 Collaboration), Phys. Rev. Lett. **81**, 5760 (1998).
- [68] A. Dzierba *et al.*, Phys. Rev. D **73**, 072001 (2006).
- [69] M. Nozar *et al.*, Phys. Rev. Lett. **102**, 102002 (2009).
- [70] A. Alekseev *et al.* (COMPASS Collaboration), arXiv:0910.5842 [hep-ex].
- [71] F.E. Close and H.J. Lipkin, *Phys. Rev. Lett.* **41**, 1263 (1978).
- [72] S.I. Bityukov et al., Sov.J.Nucl.Phys. **38**, 1205 (1983).

- [73] S.I. Bityukov et al., *Phys. Lett.* **B188**, 383 (1987).
- [74] M. Atkinson et al., *Nucl. Phys.* **B231**, 1 (1984).
- [75] Yu.M. Antipov et al., Pis'ma JETF **38**, 356 (1983).
- [76] B. Aubert et al., *Phys. Rev. D* **77**, 092002 (2008).
- [77] Valery Kubarovskiy,  $\phi\pi$  Photoproduction and Search for Exotic Meson with CLAS, CLAS-ANALYSIS Note 2000-001.
- [78] S. Janssen et. al., Nuclear Science Symposium, 1999. Conference Record. 1999 IEEE
- [79] S.J. Alsvaag et. al., IEEE transactions on Nuclear Science, Vol. 42, no.4 (1995)
- [80] S. Stepanyan et. al., CLAS Note 2009-019; S. Stepanyan et. al., 2008 IEEE nuclear Science Symposium and Medical imaging Conference
- [81] T. Barnes, N. Black and P.R. Page, *arXiv.org e-Print Archive*,**Nucl-th/0208072** (2002).
- [82] D. Bisello, et al., *Z. Phys.***C52**, 227 (1991); J. Buon, et al., *Phys. Lett.***118B**, 221 (1982).
- [83] M. Atkinson, et al., *Nucl. Phys.***B231**, 1 (1984).
- [84] F. Mane et al., (DM1), *Phys. Lett.* **112B**, 178 (1982).
- [85] J.M. Link, et al.(FOCUS),*arXiv.org e-Print Archive* **hep-ex/0208027** (2002).
- [86] F. Mane et al., (DM1),*Phys. Lett.***99B**, 261 (1981).
- [87] B. Delcourt, et al., (DM1)*Phys. Lett.***99B**, 257 (1981)
- [88] P.M.Ivanov, et al., *Phys. Lett.* **107B**, 297 (1981).
- [89] D. Bisello, et al., (DM2) *Z. Phys.* **C39**, 13 (1988).
- [90] J. Buon, et al., (DM1) *Phys. Lett.* **118B**, 221 (1982).
- [91] A. Antonelli, et al., (DM2) *Z. Phys.* **C56**, 15 (1992).
- [92] D. Aston, et al., *Phys. Lett.* **104B**, 231 (1981).
- [93] M. Atkinson, et al., *Z. Phys.* **C27**, 233 (1985).
- [94] J. Busenitz, et al., *Phys. Rev.* **D40**, 1 (1989).
- [95] A. Donnachie and P.V. Landshoff, *Phys. Lett.* **B348**, 213 (1995).
- [96] , P.D.B. Collins, and A.D. Martin, *Rep. Prog. Phys.***335**, 45 (1982).
- [97] CLAS12 Technical Design Report (2008).
- [98] M. Sargsyan, CLAS-NOTE 90-007 (1990).
- [99] M. Mestayer, SLAC Eng.Note 72 (1977).
- [100] D. Alde, et al. *Phys.Lett.* **B205**, 397 (1988).

- [101] H. Aoyagi, et.al. *Phys. Lett.* **B314**, 246 (1993).
- [102] D. R. Thompson et. al. (BNL-E852 Collaboration,) *Phys. Rev. Lett.* **79**, 1630 (1997).
- [103] G. M. Beladidze et. al. *Phys. Lett.* **B313**, 276 (1993).
- [104] C. A. Meyer and Y. Van Haarlem, *Phys. Rev.* **C82**, 025208 (2010).
- [105] D. P. Weygand, *The Status of Mesonic Exotica* **Mesons 2101**, Warsaw, Poland (2010).